



MSc in Physics

The eccentric evolution of circumbinary gas disks

Marcela Grcic

Supervised by Daniel J. D'Orazio and Martin E. Pessah

August 15, 2022



Marcela Grcic

The eccentric evolution of circumbinary gas disks

MSc in Physics, August 15, 2022

Supervisors: Daniel J. D’Orazio and Martin E. Pessah

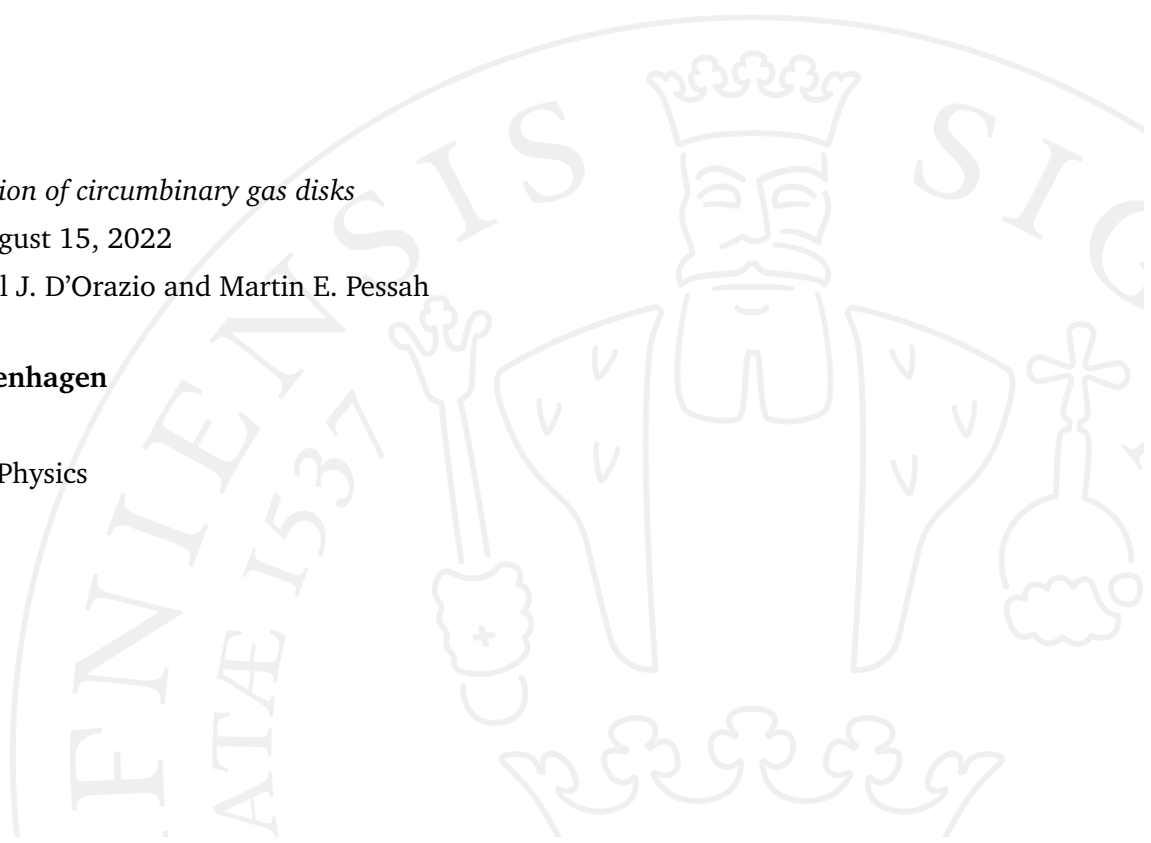
University of Copenhagen

Niels Bohr Institute

Masters Degree in Physics

Blegdamsvej 17

2100 Copenhagen



Acknowledgements

I would like to offer a special thanks to my supervisors Daniel J. D’Orazio and Martin E. Pessah. I greatly benefited from our many discussions and have been continually supported over the last year. They kept me motivated and inspired.

Abstract

Gas disks around binaries are ubiquitous in the universe, naturally arising during the formation of binary stars and playing an important role in the mergers of black holes. The interaction of these circumbinary disks with the binary still holds many open questions that are important for understanding how populations of binaries are sculpted and also the observable signatures of these systems. Recent numerical simulations of these systems have discovered a number of surprising features in the response of the gas disk to the binary's gravitational potential, including the growth of eccentric modes in the gas disk. These eccentric features have important consequences for binary evolution and observability, yet the physical means for their generation is still poorly understood.

This thesis provides an overview of the differential equations governing eccentricity growth in a circumbinary gas disk. Equations governing the eccentricity evolution of adiabatic and isothermal disks, 2d and 3d disks, circumprimary and circumbinary disks are presented. The eccentricity equation is solved for a locally isothermal circumbinary disk. The number of modes such a disk can support in terms of the disk thickness and the binary mass ratio is found. Properties of elementary and higher order modes are explained. The effect of the disk density distribution on the disk eccentricity is discussed.

Contents

I	Introduction	3
II	Eccentricity equations	9
1	Eccentricity as a way of describing the orbit	11
1.1	Binary orbit	11
1.2	A disk around a binary	13
1.3	Disk evolution as a function of eccentricity	14
2	Unforced eccentricity equation for a 2d adiabatic disk	17
2.1	Disk governing equations	19
2.1.1	The continuity equation	19
2.1.2	Equations of motion	20
2.1.3	Adiabatic equation of state	21
2.1.4	Disk equations	22
2.2	Unperturbed state of the disk	23
2.3	Series expansion of the unperturbed state	24
2.4	Disk in a perturbed state	26
2.5	Series expansion of the perturbed state	28
3	Unforced eccentricity equations for other disks	31
3.1	A locally isothermal 2D disk	31
3.2	Comparison of eccentricity equations for 2d adiabatic and 2d isothermal disks	33
3.3	3D disks	34
4	Gravitational potential	37
4.1	Circular binary.	37
4.1.1	A circumprimary disk and a small binary mass ratio	41
4.1.2	A circumbinary disk	43
4.2	Gravitational potential in a thin ring approximation	45

5	Forcing effects	51
5.1	Eccentricity generation	51
5.2	Eccentricity damping	52
6	Boundary conditions	53
7	Stationary eccentricity and Schrödinger equation	55
7.1	Schrödinger form	56
 III Locally isothermal circumbinary disk in a stationary state		 59
8	Eccentricity equation and solutions	61
8.1	The equation	61
8.2	Pressure and binary quadrupole effects	62
8.2.1	Binary quadrupole effects	63
8.2.2	Pressure effects	63
8.3	Schrödinger equation for eccentricity	64
8.4	The density profile	65
8.5	The quantization condition	67
8.6	Numerical results for the eccentricity boundary value problem	70
9	The lowest mode	73
9.1	WKB frequency	75
9.1.1	Low CFR range	76
9.1.2	High CFR range	77
9.1.3	The entire CFR range	81
9.2	Numerical BVP frequency	82
9.2.1	Low CFR range	82
9.2.2	High CFR range	83
9.2.3	The entire CFR range	87
9.3	Mode location and width	88
9.4	Summary	90
10	Higher order modes	91
10.1	The number of modes	92
10.2	Higher mode frequencies, eccentricity profiles and the location of higher order modes	96
10.3	Summary	100

11 Eccentricity solutions as a function of density	101
11.1 The torque exerted on the binary by the disk	102
11.2 The size of the disk cavity	104
11.3 The cutoff exponent	106
11.4 Illustration of the importance of the cutoff function.	108
11.5 Explanation of the dominance of the density cutoff function on all eccentricity results	111
11.6 Summary	115
12 Summary and conclusion	117
IV Appendix	119
A Polar coordinate system	121
B.1 Equations of motion	123
C Coefficients of expansion of the disk's unperturbed state	125
D Derivation of perturbed equation	127
E Eccentricity equation derivation for a locally isothermal disk	131
E.0.1 Radial equation of motion	133
E.0.2 Newton's law of motion - angular equation	135
E.0.3 Continuity equation	136
E.0.4 Pressure equation	137
F VERTICAL HYDROSTATIC EQUILIBRIUM	139
G Derivation of boundary conditions for the eccentricity equation	141
G.1 An adiabatic disk	142
H Derivation of the eccentricity potential and scaled eccentricity	145
I Scaling the eccentricity equation with a cavity radius	149
J Bibliography	151

List of Figures

1.1	Orbits of the primary (pink) and the secondary (blue) binary component. The center of mass is fixed in the origin. The primary and the secondary revolve the center of mass in similar ellipses of eccentricity $e = 0.75$. The binary mass ratio is $q = 0.5$, so the semi-major axis of the secondary is twice the size of the semi-major axis of the primary (equation (1.7)). The angle between the position of the primary and the secondary is always 180° , so the elliptical orbit of the secondary is rotated by 180° with respect to the orbit of the primary.	13
1.2	Three types of disks based on their location; a circumprimary disk is centered at the location of the primary; a circumsecondary disk is centered at the location of the secondary; a circumbinary disk is centered at the binary center of mass.	14
4.1	Orbit of a circular binary with a binary mass ratio $q = 0.5$	39
4.2	Location of a point (r, ϕ) relative to the primary and the secondary binary object.	40
4.3	An illustration of a disk (orange) around the primary (pink) centered in the origin. The secondary (blue) moves in a circle of radius a	42
4.4	Tidal potential of a uniform ring	46
7.1	An example of a potential that can trap modes in area between r_1 and r_2	57
8.1	The density profile for a disk with a central cavity.	66
8.2	Potentials in units of the binary precession frequency as a function of radius in unites of binary separation. Quadrupole eccentricity potential (orange) for $q = 1$. Pressure eccentricity potential (cyan) for $h = 0.2$). Eccentricity potential for $q = 1$ and $h = 0.2$ (dotted black).	67

8.3	Eccentricity potentials and allowed frequencies (left) and dispersion relation maps (right) for $[q, h] = [0.9, 0.1]$ (upper panels) and $[q, h] = [0.9, 0.03]$ (lower panels).	69
8.4	Lowest mode frequencies ω_0 in units of the binary orbital frequency Ω_b , as a function of the binary mass ratio q for $h = [0.01, 0.02, 0.05, 0.1, 0.2]$	70
8.5	WKB and numerical BVP frequencies of the lowest mode in units of the cavity quadrupole frequency as a function of the ratio of the cavity pressure and the cavity quadrupole frequency.	71
8.6	Eccentricity profiles $E(r)$ for $[q, h] = [0.9, 0.03]$	71
8.7	Eccentricity profiles (left) and scaled eccentricity profiles (right) for $\omega_P/\omega_Q = 0.05$ (upper panels) and $\omega_P/\omega_Q = 50$ (lower panels). The radius is scaled with the size of the cavity, and the eccentricity is scaled to $E = 1$ at the inner disk boundary.	72
9.1	CFR as a function of h and q	74
9.2	Left: The frequency of the lowest mode (ω_0) in units of the cavity quadrupole frequency (ω_Q), as a function of the cavity frequency ratio (ω_P/ω_Q) Right: eccentricity potential ($\omega_{\text{pot}}/\omega_Q$) in units of the cavity quadrupole frequency ($\omega_{\text{pot}}/\omega_Q$) as a function of radius in units of the binary separation (a). Eccentricity potentials corresponding to CFRs larger than the critical one are in blue, and those corresponding to CFRs lower than the critical one are in red. The critical CFR is in grey. Lowest mode frequencies (ω_0/ω_Q) are in thin dashed lines in the same colors as the corresponding eccentricity potentials.	75
9.3	Eccentricity potentials and potential contributions for an equal mass binary ($q = 1$) and five different values of the disks thickness h . All plot in units of binary precession frequency (Ω_b), and as a function of radius in units of the binary separation (r/a). Left: quadrupole eccentricity potential to eccentricity potential in dotted black, total eccentricity potential in solid lines. Right: quadrupole eccentricity potential in dotted black, pressure eccentricity potential in solid lines. In both plots, the cavity quadrupole frequency ω_Q is in a black dotted line for reference.	77

9.4	Left: the lowest mode frequency in units of the cavity pressure frequency, as a function of the CFR. Right: eccentricity potential in units of the cavity pressure frequency, as a function of radius in units of binary separation.	79
9.5	Eccentricity potentials in units of the binary precession frequency as a function of radius scaled with the binary separation (r/a) for $h = 2$ and $q = [10^{-6}, 10^{-4}, 10^{-2}]$. Left: pressure eccentricity potential (dotted black line) and total eccentricity potentials (solid lines). Right: pressure eccentricity potential (dotted black line) and quadrupole eccentricity potentials (solid lines).	80
9.6	ω_0 in units of Ω_b as a function of q for five different values of h (solid lines). Cavity quadrupole frequency (dotted black line).	81
9.7	Comparison of WKB and BVP frequencies as a function of CFR. Left: lowest mode frequency in units of the cavity quadrupole frequency. Right: lowest mode frequency in units of the cavity pressure frequency.	82
9.8	Numerical BVP ω_0 frequencies for $q = 0$ and $0.001 \leq h \leq 0.2$. Disk boundaries are $r_{\text{in}} = 1.875a$ and $r_{\text{out}} = 10^5a$. Left: ω_0 in units of the binary precession frequency, as a function of the disk's thickness. Right: ω_0 in units of the cavity pressure frequency, as a function of the disk's thickness.	84
9.9	Frequency dependence as a function of ω_P/ω_Q for eight values of the outer disk radius. Upper panel: frequencies in units of the quadrupole cavity frequency. For larger outer radii, frequencies are smaller, but they diverge to a cyan line for $r_{\text{out}} > 500a$. We see that $\omega_0/\omega_Q = 0.18$ behaviour stops for sufficiently large CFR. Lower panel: frequencies in units of the pressure cavity frequency. We plot the numerical BVP solution for $q = 0$ (equation 9.23) in a dashed black line. We see that this value is in agreement with numerical BVP solutions for $\omega_Q/\omega_P > 10^5$	86
9.10	Numerical BVP lowest mode frequency in units of the binary precession frequency, as a function of the binary mass ratio.	87
9.11	Dispersion relation maps.	88
9.12	Dispersion relation maps.	88

10.1	The highest possible mode order as a function of the binary mass ratio and the thickness of the disk (colored lines). Lines $n_{\max} = [5, 10, 20, 40, 80]$ is solid black lines for reference. The area where the WKB approximation gives correct ω_0 values is below the dotted black line. The cavity size of the disk is taken to be $R_{\text{cav}} = 2.5a$	93
10.2	Maximum number of possible modes as a function of binary mass ratio and the thickness of the disk for a disk with a cavity size $R_{\text{cav}} = 2.5a$ Same as figure (10.1), but in a linear scale.	94
10.3	Left panel: eccentricity potential (black) as a function of radius scaled with binary separation in units of the quadrupole frequency at the cavity radius. Frequencies of all possible modes ω_n (purple). Right panel: same as left, with five highlighted modes ($n \in [0, 1, 10, 20, 90]$).	97
10.4	Frequency dispersion maps for 0-th (purple), 1-st (orange), 10-th (red), 20-th (cyan), and 90-th (green) mode in a disk of thickness $h = 0.001$ around an equal mass binary ($q = 1$).	98
10.5	Absolute values of eccentricity profiles as functions of radius in units of the binary separation (a) for five modes in a thin disk ($h = 10^{-3}$) around an equal mass binary ($q = 1$). All five eccentricity profiles are scaled to $E = 1$ at the inner boundary. Upper left: eccentricity profiles of the 0-th mode (purple) and the 1-st mode (orange). Upper right: eccentricity profiles of the 10-th mode (red) and the 20-th mode (cyan). Lower panel: eccentricity profiles of the 90-th mode (green).	99
11.1	Radial density profiles of a disk with a cavity of size $R_{\text{cav}} = 2.5a$ and cavity slope $Z = 12$ for $L = [0, 0.5, 0.7, 0.9, 1]$	102
11.2	The lowest mode frequency in units of the cavity quadrupole frequency as a function of the CFR for $L = [0, 0.5, 0.7, 0.9, 1]$	103
11.3	Radial density profiles of a disk with $Z = 12$ and $L = 0.7$ for cavity sizes $R_{\text{cav}} = [1.5a, 4a, 6a, 10a]$	104
11.4	The lowest mode frequency in units of the cavity quadrupole frequency, as a function of the CFR. $L = 0.7$ and $r_{\text{out}} = 450a$. The disk cavity size is $R_{\text{cav}} = [1.5a, 4a, 6a, 10a]$, and the inner disk radius is taken to be $r_{\text{out}} = 0.8r_{\text{cav}}$	105
11.5	Radial density profiles of a disk with $R_{\text{cav}} = 2.5a$ and $L = 0.7$ for $Z = [4, 6, 12, 18]$	106
11.6	Caption	106

11.7	Comparison of WKB and numerical BVP frequencies ω_0 for each Z .	107
11.8	Frequency solutions ω_0/ω_Q as a function of the CFR. Comparison of results obtained using just the cutoff function (solid lines) and results obtained using the full density profile (dashed lines). . . .	108
11.9	Radial eccentricity profiles for $h = 1$ and $q = [0.1, 0.2, 0.4, 0.6, 1]$. Comparison of results obtained using just the cutoff function (solid lines) and results obtained using the full density profile (dashed lines).	109
11.10	Scaled eccentricity profiles (left panels) and eccentricity profiles (right panels) for $\omega_P/\omega_Q = 0.05$ (upper panels) and $\omega_P/\omega_Q = 50$ (lower panels). Comparison of results obtained using just the cutoff function (solid lines) and results obtained using the full density profile (dashed lines).	110
11.11	Density profiles of cut, extended and combined disks.	111
11.12	Pressure eccentricity potentials for a cut, extended, and a combined disk.	112
11.13	Total pressure eccentricity potential in pink. Each of the four terms contributing to this potential (equation (11.7)) in blue. . .	113
A.1	Polar coordinate system.	121

Part I

Introduction

In this thesis, we explore gas disks in binary systems. Specifically, we describe the evolution of such a disk through the evolution of its eccentricity.

Binary-disk systems

We first explain the importance of binary systems and disks and what part the eccentricity of the disk plays in the evolution of such systems.

A binary is a system of two objects that are gravitationally bound. Since all astrophysical objects interact gravitationally, binaries can range from asteroid binaries to supermassive black hole binaries. Some of them are well observed, such as star-planet binaries. Another example is stellar binaries; Tian *et al.* (2018) estimate that up to 80% of 0.15 million observed dwarf stars form a binary system. The existence of solar mass black hole binaries was confirmed by their merger; LIGO (Laser Interferometer Gravitational-Wave Observatory) detected gravitational waves radiated by such mergers (The LIGO Scientific Collaboration *et al.*, 2021). The existence of supermassive black hole binaries is not yet confirmed but will be tested by upcoming low-frequency GW experiments such as LISA (Laser Interferometer Space Antenna)(e.g., Amaro-Seoane *et al.*, 2022) and PTA (Pulsar Time Arrays) (e.g., Arzoumanian *et al.*, 2020; Lommen, 2012).

Stars and planets are formed out of gas in gas rich environments, so we expect gas to be present around them and to influence the dynamics of the system. One example is a planet embedded in a disk around a star; the planet can grow in mass (because it accretes gas from the disk), and can migrate inwards (because of angular momentum lost to friction between the planet and the disk) (Duffell *et al.*, 2020a). In general, an accreting disk can change binary parameters, such as binary eccentricity, binary mass ratio, or binary separation (Bogdanovic *et al.*, 2021). Since observational properties of the binary depend on its orbital properties, the detectability of a binary is influenced by the disk. The binary can also change the eccentricity and precession frequency of the accretion disk (D’Orazio *et al.*, 2016). Since the eccentricity evolution of the disk depends on binary parameters, observations of the disk can provide information on the binary. In addition, black holes can be observed in the EM spectrum only if they are accreting gas, and the EM signal properties depend on the disk orbital parameters (D’Orazio *et al.*, 2013).

Disks around massive black hole binaries (MBHBs) are interesting because they could provide a way for a MBHB merger to be detected in two different ways.

First, a space based gravitational wave detector LISA (Laser Interferometer Space Antenna) should be able to detect gravitational waves with frequencies in range of MBHB merges ($10^{-4} - 10^{-6}$ Hz) ((w.g., Amaro-Seoane *et al.*, 2017; Klein *et al.*, 2016). Furthermore, those mergers could be observed in the electromagnetic spectrum as well (Bogdanovic *et al.*, 2021). However, the possibility of those mergers is under question and is known as the final parsec problem. Gravitation radiation can cause MBHB merger on timescales shorter than the Hubble time, but only if the black holes are separated by less than roughly one-tenth of a parsec. Dynamical friction between the MBH and the stars surrounding them can only explain how the binary separation gets down to a few parsecs (Begelman *et al.*, 1980). A process that might make it possible for the binary separation to go from a few parsecs down to less than a parsec is an angular momentum transfer involving a circumbinary disk and circumsingle disks around each black hole (e.g., MacFadyen and Milosavljević, 2008; Cuadra *et al.*, 2009). Another problem is the value of the Hubble constant; there is a disagreement between the values of the Hubble constant obtained in two different indirect ways (Perivolaropoulos and Skara, 2022). The detection of electromagnetic waves and gravitational waves from the same source is a direct way of calculating the Hubble constant (Bogdanovic *et al.*, 2021). As we mentioned, a good candidate for an accreting MBHB.

Ways to approach the problem.

In this thesis, we use hydrodynamic equations to derive an equation that determines the evolution of the disk eccentricity, and we use analytical and semi-analytical methods to solve that equation. We now briefly explain the motivation for choosing this approach.

There are two main categories of approaches one can choose to use to further the understanding of a binary-disk system; numerical simulations and analytical formulations of the problem. For example, works such as D’Orazio *et al.* (2016) and D’Orazio and Duffell (2021) use numerical simulations to show that the disk influences the evolution of the binary and vice versa.

The main motivation is to understand binary-disk systems intuitively. Simulations provide results on how a disk will behave in given conditions, but they do

not provide us with an explanation as to why the disk behaves that way. Therefore, to gain physical insight, we turn to an analytic approach. The basis for an analytical approach to the eccentricity problem was laid out by Goodchild and Ogilvie (2006) and expanded by, among many others, Teyssandier and Ogilvie (2016). They formulated eccentricity equations for accretion disks, showing the physical processes behind the disk's evolution. This formulation of the disk eccentricity problem is used because it applies to a wide range of binary disk systems; both adiabatic (Goodchild and Ogilvie, 2006) and locally isothermal disks (Muñoz and Lithwick, 2020); on both circumsingle (Goodchild and Ogilvie, 2006) and circumbinary disks (Teyssandier and Ogilvie, 2016); on both steady disks (Muñoz and Lithwick, 2020) and disks that did not yet reach a steady state (Goodchild and Ogilvie, 2006); on both both 2d and 3d disks (Teyssandier and Ogilvie, 2016).

Another motivating factor is our wish to compare the behavior of disks with a great variety of different settings so we need to solve multiple different eccentricity problem settings efficiently. Currently, the usage of numerical simulations of accretion disks is limited because the method is time-consuming, making it hard to explore many different subsets of possible physical parameters. In comparison, using a trustworthy analytical approach makes it possible to quickly consider a virtually arbitrarily large subset of any parameter or even all of them.

There is another limit imposed on numerical simulations we wish to find a way around; the span of physical parameters. So far, only relatively thick disks have been explored utilizing numerical simulations. Simulations of thin disks require higher resolution and can result in loss of stability in employed the numerical methods (Tiede *et al.*, 2020).

To summarize, if we can describe the physics of accretion disks for disk settings used in numerical simulations and results from both approaches are consistent, then we are in a position to apply the same analytical approach to disks in ranges that numerical simulations did not tackle yet.

Layout of the thesis.

First, in chapter (1), we show how the orbit of a precessing body can be described using eccentricity. In chapter (2), we derive in detail the eccentricity equation for a 2d adiabatic disk. Next, in chapter (3), we show how to use a straightforward procedure and results for adiabatic 2d disk to derive the eccentricity equation for a 2d locally isothermal disk. We also write results for 3d disks. Then, in chapter (4), we explain how to adapt the eccentricity equation for disks in different locations; Within and outside the orbit of the binary. After that, in chapter (5), we list some of the known mechanisms that cause damping or excitation of the eccentricity and explain how to include these effects in the eccentricity equation. In chapter (6), we derive boundary conditions for eccentricity equations. Finally, in chapter (7.1), we define a stationary eccentricity solutions and show how to write a stationary eccentricity solution in the form of a Schrödinger equation.

In essence, part II provides a cookbook for writing the eccentricity equation for any combination of the disk type, forcing effects, and the disk's location. Once this is done, we are ready to choose a disk setting and solve the eccentricity equation.

In part III, we focus on stationary eccentricity solutions for a locally isothermal circumbinary disk.

In chapter (8), we analyze the work done by Muñoz and Lithwick (2020) for several reasons. First, we use it as an example of how the prescription from part II is used to formulate the eccentricity problem. In part II, we show how to write the eccentricity problem, but we do not show any methods for solving it. Therefore, we use Muñoz and Lithwick (2020) analysis to learn a numerical method of solving the boundary value problem and to learn a semi-analytical method of finding solutions to Schrödinger equation. We then reproduce solutions from Muñoz and Lithwick (2020) to verify that our understanding of the methods is correct, and to gain an insight of what the solutions mean.

To analyze a locally isothermal circumbinary disk in more detail, we focus our attention to areas unexplored by that paper (Muñoz and Lithwick, 2020). In chapter (9), we look for eccentricity solution for thinner disks and for disks

around binaries whose components have vastly different masses. In chapter (10), we look for the number of possible solutions of the eccentricity problem, and find how that number depends on the parameters of the disk and the binary. In chapter (11), we show how solutions of the eccentricity problem depend on the density distribution within the disk.

Part II

Eccentricity equations

Eccentricity as a way of describing the orbit

1.1 Binary orbit

We are interested in systems consisting of a binary and a disk. A binary is a system of two gravitationally bound objects. The more massive binary object is called the primary, its mass is M_p , and its position is \vec{r}_p . The less massive binary object is called the secondary, its mass is M_s , and its position is \vec{r}_s . In the absence of outer forces acting on the binary, the binary motion is co-planar (the motion of both bodies is in the same plane at all times), and we can describe it with a 2d coordinate system. We choose the polar coordinate system (Appendix A). We put the binary center of mass in the origin so that:

$$M_p \vec{r}_p + M_s \vec{r}_s = \vec{0}. \quad (1.1)$$

From equation (1.1), it follows that the angle between the position of the primary and the secondary is always π :

$$\angle(\vec{r}_p, \vec{r}_s) = \pi. \quad (1.2)$$

In general, both the primary and the secondary move in ellipses of eccentricity e . We choose the reference direction (for which $\phi = 0$) as the direction of the maximum distance of the primary from the origin. If the semi-major axis of the primary is a_p , its orbit is:

$$r_p(\phi) = \frac{a_p (1 - e^2)}{1 - e \cos \phi}. \quad (1.3)$$

If the semi-major axis of the secondary is a_s , its orbit is:

$$r_s(\phi) = \frac{a_s (1 - e^2)}{1 - e \cos(\phi + \pi)}. \quad (1.4)$$

We define the binary mass ratio as:

$$q \equiv \frac{M_s}{M_p}, \quad (1.5)$$

which is always in range:

$$0 \leq q \leq 1. \quad (1.6)$$

Equations (1.1) and (1.5) allow us to write the ratio of primary and secondary semi-major axis as:

$$\frac{a_p}{a_s} = \frac{M_s}{M_p} = q. \quad (1.7)$$

We define binary separation as a :

$$a \equiv a_p + a_s, \quad (1.8)$$

which is the mean value of the maximum and minimum separation of the primary and the secondary. Total mass of the binary is:

$$M \equiv M_p + M_s. \quad (1.9)$$

The orbital frequency of both the primary and the secondary around the origin (binary orbital frequency) is:

$$\Omega_b = \frac{GM}{a^3}. \quad (1.10)$$

Binary orbit for $q = 0.5$ and $e = 0.75$ is illustrated in figure (1.1).

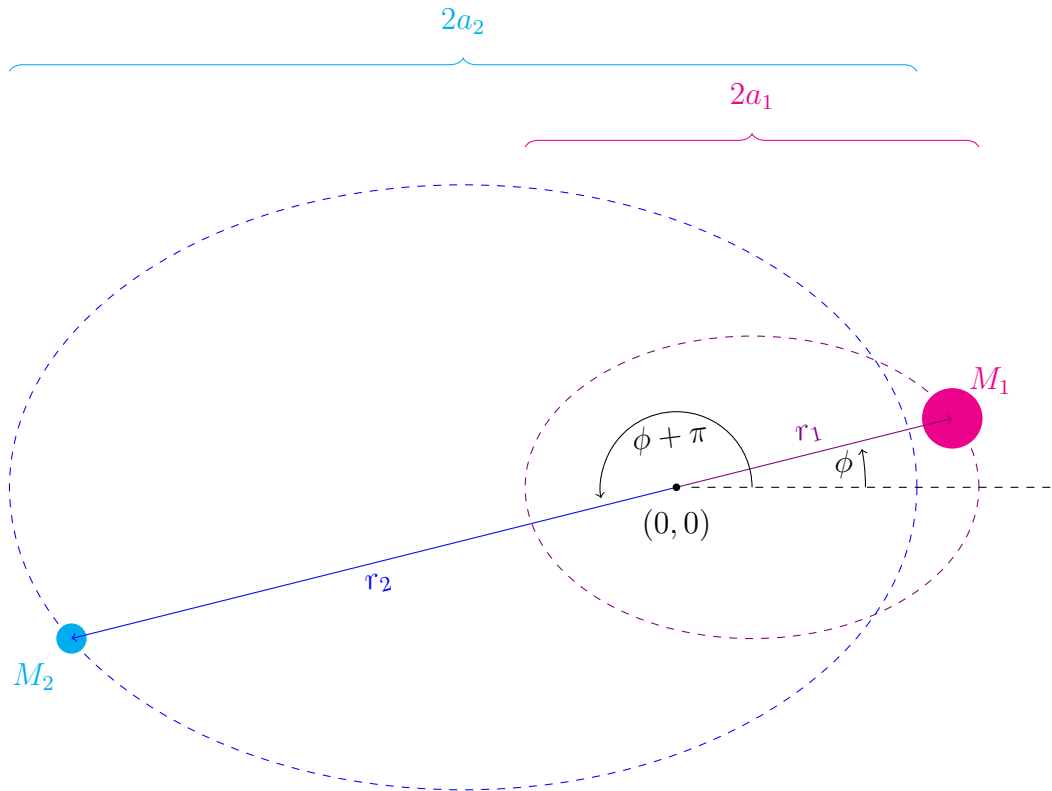


Figure 1.1.: Orbits of the primary (pink) and the secondary (blue) binary component. The center of mass is fixed in the origin. The primary and the secondary revolve the center of mass in similar ellipses of eccentricity $e = 0.75$. The binary mass ratio is $q = 0.5$, so the semi-major axis of the secondary is twice the size of the semi-major axis of the primary (equation (1.7)). The angle between the position of the primary and the secondary is always 180° , so the elliptical orbit of the secondary is rotated by 180° with respect to the orbit of the primary.

1.2 A disk around a binary

A gaseous disk can interact with the binary. Depending on the location of such a disk, we can distinguish between two types of disks; circumbinary disks and circumsingle disks. A circumbinary disk orbits both the primary and the secondary object. A circumsingle disk is a disk orbiting only one of the binary objects. If the circumsingle disk orbits the primary object, it is called a circumprimary disk. If the circumsingle disk orbits the secondary object, it is called a circumsecondary disk. A binary-disk system can contain any combination of these three disks. We assume that the midplane of the disk lies in the same plane as the binary at all times and we can use the coordinate system as illustrated in figure (1.1) to model the binary-disk system. A simple

visualisation of a system with a binary and all three disks types is drawn in figure 1.2.

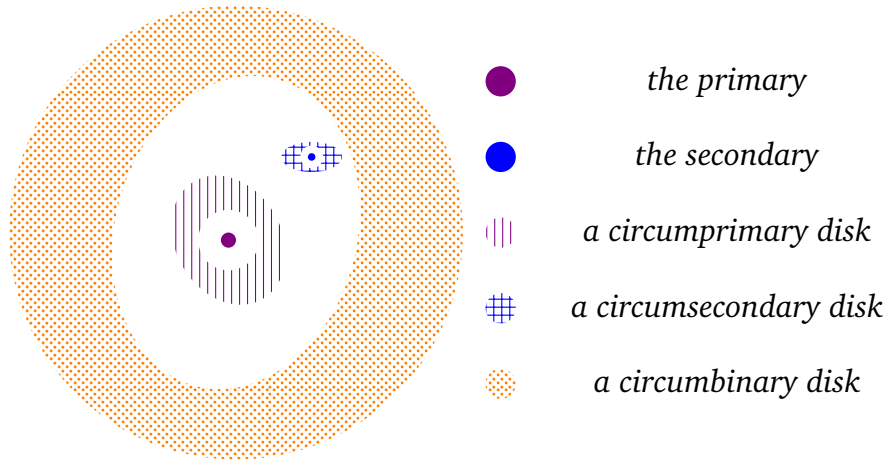


Figure 1.2.: Three types of disks based on their location; a circumprimary disk is centered at the location of the primary; a circumsecondary disk is centered at the location of the secondary; a circumbinary disk is centered at the binary center of mass.

The pressure of the disk is $p(r, \phi, t)$, its density is $\Sigma(r, \phi, t)$. The gravitational potential is $\Phi(r, \phi, t)$. The radial velocity of a disk fluid element is $u(r, \phi, t)$, its angular velocity is $v(r, \phi, t)$, so the total velocity vector of a disk fluid element is:

$$\vec{V} = u\hat{r} + v\hat{\phi}. \quad (1.11)$$

1.3 Disk evolution as a function of eccentricity

The orbit of each fluid element of a gaseous disk can be written in a way similar to equations (1.3) and (1.4). Meaning, its orbit $r_D(\phi, t)$ could be expressed in terms of semi-major axis a_D , eccentricity e_D , and the angle of the orbit pericenter α_D :

$$r_D(\phi) = \frac{a_D (1 - e_D^2)}{1 - e_D \cos(\phi - \alpha_D)}. \quad (1.12)$$

However, unlike a point mass primary/secondary, the disk is spread out over a range of radii. Moreover, the disk is influenced by forces other than the central gravity force, such as non-central gravity or viscous and pressure forces.

This means that, in general, all orbit parameters such as eccentricity e_D vary within the disk. Therefore, the disk can be divided into ellipses of infinitesimal width, each of which has a different eccentricity, orientation, and angular frequency. In this part, we derive an equation that describes the radial and time dependence of the eccentricity within the disk. From now on, we call that equation the eccentricity equation.

In chapter (2), we derive the eccentricity equation for a 2d adiabatic disk whose behavior is governed by only two forces; the force caused by the pressure gradient within the disk and the force caused by the gravitation potential of the binary. We ignore self-gravity, viscosity, and any other possible mechanisms of eccentricity damping and eccentricity forcing. Then, in chapter (3), we show how to modify the eccentricity equation for a 2d isothermal disk and 3d disks. Next, in chapter (4), we discuss the gravitational potential of the binary and how this affects the eccentricity equations for a circumbinary and a circumsingle disk. After that, in chapter (5), we list eccentricity damping and eccentricity forcing possibilities and explain how to add those terms to the eccentricity equation. Finally, in chapter (6), we derive boundary conditions for the eccentricity equation.

Unforced eccentricity equation for a 2d adiabatic disk

In order to find the unforced eccentricity equation for 2d adiabatic disks, we use the procedure described in Goodchild and Ogilvie (2006). We can sum up the procedure as:

- In section (2.1), we use the mass continuity equation, Newton's second law of motion, and the adiabatic gas equation of state to find a system of four equations that describe the disk.
- Next, in section (2.2), we define an unperturbed state. We find what equations from section (2.1) look like for the unperturbed state.
- In section (2.3), we define a new order parameter $\epsilon < 1$, and use it to expand the unperturbed state in a power series:

$$X_{\text{unp}} = \sum_k \epsilon^k X_{\text{unp},k}.$$

We then find what the two lowest expansion terms' equations from section (2.2) look like.

- In section (2.4), we introduce perturbations in such way that the total value of each quantity X can be written as:

$$X = X_{\text{unp}} + X_{\text{perturbation}}.$$

The form of those perturbations is:

$$X_{\text{perturbation}} = X' e^{-i\phi}.$$

We then find what the perturbed state's equations from section (2.1) look like.

- In section (2.5) we expand the perturbed state in terms of ϵ , just like we did with the unperturbed state:

$$X' = \sum_k \epsilon^k X'_k.$$

This allows us to define the eccentricity function in terms of perturbed quantities. Finally, we solve this chapter's full set of equations to find an eccentricity equation that depends only on the disk's unperturbed state values.

2.1 Disk governing equations

2.1.1 The continuity equation

The continuity equation shows how a quantity y and its flux \vec{Y} are influenced by the generation of that quantity σ_y :

$$\frac{\partial y}{\partial t} + \vec{\nabla} \cdot \vec{Y} = \sigma_y. \quad (2.1)$$

We can use the continuity equation for density:

$$y = \rho, \quad (2.2)$$

with a density flux:

$$\vec{Y} = \rho \vec{v}. \quad (2.3)$$

Since the total mass is conserved, the density generation function is:

$$\sigma_\rho = 0, \quad (2.4)$$

so the density continuity equation is:

$$\frac{\partial \rho}{\partial t} + \vec{\nabla} \cdot (\rho \vec{v}) = 0. \quad (2.5)$$

We rewrite equation(2.5) using the product rule:

$$\frac{\partial \rho}{\partial t} + \vec{v} \cdot (\vec{\nabla} \rho) + \rho (\vec{\nabla} \cdot \vec{v}) = 0. \quad (2.6)$$

Now we use equations (1.11), (A.9) and (A.10) to write equation (2.6) as:

$$\frac{\partial \rho}{\partial t} + [u \hat{r} + v \hat{\phi}] \left[\frac{\partial \rho}{\partial r} \hat{r} + \frac{1}{r} \frac{\partial \rho}{\partial \phi} \hat{\phi} \right] + \rho \left[\frac{1}{r} \frac{\partial}{\partial r} (ru) + \frac{1}{r} \frac{\partial v}{\partial \phi} \right] = 0. \quad (2.7)$$

We now use equation (A.8) to write:

$$\frac{\partial \rho}{\partial t} + u \frac{\partial \rho}{\partial r} + \frac{v}{r} \frac{\partial \rho}{\partial \phi} = -\frac{\rho}{r} \left[\frac{\partial}{\partial r} (ru) + \frac{\partial v}{\partial \phi} \right], \quad (2.8)$$

which is a mass conservation equation in polar coordinates.

2.1.2 Equations of motion

Newton's second law of motion shows how the momentum of a body of mass m changes when it is influenced by force \vec{F} :

$$m \frac{d\vec{v}}{dt} = \vec{F}. \quad (2.9)$$

We write mass in terms of volume V and density ρ :

$$m = V\rho, \quad (2.10)$$

and define force volume density as:

$$\vec{f} \equiv \frac{\vec{F}}{V}, \quad (2.11)$$

to write equation (2.9) as:

$$\rho \frac{d\vec{v}}{dt} = \vec{f}. \quad (2.12)$$

We consider two forces; gravity and the force caused by the pressure gradient in the disk:

$$\vec{f} = -\vec{\nabla}p - \rho\vec{\nabla}\Phi. \quad (2.13)$$

If we write the Lagrangian time derivative as:

$$\frac{d}{dt} = \frac{\partial}{\partial t} + (\vec{v} \cdot \vec{\nabla}), \quad (2.14)$$

the motion equation in vector form becomes:

$$\rho \left[\frac{\partial \vec{v}}{\partial t} + (\vec{v} \cdot \vec{\nabla})\vec{v} \right] = -\vec{\nabla}p - \rho\vec{\nabla}\phi. \quad (2.15)$$

Equation (2.15) is the momentum vector continuity equation, its radial component is:

$$\frac{\partial u}{\partial t} + u \frac{\partial u}{\partial r} + \frac{v}{r} \frac{\partial u}{\partial \phi} - \frac{v^2}{r} = -\frac{1}{\rho} \frac{\partial p}{\partial r} - \frac{\partial \Phi}{\partial r}, \quad (2.16)$$

and its azimuthal component is:

$$\frac{\partial v}{\partial t} + u \frac{\partial v}{\partial r} + \frac{v}{r} \frac{\partial v}{\partial \phi} + \frac{uv}{r} = -\frac{1}{\rho r} \frac{\partial p}{\partial \phi} - \frac{1}{r} \frac{\partial \Phi}{\partial \phi}. \quad (2.17)$$

Equation (2.16) is the radial momentum continuity equation. If there were no radial forces, the total radial momentum of a fluid element would be conserved. Similarly, equation (2.17) is the angular momentum continuity equation. If there were no radial forces, the total angular momentum of a fluid element would be conserved.

2.1.3 Adiabatic equation of state

A thermodynamic equation of state says that thermodynamic parameters of a fluid (pressure p , volume V , and temperature T) are not all mutually independent: Its general form is:

$$f(p, V, T, n) = 0. \quad (2.18)$$

The general equation of state for an ideal gas is:

$$pV - nRT = 0. \quad (2.19)$$

For an ideal gas undergoing an adiabatic or isothermal process, the equation of state is barotropic, meaning the pressure is a function of density only:

$$p = p(\rho). \quad (2.20)$$

The equation of state for an ideal adiabatic gas is:

$$p = K\rho^\gamma. \quad (2.21)$$

Constant γ is called the adiabatic index, its value depends mostly on the gas composition, but it also a function of temperature. Here, we assume that there is no temperature dependence and that γ is a function of disk composition only. K is a constant throughout the process, and its value depends on the system in question. It can be determined if at any point in time, we know the pressure, density and the adiabatic constant. We do not know the value of K , but we can use a trick to write a gas equation that does not include K . First, we use equation (2.14) to write:

$$\frac{d\rho}{dt} = -\rho(\vec{\nabla} \cdot \vec{v}). \quad (2.22)$$

Next, we use equations (2.21) and (2.22) to write the time derivative of pressure as:

$$\frac{dp}{dt} = \frac{dp}{d\rho} \frac{d\rho}{dt} = K\rho^{\gamma-1}\gamma(-\rho)(\vec{\nabla} \cdot \vec{v}) = -\gamma p \vec{\nabla} \cdot \vec{v} = -\frac{\gamma p}{r} \left[\frac{\partial(ru)}{\partial r} + \frac{\partial v}{\partial \phi} \right]. \quad (2.23)$$

We then use 2.14 to write the time derivative of pressure in another form:

$$\frac{dp}{dt} = \frac{\partial p}{\partial t} + (\vec{v} \cdot \vec{\nabla})p = \frac{\partial p}{\partial t} + u \frac{\partial p}{\partial r} + \frac{v}{r} \frac{\partial p}{\partial \phi}. \quad (2.24)$$

Finally, we compare equations (2.23) and (2.24), to write:

$$\frac{\partial p}{\partial t} + u \frac{\partial p}{\partial r} + \frac{v}{r} \frac{\partial p}{\partial \phi} = -\frac{\gamma p}{r} \left[\frac{\partial(ru)}{\partial r} + \frac{\partial v}{\partial \phi} \right]. \quad (2.25)$$

Equation (2.25) is a continuity equation for pressure in polar coordinates and shows how the velocity of a fluid can generate pressure.

2.1.4 Disk equations

To sum this section up, we found four equations for the density, radial velocity, angular velocity, and the pressure of a disk fluid element.

Four equations in polar coordinates that determine the behaviour of a 2d adiabatic disk

$$\frac{\partial \rho}{\partial t} + u \frac{\partial \rho}{\partial r} + \frac{v}{r} \frac{\partial \rho}{\partial \phi} = -\frac{\rho}{r} \left[\frac{\partial}{\partial r}(ru) + \frac{\partial v}{\partial \phi} \right] \quad (2.26a)$$

$$\frac{\partial u}{\partial t} + u \frac{\partial u}{\partial r} + \frac{v}{r} \frac{\partial u}{\partial \phi} - \frac{v^2}{r} = -\frac{1}{\rho} \frac{\partial p}{\partial r} - \frac{\partial \Phi}{\partial r} \quad (2.26b)$$

$$\frac{\partial v}{\partial t} + u \frac{\partial v}{\partial r} + \frac{v}{r} \frac{\partial v}{\partial \phi} + \frac{uv}{r} = -\frac{1}{\rho r} \frac{\partial p}{\partial \phi} - \frac{1}{r} \frac{\partial \Phi}{\partial \phi} \quad (2.26c)$$

$$\frac{\partial p}{\partial t} + u \frac{\partial p}{\partial r} + \frac{v}{r} \frac{\partial p}{\partial \phi} = -\frac{\gamma p}{r} \left[\frac{\partial(ru)}{\partial r} + \frac{\partial v}{\partial \phi} \right] \quad (2.26d)$$

Because an ellipse is a perturbed circle, we want to write the orbit of the disk in terms of a perfectly circular orbit (unperturbed state) and a perturbation to that orbit.

2.2 Unperturbed state of the disk

Since we want an unperturbed state to describe a circular orbit, we define it as the state of a disk that satisfies five conditions. The first condition says that the Eulerian time derivative is zero:

$$\frac{\partial}{\partial t} = 0. \quad (2.27)$$

Solutions that do not explicitly depend on time are called steady state solutions, and equation (2.27) is called the steady-state condition. The second condition is axial symmetry:

$$\frac{\partial}{\partial \phi} = 0, \quad (2.28)$$

the third condition is the lack of radial motion:

$$u = 0. \quad (2.29)$$

and the fourth condition is that there is no vertical motion. For a non-self gravitating disk, this leads to (Appendix F):

$$p_{\text{unp}} \propto \rho_{\text{unp}}(H/r)^2, \quad (2.30)$$

where H is the disk's characteristic thickness.

We now apply steady basic state conditions on equations (2.26). The only non-trivial equation is equation (2.26b) and it reduces to:

$$-\frac{v_{\text{unp}}^2}{r} = -\frac{1}{\rho_{\text{unp}}} \frac{\partial p_{\text{unp}}}{\partial r} - \frac{\partial \Phi_{\text{unp}}}{\partial r}. \quad (2.31)$$

To sum up, in this section we learned that the unperturbed state of the disk can be described with a single equation.

Unperturbed state of a 2d adiabatic disk.

$$-\frac{v_{\text{unp}}^2}{r} = -\frac{1}{\rho_{\text{unp}}} \frac{\partial p_{\text{unp}}}{\partial r} - \frac{\partial \Phi_{\text{unp}}}{\partial r} \quad (2.32)$$

Equation (2.32) simply states that if there are two radial forces acting on a fluid element, and if the fluid element is in a steady state, then the sum of those two forces has to be balanced out by the centripetal force.

2.3 Series expansion of the unperturbed state

Functions $u(r, \phi, t)$, $v(r, \phi, t)$, $\rho(r, \phi, t)$, $\Phi(r, \phi, t)$, and $p(r, \phi, t)$ are unknown functions of radius. We expand those functions in a series and approximate them with their lowest two non-zero terms. Before we can do that, we need to choose an appropriate order parameter ϵ . Since we already found that $p \propto \rho(H/r)^2$, and for a thin disk we have $H/r < 1$, a good choice is:

$$\epsilon \equiv H/r. \quad (2.33)$$

For $X = u, v, \rho, p, \Phi, p$, we write:

$$X_{\text{unp}} = \sum_{k \geq 0} \epsilon^k X_{\text{unp},k}. \quad (2.34)$$

There is no a priori reason for the disk to be asymmetric with respect to $z = 0$, so we write:

$$X(-H) = X(H). \quad (2.35)$$

For equation (2.35) to be true, in expansion (2.34) all odd powers of ϵ have to be zero so:

$$X_{\text{unp}} = \sum_{k \geq 0, \text{even}} \epsilon^k X_{\text{unp},k}. \quad (2.36)$$

In Appendix C we find lowest two nonvanishing terms of expansion for all quantities. Those are:

$$\begin{aligned} v_{\text{unp}} &= v_0 + v_2 \epsilon^2 \\ \rho_{\text{unp}} &= \rho_0 + \rho_2 \epsilon^2 \\ \Phi_{\text{unp}} &= \Phi_0 + \Phi_2 \epsilon^2 \\ p_{\text{unp}} &= p_2 \epsilon^2 + p_4 \epsilon^4. \end{aligned} \quad (2.37)$$

Now we put (Appendix C) equations (2.37) in the unperturbed state equation that we have obtained (equation (2.32)):

$$-\frac{v_0^2 + 2v_0 v_2 \epsilon^2}{r} = \frac{-1}{\rho_0} \frac{\partial p_2 \epsilon^2}{\partial r} + \frac{\partial(\Phi_0 + \epsilon^2 \Phi_2)}{\partial r}. \quad (2.38)$$

We can define two new functions as:

$$\Omega_0 \equiv \frac{v_0}{r}, \quad (2.39)$$

and

$$\Omega_2 \equiv \frac{v_2}{r}. \quad (2.40)$$

This allows us to write the lowest order (ϵ^0) of equation (8.10) as:

$$r\Omega_0^2 = \frac{\partial\Phi_0}{\partial r}, \quad (2.41)$$

and the next order (ϵ^2) of equation (8.10) as:

$$2r\Omega_0\Omega_2 = \frac{\partial\Phi_2}{\partial r} + \frac{1}{\rho_0} \frac{\partial p_2}{\partial r}. \quad (2.42)$$

Two lowest order equation for the unperturbed state of a 2d adiabatic disk

$$r\Omega_0^2 = \frac{\partial\Phi_0}{\partial r} \quad (2.43a)$$

$$2r\Omega_0\Omega_2 = \frac{\partial\Phi_2}{\partial r} + \frac{1}{\rho_0} \frac{\partial p_2}{\partial r} \quad (2.43b)$$

Equation (2.43a) says that in lowest approximation, the motion of the fluid is the motion of a particle in a gravitational field of point mass. Equation (2.43b) says that a non point binary mass distribution and the pressure of the disk change the angular velocity of the fluid element. In any case, the total motion of the disk fluid particle is angular, and higher orders of the unperturbed state expansion just change the magnitude of the angular velocity.

The definition of angular velocity

We should keep in mind that with Ω_0 defined as (2.39), and Ω_2 defined as (2.40):

$$\Omega_{\text{unp}} \neq \Omega_0 + \epsilon^2\Omega_2 = \frac{v_0^2}{r} + \epsilon^2 \frac{v_2^2}{r}. \quad (2.44)$$

To see this, we write:

$$\begin{aligned}\Omega_{\text{unp}} &= \frac{v^2}{r} = \frac{(v_0 + \epsilon^2 v_2)^2}{r} = \frac{v_0^2 + 2\epsilon^2 v_0 v_2 + \epsilon^4 v_2^2}{r} \\ &= r\Omega_0 + 2r\Omega_0\Omega_2\epsilon^2.\end{aligned}\tag{2.45}$$

However, if we were to define Ω_{00} as:

$$\Omega_{00} \equiv \frac{v_0^2}{r},\tag{2.46}$$

and Ω_{22} as:

$$\Omega_{22} \equiv \frac{2v_0 v_2}{r},\tag{2.47}$$

we could write:

$$r\Omega_{00}^2 = \frac{\partial\Phi_0}{\partial r},\tag{2.48}$$

$$r\Omega_{22} = \frac{\partial\Phi_2}{\partial r} + \frac{1}{\rho_0} \frac{\partial p_2}{\partial r},\tag{2.49}$$

and:

$$\Omega_{\text{unp}} = \Omega_{00} + \epsilon^2\Omega_{22}.\tag{2.50}$$

2.4 Disk in a perturbed state

We introduce perturbations to the unperturbed state. In analogy to the binary eccentric orbit, we allow disk perturbations to have both radial and angular dependency. The perturbation need to satisfy:

$$X_{\text{perturbation}}(r, \phi = 0) = X_{\text{perturbation}}(r, \phi = 2\pi),\tag{2.51}$$

so we can write it as a fourier series of a function that is periodic in ϕ with a period $P = 2\pi$:

$$X_{\text{perturbation}} = \sum f_n(r)e^{in\phi}\tag{2.52}$$

Term $n = 0$ results in a radially symmetric movement. Term $n = 1$ results in a motion with two angular turning points. Terms $n \geq 2$ result in n angular turning points. Since we are looking for a solution that is similar to an ellipse, the only term we can work with is $n = 1$. We rename the radial part as:

$$f_1(r) = X'(r),\tag{2.53}$$

to write the perturbation as:

$$X_{\text{perturbation}} = X'(r)e^{-i\phi}. \quad (2.54)$$

The total state of every quantity X is then:

$$X = X_{\text{unp}} + X_{\text{perturbation}} = X_{\text{unp}} + X'e^{-i\phi}. \quad (2.55)$$

So, the total velocity, pressure and density can be written as:

$$u = u_{\text{unp}} + u'e^{-i\phi} = 0 + u'e^{-i\phi} = u'e^{-i\phi}, \quad (2.56)$$

$$v = v_{\text{unp}} + v'e^{-i\phi}, \quad (2.57)$$

$$p = p_{\text{unp}} + p'e^{-i\phi}, \quad (2.58)$$

and

$$\rho = \rho_{\text{unp}} + \rho'e^{-i\phi} \quad (2.59)$$

where unperturbed values are given in the previous section. We use equations (2.56), (2.57), (2.58), (2.59), and equations 2.26 to get equations for perturbed values. We keep (Appendix D) only the lowest two orders of those expressions:

Equations for perturbed quantities of a 2d adiabatic disk

$$\frac{\partial u'}{\partial t} - iu'\Omega_{\text{unp}} + 2\Omega_{\text{unp}}v' = -\frac{1}{\rho_{\text{unp}}}\frac{\partial p'}{\partial r} + \frac{\rho'}{\rho_{\text{unp}}^2}\frac{\partial p_{\text{unp}}}{\partial r} \quad (2.60a)$$

$$\frac{\partial v'}{\partial t} - iv'\Omega_{\text{unp}} + \frac{u'}{r}\frac{\partial}{\partial r}(r^2\Omega_{\text{unp}}) = \frac{ip'}{r\rho_{\text{unp}}} \quad (2.60b)$$

$$\frac{\partial \rho'}{\partial t} - i\rho'\Omega_{\text{unp}} + u'\frac{\partial \rho_{\text{unp}}}{\partial r} = -\frac{\rho_{\text{unp}}}{r}\left[\frac{\partial(ru')}{\partial r} - iv'\right] \quad (2.60c)$$

$$\frac{\partial p'}{\partial t} - ip'\Omega_{\text{unp}} + u'\frac{\partial p_{\text{unp}}}{\partial r} = -\frac{\gamma p_{\text{unp}}}{r}\left[\frac{\partial(ru')}{\partial r} - iv'\right] \quad (2.60d)$$

2.5 Series expansion of the perturbed state

A result that will be useful in further derivations is:

$$\frac{\partial}{\partial r} (r^2 \Omega_0) = \frac{\partial}{\partial r} (r^2 \sqrt{GM} r^{-3/2}) \frac{1}{2} \sqrt{GM} r^{-1/2} = \frac{1}{2} r \Omega_0. \quad (2.61)$$

We expand every perturbation X' in a series just like we did with the unperturbed state:

$$X' = X'_0 + X'_2 \epsilon^2. \quad (2.62)$$

Now we find lowest two orders of equations (2.60a)-(2.60d). To do that, we need an estimate of the magnitude of $\partial/\partial t$. We take it to be of the order ϵ^2 . Lowest (ϵ^0) order of equation (2.60a) is:

$$-i \frac{v_0 v'_0}{r} - 2 \frac{v_0 v'_0}{r} = 0 \quad (2.63)$$

Lowest (ϵ^0) order of equation (2.60b) is:

$$-i \frac{v_0 v'_0}{r} - \frac{1}{2} \frac{v_0 u'_0}{r} = 0 \quad (2.64)$$

Both of these equations lead to a proportionality of radial and angular velocity perturbations:

$$u'_0 = i \frac{1}{2} v'_0. \quad (2.65)$$

The radial velocity of a fluid element is:

$$u \approx u_{\text{unp}} + \text{Re}(u'_0 e^{-i\phi}) = \text{Re}(u'_0 e^{-i\phi}). \quad (2.66)$$

The angular velocity of a fluid element is:

$$\begin{aligned} v &\approx v_{\text{unp}} + \text{Re}(v'_0 e^{-i\phi}) = \Omega_0 r + \frac{1}{2\Omega_0} \left[\frac{\partial \Phi_2}{\partial r} + \frac{1}{\rho_0} \frac{\partial p_2}{\partial r} \right] - \text{Re}(2iu'_0 e^{-i\phi}) \\ &= \Omega_0 r \left[1 + \frac{1}{2\Omega_0} \left[\frac{\partial \Phi_2}{\partial r} + \frac{1}{\rho_0} \frac{\partial p_2}{\partial r} \right] + \text{Re}\left(\frac{2iu'_0}{\Omega_0 r} e^{-i\phi}\right) \right], \end{aligned} \quad (2.67)$$

so the ratio of the two is:

$$\frac{u}{v} = \frac{\text{Re}(u'_0 e^{-i\phi})}{\Omega_0 r \left[1 + \frac{1}{2\Omega_0} \left[\frac{\partial \Phi_2}{\partial r} + \frac{1}{\rho_0} \frac{\partial p_2}{\partial r} \right] + \text{Re}\left(\frac{2iu'_0}{\Omega_0 r} e^{-i\phi}\right) \right]}. \quad (2.68)$$

For an ellipse:

$$r_D(\phi) = \frac{a_D (1 - e_D^2)}{1 - e_D \cos(\phi - \alpha_D)}, \quad (2.69)$$

we can write:

$$\frac{dr}{dt} = \frac{dr}{d\phi} \frac{d\phi}{dt}, \quad (2.70)$$

so:

$$\begin{aligned} \frac{u}{v} &= \frac{dr}{d\phi} = \frac{a_D (1 - e_D^2)}{(1 - e_D \cos(\phi - \alpha_D))^2} \sin(\phi - \alpha_D) \\ &\approx \frac{dr}{d\phi} = \frac{a_D \sin(\phi - \alpha_D)}{1 - 2e_D \cos(\phi - \alpha_D)}. \end{aligned} \quad (2.71)$$

Comparing equations (2.68) and (2.71), we can see that we can define the eccentricity of a fluid element as:

$$e_D \equiv \frac{-iu'_0}{\Omega_0 r}. \quad (2.72)$$

We call a function that describes the disk eccentricity at any location and at any time the eccentricity equation $E(r, t)$. To find that function, we use all perturbed and unperturbed equations, and eliminate all perturbed quantities except for perturbed velocity. Then we replace velocity with eccentricity (equation (2.72)) (Appendix D). Finally, we get an eccentricity equation:

Unforced eccentricity equation for a 2d adiabatic disk

$$2r\Omega \frac{\partial E}{\partial t} = -\frac{iE}{r} \frac{\partial}{\partial r} \left(r^2 \frac{\partial \Phi_2}{\partial r} \right) + \frac{iE}{\rho} \frac{\partial p}{\partial r} + \frac{i}{r^2 \rho} \frac{\partial}{\partial r} \left[\gamma p r^3 \frac{\partial E}{\partial r} \right], \quad (2.73)$$

where all unsubscribed values are the lowest order unperturbed values, meaning

$$\begin{aligned} \Omega &= \Omega_0, \\ p &= p_2 \\ \rho &= \rho_0. \end{aligned} \quad (2.74)$$

Unforced eccentricity equations for other disks

3.1 A locally isothermal 2D disk

The procedure of deriving the eccentricity equation for a locally isothermal disk is identical to that of an adiabatic disk. So instead of carefully calculating every step, we just show what adjustments have to be made to relevant equations from Part II, Chapter 2. We then use those modified equations to derive the eccentricity equation. The isothermal equation of state is:

$$p = \rho c_s^2, \quad (3.1)$$

where c_s is sound speed.

Since, unlike with adiabatic equation, there is no unknown constant that we need to find a way to get rid of, we just plug equation (3.1) into equations (2.26a), (2.26b) and (2.26c):

Three equations that determine the behaviour of a locally isothermal disk

$$\frac{\partial \rho}{\partial t} + u \frac{\partial \rho}{\partial r} + \frac{v}{r} \frac{\partial \rho}{\partial \phi} = -\frac{\rho}{r} \left[\frac{\partial}{\partial r} (ru) + \frac{\partial v}{\partial \phi} \right] \quad (3.2a)$$

$$\frac{\partial u}{\partial t} + u \frac{\partial u}{\partial r} + \frac{v}{r} \frac{\partial u}{\partial \phi} - \frac{v^2}{r} = -\frac{1}{\rho} \frac{\partial (\rho c_s^2)}{\partial r} - \frac{\partial \Phi}{\partial r} \quad (3.2b)$$

$$\frac{\partial v}{\partial t} + u \frac{\partial v}{\partial r} + \frac{v}{r} \frac{\partial v}{\partial \phi} + \frac{uv}{r} = -\frac{1}{\rho r} \frac{\partial (\rho c_s^2)}{\partial \phi} - \frac{1}{r} \frac{\partial \Phi}{\partial \phi} \quad (3.2c)$$

Unperturbed state conditions (equations (2.27)) reduce the above set of equation to a single one:

Unperturbed state of a 2d locally isothermal disk

$$-\frac{v_{\text{unp}}^2}{r} = -\frac{1}{\rho_{\text{unp}}} \frac{\partial(\rho_{\text{unp}} c_s^2)}{\partial r} - \frac{\partial\Phi_{\text{unp}}}{\partial r} \quad (3.3)$$

We know (vertical hydrostatic equilibrium) that:

$$p = c_s^2 \rho, \quad (3.4)$$

and that $c_s^2 \propto H/r$ so the only part of the pressure that we can perturb is the density:

$$p' = c_s^2 \rho'. \quad (3.5)$$

Using the same procedure we used for for the adiabatic disk, we get:

Equations for the perturbed state of a 2d locally isothermal disk

$$\begin{aligned} \frac{\partial u'}{\partial t} - iu'\Omega + 2\Omega v' &= -\frac{1}{\rho_{\text{unp}}} \frac{\partial(c_s^2 \rho')}{\partial r} + \frac{\rho'}{\rho_{\text{unp}}^2} \frac{\partial(c_s^2 \rho_{\text{unp}})}{\partial r} \\ &= -c_s^2 \frac{\partial}{\partial r} \left(\frac{\rho'}{\rho} \right) \end{aligned} \quad (3.6a)$$

$$\frac{\partial v'}{\partial t} - iv'\Omega + \frac{u'}{r} \frac{\partial}{\partial r} (r^2 \Omega) = \frac{ic_s^2 \rho'}{r \rho_{\text{unp}}} \quad (3.6b)$$

$$\frac{\partial \rho'}{\partial t} - i\rho'\Omega + u' \frac{\partial \rho_{\text{unp}}}{\partial r} = -\frac{\rho_{\text{unp}}}{r} \left[\frac{\partial(ru')}{\partial r} - iv' \right] \quad (3.6c)$$

Just like for a 2d adiabatic disk, the lowest order of equations for perturbed quantities ((ϵ^0) order of equation (3.6a) and (3.6b)) gives:

$$u'_0 = 2iv'_0. \quad (3.7)$$

We define eccentricity $E(r, \phi, t)$ of a 2d isothermal disk in the same way we did for the adiabatic one:

$$\begin{aligned} u'_0 &= ir\Omega_0 E, \\ v'_0 &= \frac{1}{2}r\Omega_0 E. \end{aligned} \quad (3.8)$$

Applying a procedure similar top the one for the adiabatic disk (Appendix E), we get the eccentricity equation for a 2d isothermal disk:

$$\begin{aligned}
 2r^2 \rho_0 \Omega_0 \frac{\partial E}{\partial t} = & -i\rho E \frac{\partial}{\partial r} \left[r^2 \frac{\partial \Phi_2}{\partial r} \right] + \frac{i}{r} \frac{\partial}{\partial r} \left(\rho c_s^2 r^3 \frac{\partial E}{\partial r} \right) + irE \frac{\partial(\rho_0 c_s^2)}{\partial r} \\
 & - \frac{i}{r} \frac{\partial}{\partial r} \left(\rho_0 E r^3 \frac{\partial c_s^2}{\partial r} \right).
 \end{aligned}
 \tag{3.9}$$

3.2 Comparison of eccentricity equations for 2d adiabatic and 2d isothermal disks

In this section, we point out the differences between eccentricity equations for adiabatic and isothermal disks. First, we compare gas equations of state. The equation of state for adiabatic gas is:

$$p = K\rho^\gamma, \tag{3.10}$$

and the equation of state for isothermal gas is:

$$p = c_s^2 \rho. \tag{3.11}$$

From this we see that we can use adiabatic equation of state to get isothermal equation of state by making a change $K \rightarrow c_s^2$, and $\gamma \rightarrow 1$. We can see that the two eccentricity equations ((2.73) and (3.1)) are similar. Here, we show that it is not possible to use any of the two equations to get the other by simply interchanging $c_s^2 \rho \leftrightarrow p$.

If we were to use adiabatic equation and set $\gamma = 1$ and $K = c_s^2$, we would be missing a term $-\frac{i}{r} \frac{\partial}{\partial r} \left(\rho E r^3 \frac{\partial c_s^2}{\partial r} \right)$. The reason for this is that in the derivation of the adiabatic equation, from the start we assumed that K is a constant and the information on it's radial derivative is lost.

If, on the other hand, we tried to use isothermal equation and use ($c_s^2 \rho \rightarrow p$) along with ($c_s^2(r) \rightarrow K$) \Rightarrow ($\partial c_s^2 / \partial r \rightarrow 0$), we would not get adiabatic eccentricity equation either. Specifically, the first pressure term would be

reduced by a factor of γ ; i.e. $\frac{i}{r} \frac{\partial}{\partial r} \left(pr^3 \frac{\partial E}{\partial r} \right)$ instead of $\frac{i}{r} \frac{\partial}{\partial r} \left(\gamma pr^3 \frac{\partial E}{\partial r} \right)$. The reason for this is that the γp factor appears as a result of calculating $\frac{dp}{d\rho} \rho$ (as seen in equation (2.23)), which in the case of an isothermal disk is:

$$\frac{dp}{d\rho} \rho = \frac{d(c_s^2 \rho)}{d\rho} \rho = c_s^2 \rho = p, \quad (3.12)$$

whereas for adiabatic disk, the result is:

$$\frac{dp}{d\rho} \rho = \frac{d(K\rho^\gamma)}{d\rho} \rho = \gamma p. \quad (3.13)$$

3.3 3D disks

The method of deriving elementary eccentricity equations for 3d disks (Teyssandier and Ogilvie, 2016) is identical to the one used for 2d cases. Here, we just list final eccentricity equations.

Unforced eccentricity equation for a 3d adiabatic disk

$$2r\Omega \frac{\partial E}{\partial t} = \frac{i}{r} \frac{\partial}{\partial r} \left[\left(2 - \frac{1}{\gamma} \right) pr^3 \frac{\partial E}{\partial r} \right] + i \left(4 - \frac{3}{\gamma} \right) r \frac{dp}{dr} E + 3ipE \left(1 + \frac{1}{\gamma} \right) \quad (3.14)$$

Unforced eccentricity equation for a 3d locally isothermal disk

$$2r^2 \rho \Omega \frac{\partial E}{\partial t} = -i\rho E \frac{\partial}{\partial r} \left[r^2 \frac{\partial \Phi_2}{\partial r} \right] + \frac{i}{r} \frac{\partial}{\partial r} \left(\rho c_s^2 r^3 \frac{\partial E}{\partial r} \right) + irE \frac{\partial(\rho c_s^2)}{\partial r} - \frac{i}{r} \frac{\partial}{\partial r} \left(\rho E r^3 \frac{\partial c_s^2}{\partial r} \right) + \frac{3i\rho E}{r} (c_s^2 r^2) \quad (3.15)$$

The eccentricity equation for a 3d adiabatic disk, compared to the 2d adiabatic disk equation, has one additional term and different coefficients connected to the adiabatic index. Likewise, the eccentricity equation for a 3d isothermal disk has one extra term compared to the 2d equation. Those are the result of allowing vertical variations of quantities.

Works such as Ogilvie (2008) and Teyssandier and Ogilvie (2016) discuss 3d disks. These show that 2d and 3d approximations can lead to different results. However, the exact importance of this choice is not clear. Results from Teyssandier and Ogilvie (2016) show that the eccentricity profile differs for 2d and 3d disks. This difference is significant for adiabatic disks but not as large for isothermal disks. Another result shows that in both adiabatic and isothermal disks, the choice of the dimension can make a difference between prograde and retrograde modes. Nevertheless, even that possibility depends on many parameters, including the mode order. From the examples discussed there, it is clear that there are many contributing factors in determining how significant the difference between 2d and 3d disks will be. Works such as Ogilvie (2008) even show that sometimes only a 3d disk can trap modes. However, that analysis was done for a disk around a single star. It is unclear if we can apply any of those solutions to our systems.

Gravitational potential

Now that we have derived the eccentricity equation for adiabatic and locally isothermal disks, we can see that both equations include a second-order contribution to gravitational potential Φ_2 . The contribution of higher order gravitational potential to total disk eccentricity can be described as:

$$2r^2\rho\Omega\frac{\partial E}{\partial t}\Bigg|_{\text{grav}} = -i\rho E\frac{\partial}{\partial r}\left[r^2\frac{\partial\Phi_2}{\partial r}\right]. \quad (4.1)$$

In this section, we derive a form of equation (4.1) that is easier to use. To do so, we first remind ourselves of the assumptions we have made before that allow us to restrict how we model second-order gravitational potential in two ways. We wrote unperturbed gravitational potential as:

$$\Phi = \Phi_0 + \epsilon^2\Phi_2, \quad (4.2)$$

and one of the unperturbed state requirements was:

$$\frac{\partial\Phi}{\partial\phi} = \frac{\partial\Phi_0}{\partial\phi} = \epsilon^2\frac{\partial\Phi_2}{\partial\phi} = 0. \quad (4.3)$$

To be consistent, our potential model must not depend on the angular coordinate.

4.1 Circular binary.

A circular binary is a binary whose both components (the primary and the secondary) move in circles. We use equations (1.3) and (1.4), and $e = 0$ to find the radius of their orbit around their center of mass:

$$r_p = a_p = \text{const}, \quad (4.4)$$

and:

$$r_s = a_s = \text{const.} \quad (4.5)$$

Their separation is constant:

$$|\vec{r}_s - \vec{r}_p| = a_p + a_s = a. \quad (4.6)$$

We use equation (1.7) and (1.8) to write:

$$a_p = \frac{aM_s}{M_p + M_s}, \quad (4.7)$$

and:

$$a_s = \frac{aM_p}{M_p + M_s}. \quad (4.8)$$

In figure (4.1), we illustrate the binary orbit. A fluid element at position (r, ϕ) will feel a gravitational potential that depends on the distance from the primary d_p , and the distance from the secondary d_s :

$$\Phi(r, \phi) = -\frac{GM_p}{d_p} - \frac{GM_s}{d_s}. \quad (4.9)$$

We can use the law of cosines to write:

$$d_{p,s}^2 = a_{p,s}^2 + r^2 - 2ra_{p,s} \cos(\phi - \phi_{p,s}), \quad (4.10)$$

and:

$$\Phi(r, \phi) = \frac{-GM_p}{\sqrt{a_p^2 + r^2 - 2ra_p \cos(\phi - \phi_p)}} + \frac{-GM_s}{\sqrt{a_s^2 + r^2 - 2ra_s \cos(\phi_s - \phi)}}. \quad (4.11)$$

In figure (4.2), we illustrate the relative positions of the primary, the secondary and the disk fluid element. Equation (4.11) shows that the potential depends on the angular coordinate, which is at odds with equation (4.3). To find the potential independent on ϕ , we find the mean value of the potential (4.11) at distance r :

$$\Phi(r) \equiv \frac{1}{2\pi} \int_0^{2\pi} \left[\frac{-GM_p}{\sqrt{a_p^2 + r^2 - 2ra_p \cos(\phi - \phi_p)}} + \frac{-GM_s}{\sqrt{a_s^2 + r^2 - 2ra_s \cos(\phi_s - \phi)}} \right] d\phi \quad (4.12)$$

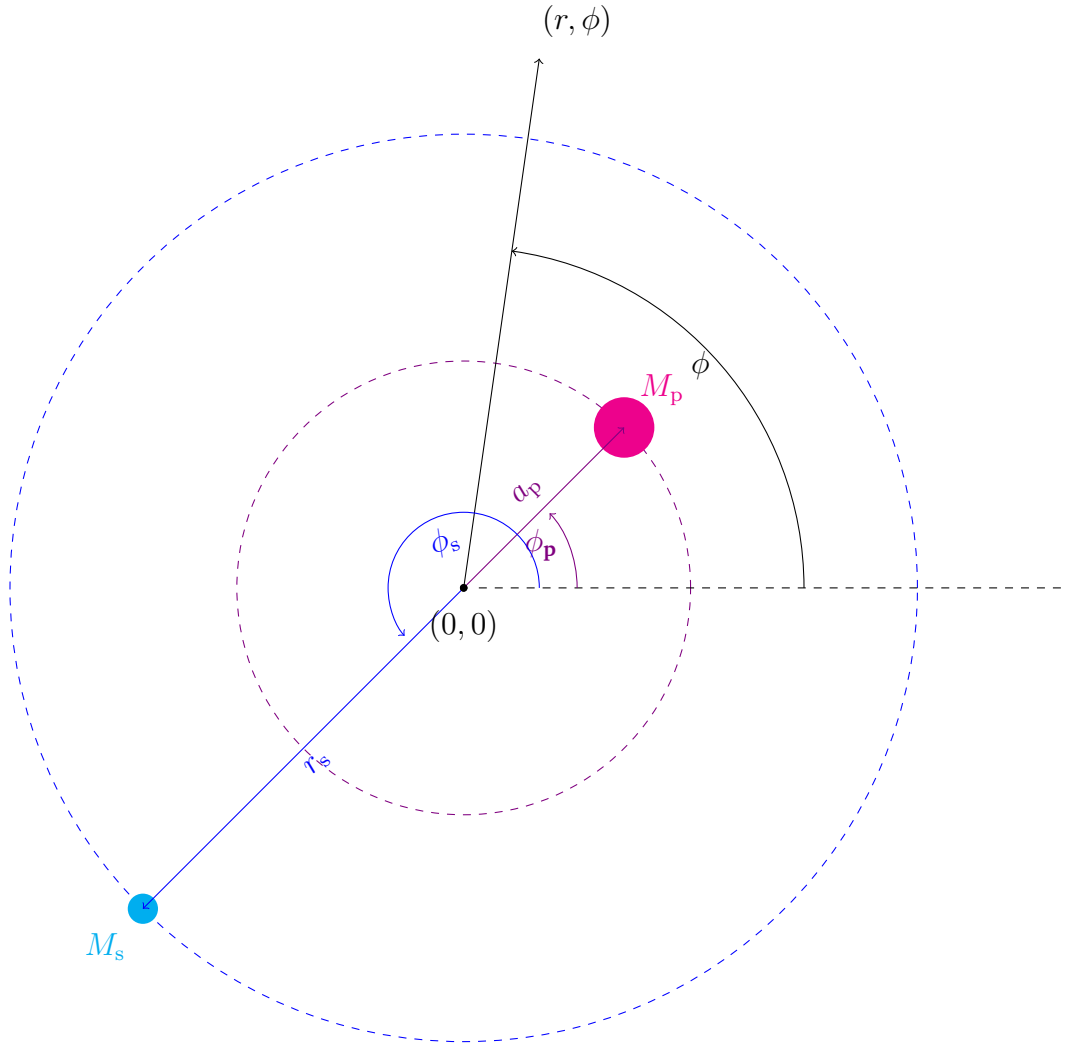


Figure 4.1.: Orbit of a circular binary with a binary mass ratio $q = 0.5$.

The initial angles of the primary and the secondary are irrelevant for integration over the entire range $\phi \in [0, 2\pi]$:

$$\Phi(r) \equiv \frac{1}{2\pi} \int_0^{2\pi} \left[\frac{-GM_p}{\sqrt{a_p^2 + r^2 - 2ra_p \cos(\phi)}} + \frac{GM_s}{\sqrt{a_s^2 + r^2 - 2ra_s \cos(\phi)}} \right] d\phi. \quad (4.13)$$

We use Lagandre expansion to write the subintegral function as:

$$\frac{1}{\sqrt{a_{p,s}^2 + r^2 - 2ra_{p,s} \cos(\phi)}} \approx \frac{1}{r_{>,p,s}} \left[1 + \cos \phi \frac{r_{<,p,s}}{r_{>,p,s}} + \frac{1}{2} \frac{r_{<,p,s}^2}{r_{>,p,s}^2} (3 \cos^2 \phi - 1) \right], \quad (4.14)$$

where:

$$r_{>,p} = \max[r, a_p], \quad (4.15)$$

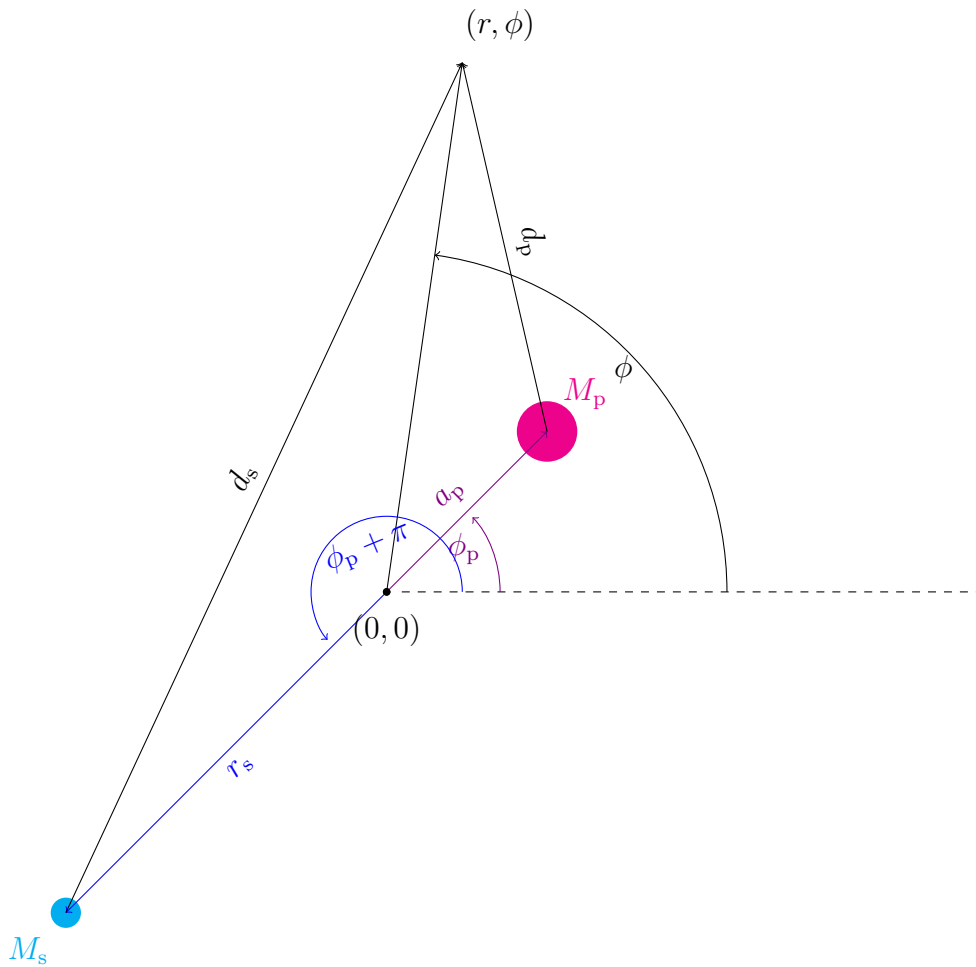


Figure 4.2.: Location of a point (r, ϕ) relative to the primary and the secondary binary object.

$$r_{>,s} = \max[r, a_s], \quad (4.16)$$

$$r_{<,p} = \min[r, a_p], \quad (4.17)$$

and

$$r_{<,s} = \min[r, a_s]. \quad (4.18)$$

We use:

$$\begin{aligned} \int_0^{2\pi} d\tau &= 2\pi, \\ \int_0^{2\pi} \cos \tau d\tau &= 0, \\ \int_0^{2\pi} \cos^2 \tau d\tau &= \pi, \end{aligned} \quad (4.19)$$

to write:

Averaged gravitational potential of a circular secondary

$$\Phi_s(r) = -\frac{GM_s}{2\pi} \frac{1}{r_{>,s}} \left[2\pi + \frac{1}{2} \frac{r_{<,s}^2}{r_{>,s}^2} (3\pi - 2\pi) \right] = -GM_s \frac{1}{r_{>,s}} \left[1 + \frac{1}{4} \frac{r_{<,s}^2}{r_{>,s}^2} \right], \quad (4.20)$$

and:

Average gravitational potential of a circular primary

$$\Phi_p(r) = -\frac{GM_p}{2\pi} \frac{1}{r_{>,p}} \left[2\pi + \frac{1}{2} \frac{r_{<,p}^2}{r_{>,p}^2} (3\pi - 2\pi) \right] = -GM_p \frac{1}{r_{>,p}} \left[1 + \frac{1}{4} \frac{r_{<,p}^2}{r_{>,p}^2} \right]. \quad (4.21)$$

4.1.1 A circumprimary disk and a small binary mass ratio

If $q \ll 1$, the center of mass is approximately the same as the center of mass of the primary so the primary is fixed in the origin, and the secondary revolves around it with a radius a :

$$\frac{a_p}{a_s} = q \ll 1 \rightarrow a_p \approx 0 \quad (4.22)$$

$$a_p + a_s = a \rightarrow a_s \approx a.$$

$$\Phi_s(r) = -\frac{GM_s}{a} \left[1 + \frac{1}{4} \frac{r^2}{a^2} \right], \quad (4.23)$$

and:

$$\Phi_p(r) = -\frac{GM_p}{r} \left[1 + \frac{1}{4} \frac{a_p^2}{r^2} \right] \approx -\frac{GM_p}{r}, \quad (4.24)$$

so the total potential is:

$$\Phi(r) = -\frac{GM_s}{a} \left[1 + \frac{1}{4} \frac{r^2}{a^2} \right] - \frac{GM_p}{r} = -\frac{GM_p}{r} - \frac{GM_s}{a} - \frac{1}{4} \frac{GM_s r^2}{a^2}, \quad (4.25)$$

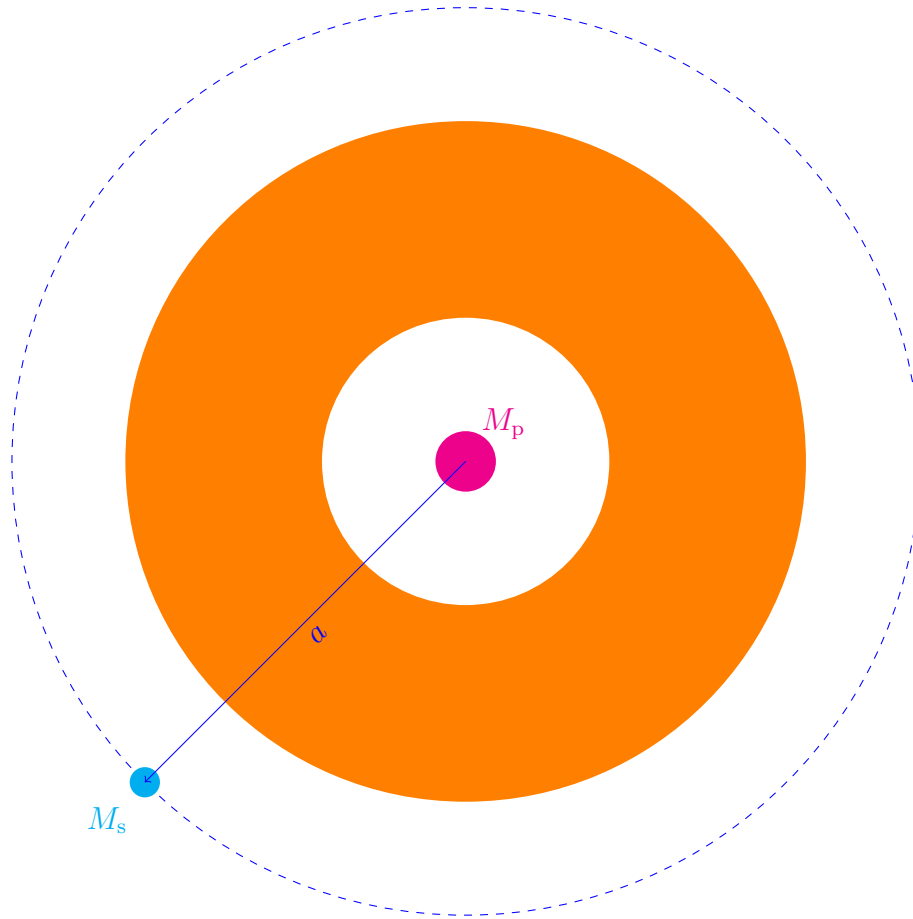


Figure 4.3.: An illustration of a disk (orange) around the primary (pink) centered in the origin. The secondary (blue) moves in a circle of radius a .

and we can identify the second order potential as:

$$\Phi_2(r) = -\frac{1}{4} \frac{GM_s r^2}{a^2}. \quad (4.26)$$

The eccentricity contribution of Φ_2 is then:

$$2r^2 \rho \Omega \left. \frac{\partial E}{\partial t} \right|_{\text{grav}} = -i\rho E \frac{\partial}{\partial r} \left[r^2 \frac{\partial \Phi_2}{\partial r} \right] = -i\rho E \frac{\partial}{\partial r} \left[r^2 \frac{2}{4} \frac{GM_s r}{a^3} \right] = -i\rho E \frac{3}{2} \frac{GM_s r^2}{a^3}. \quad (4.27)$$

We find:

$$GM_s = GM_s \frac{M_p r^3}{M_p r^3} = \frac{M_s}{M_p} \frac{GM_p}{r^3} r^3 = q\Omega_0 r^{-3}, \quad (4.28)$$

so that we can write equation (4.27) in terms of binary parameters:

The effect of second order gravitational potential on eccentricity of a circumpriary disk around a circular binary.

$$\left. \frac{\partial E}{\partial t} \right|_{\text{grav}} = i\Omega_0 E \frac{3qr^3}{4(1+q)^2 a^3}. \quad (4.29)$$

4.1.2 A circumbinary disk

A circumbinary disk surrounds both the primary and the secondary so we can write:

$$\begin{aligned} r_{>,p} &= r, \\ r_{>,s} &= r, \\ r_{<,p} &= a_p, \\ r_{<,s} &= a_s. \end{aligned} \quad (4.30)$$

We write equation (4.20) as:

$$\Phi_s(r) = -GM_s \frac{1}{r} \left[1 + \frac{1}{4} \frac{a_s^2}{r^2} \right], \quad (4.31)$$

and equation (4.21) as:

$$\Phi_p(r) = -GM_p \frac{1}{r} \left[1 + \frac{1}{4} \frac{a_p^2}{r^2} \right]. \quad (4.32)$$

The total gravitational potential is then:

$$\begin{aligned} \Phi(r) &= -GM_p \frac{1}{r} \left[1 + \frac{1}{4} \frac{a_p^2}{r^2} \right] - GM_s \frac{1}{r} \left[1 + \frac{1}{4} \frac{a_s^2}{r^2} \right] \\ &= -\frac{G}{r} \left[M_p + M_p \frac{1}{4} \frac{a_p^2}{r^2} + M_s + M_s \frac{1}{4} \frac{a_s^2}{r^2} \right] \\ &= -\frac{G(M_p + M_s)}{r} - \frac{G}{4r^3} [M_p a_p^2 + M_s a_s^2]. \end{aligned} \quad (4.33)$$

We use equations (4.7) and (4.8) to write the gravitational potential as:

$$\begin{aligned}
\Phi(r) &= -\frac{G(M_p + M_s)}{r} - \frac{G}{4r^3} \left[M_p \frac{a^2 M_s^2}{(M_p + M_s)^2} + M_2 \frac{a^2 M_p^2}{(M_p + M_s)^2} \right] \\
&= -\frac{G(M_p + M_s)}{r} - \frac{G}{4r^3} \left[M_p \frac{a^2 M_2^2 / M_p^2}{(1+q)^2 r^3} + M_2 \frac{a^2}{(1+q)^2} \right] \\
&= -\frac{G(M_p + M_s)}{r} - \frac{Ga^2}{4(1+q)^2 r^3} \left[\frac{M_s^2}{M_p} + M_2 \frac{M_p}{M_p} \right] \\
&= -\frac{G(M_p + M_s)}{r} - \frac{Ga^2}{4(1+q)^2} [M_s q + M_p q] \\
&= -\frac{G(M_p + M_s)}{r} - \frac{Ga^2 q (M_p + M_s)}{4(1+q)^2 r^3} \\
&= -\frac{GM}{r} - \frac{Ga^2 q M}{4(1+q)^2 r^3}.
\end{aligned} \tag{4.34}$$

Comparing equations (4.2) and (4.34), we see that we can write the first order gravitational potential as:

$$\Phi_0(r) = -\frac{GM}{r}, \tag{4.35}$$

and the second order potential as:

$$\Phi_2(r) = -\frac{Ga^2 q M}{4(1+q)^2 r^3}. \tag{4.36}$$

The lowest order orbital frequency is then:

$$\Omega_0 = \frac{1}{r} \frac{\partial \Phi_0(r)}{\partial r} = \frac{GM}{r^3}, \tag{4.37}$$

and the eccentricity contribution of the second order gravitational potential is:

$$\begin{aligned}
2r^2 \rho \Omega \frac{\partial E}{\partial t} \Big|_{\text{grav}} &= -i\rho E \frac{\partial}{\partial r} \left[r^2 \frac{\partial \Phi_2}{\partial r} \right] = -i\rho E \frac{\partial}{\partial r} \left[r^2 \frac{GM3qa^2}{4(1+q)^2 r^4} \right] \\
&= 2i\rho E \frac{GM3qa^2}{4(1+q)^2 r^3} = 2i\rho E \Omega^2 \frac{3qa^2}{4(1+q)^2},
\end{aligned} \tag{4.38}$$

or:

The effect of second order gravitational potential on eccentricity of a circumbinary disk around a circular binary.

$$\left. \frac{\partial E}{\partial t} \right|_{\text{grav}} = i\Omega E \frac{3qa^2}{4(1+q)^2 r^2}. \quad (4.39)$$

4.2 Gravitational potential in a thin ring approximation

The approach usually used to get the gravitational potential is to approximate the gravitational potential of a binary object with the gravitational potential of a thin uniform ring. This approximation is valid because a fluid element in the disk precesses with a frequency much smaller than the precession frequency of the binary element and the fluid element 'sees' the binary object as a ring of smeared mass. We show that this approach yields the same potential equation and write the gravitation potential in terms of Laplace coefficients. This setup is illustrated in figure (4.4). The gravitational potential at point (r, ϕ) caused by any mass distribution with total mass M_2 can be expressed as:

$$\Phi_{\text{p,s}}(r, \phi) = \int_0^{M_{\text{p,s}}} \frac{G}{l} dm. \quad (4.40)$$

In the case of a thin ring of uniform mass distribution, we can write the mass differential as:

$$dm = \lambda dC, \quad (4.41)$$

where C is the circumference of the ring and we can write it as:

$$dC = a d\phi_{\text{p,s}}. \quad (4.42)$$

We can use the law of cosines to write:

$$l^2 = a_{\text{p,s}}^2 + r^2 - 2ra_{\text{p,s}} \cos(\phi - \phi_{\text{p,s}}). \quad (4.43)$$

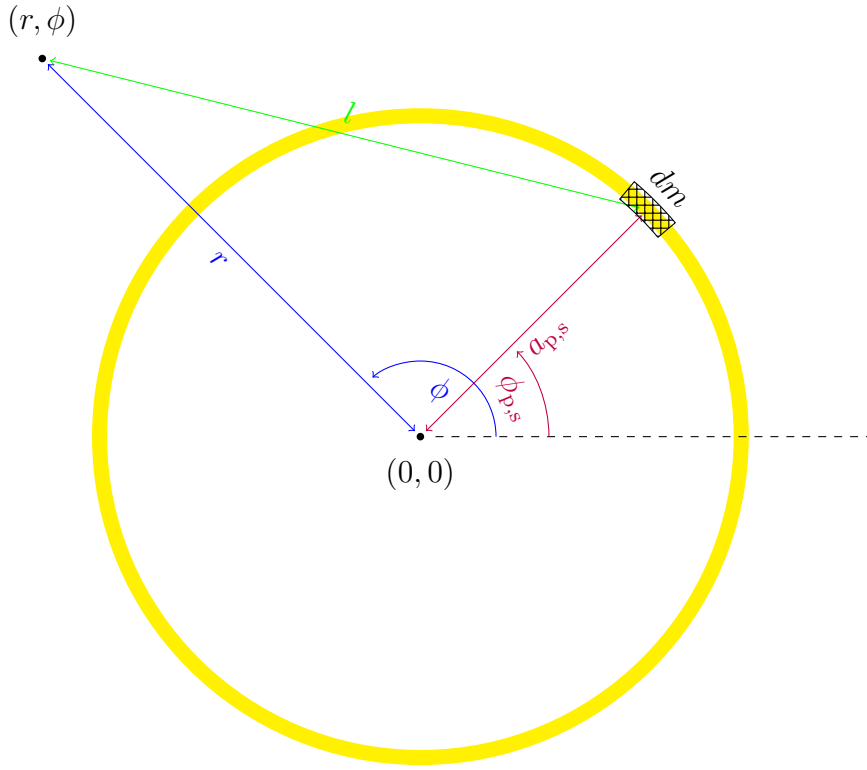


Figure 4.4.: Tidal potential of a uniform ring

Next, we can use equations (4.40), (4.41), (4.42) and (4.43) to write the gravitational potential of the secondary object as:

$$\begin{aligned}\Phi_{p,s}(r, \phi) &= - \int_0^{2\pi} \frac{GM_{p,s}}{2\pi \sqrt{a_{p,s}^2 + r^2 - 2ra_{p,s} \cos(\phi - \phi_{p,s})}} d\phi_{p,s} \\ &= - \int_0^{2\pi} \frac{GM_{p,s}}{2\pi \sqrt{a_{p,s}^2 + r^2 - 2ra_{p,s} \cos(\phi)}} d\phi.\end{aligned}\quad (4.44)$$

We now see that potential (4.44) is identical to what we found for a potential of a fixed points mass, averaged over all angles of the disk. Instead of expanding it to a series in terms of radius, this potential is often written in terms of Laplace coefficients that are defined as:

$$b_{s/2}^{(j)}(\alpha) = \frac{1}{\pi} \int_0^{2\pi} \frac{\cos(j\Psi)}{(1 + \alpha^2 - 2\alpha \cos \Psi)^{s/2}} d\Psi, \quad (4.45)$$

for $0 \leq \alpha \leq 1$. Comparing equations (4.44) and (4.45), we see that we need a Laplace coefficient with $j = 0$, $s = 0.5$.

A circumprimary disk

If the disk is located inside the orbit of the binary object, the appropriate choice for α is:

$$\alpha = \frac{r}{a}, \quad (4.46)$$

so the Laplace coefficient is:

$$b_{1/2}^{(0)}\left(\frac{r}{a_{p,s}}\right) = \frac{1}{\pi} \int_0^{2\pi} \frac{1}{\left(1 + \left(\frac{r}{a_{p,s}}\right)^2 - 2\frac{r}{a_{p,s}} \cos \Psi\right)^{1/2}} d\Psi. \quad (4.47)$$

We use equation (4.47) to write equation (4.44) as:

$$\Phi_{p,s}(r, \phi) = -\frac{GM_{p,s}}{2a_{p,s}} b_{1/2}^{(0)}\left(\frac{r}{a_{p,s}}\right). \quad (4.48)$$

The resulting eccentricity is:

$$\begin{aligned} 2r^2 \rho \Omega \frac{\partial E}{\partial t} \Big|_{\text{grav}} &= -i\rho E \frac{\partial}{\partial r} \left[r^2 \frac{\partial \Phi_2}{\partial r} \right] = -\rho i E \frac{\partial}{\partial r} \left(r^2 \frac{-GM_2}{2a} \frac{\partial}{\partial r} [b_{1/2}^{(0)}] \right) \\ &= \frac{iEGM_2\rho}{2a} \left[2r \frac{\partial b_{1/2}^{(0)}(\alpha)}{\partial r} + r^2 \frac{\partial^2 b_{1/2}^{(0)}(\alpha)}{\partial r^2} \right] \\ &= \frac{iEGM_2\rho}{2a} \left[2\alpha \frac{\partial b_{1/2}^{(0)}(\alpha)}{\partial \alpha} + \alpha^2 \frac{\partial^2 b_{1/2}^{(0)}(\alpha)}{\partial \alpha^2} \right]. \end{aligned} \quad (4.49)$$

We use a Laplace coefficient identity:

$$2\alpha \frac{\partial b_{1/2}^{(0)}(\alpha)}{\partial \alpha} + \alpha^2 \frac{\partial^2 b_{1/2}^{(0)}(\alpha)}{\partial \alpha^2} = \alpha b_{3/2}^{(1)}(\alpha), \quad (4.50)$$

to write equation (4.49) as:

Gravity induced eccentricity for a circumprimary disk in terms of Laplace coefficients

$$2r^2 \rho \Omega \frac{\partial E}{\partial t} \Big|_{\text{grav,p,s}} = \frac{iGM_{p,s}\rho Er}{2a_{p,s}^2} \left[b_{3/2}^{(1)}\left(\frac{r}{a_{p,s}}\right) \right]. \quad (4.51)$$

A circumbinary disk

If the disk is located outside the orbit of the binary object, the appropriate choice for α is:

$$\alpha = \frac{a}{r} \leq 1, \quad (4.52)$$

so the Laplace coefficient is:

$$b_{1/2}^{(0)}\left(\frac{a_{p,s}}{r}\right) = \frac{1}{\pi} \int_0^{2\pi} \frac{1}{(1 + (\frac{a_{p,s}}{r})^2 - 2\frac{a_{p,s}}{r} \cos \Psi)^{1/2}} d\Psi, \quad (4.53)$$

and the potential is:

$$\Phi_{p,s}(r, \phi) = -\frac{GM_{p,s}}{2r} b_{1/2}^{(0)}\left(\frac{p,s}{r}\right). \quad (4.54)$$

For:

$$\alpha \equiv \frac{a_{p,s}}{r}, \quad (4.55)$$

we write:

$$\frac{\partial}{\partial \alpha} = \frac{\partial}{\partial (a_{p,s}/r)} = -\frac{r^2}{a_{p,s}} \frac{\partial}{\partial r}. \quad (4.56)$$

We perform a calculation similar to one we did for circumsingle discs:

$$\begin{aligned} 2r^2 \rho \Omega \frac{\partial E}{\partial t} \Big|_{\text{grav}} &= -i\rho E \frac{-a}{r^2} \frac{\partial}{\partial \alpha} \left[r^2 \frac{-a}{r^2} \frac{\partial \Phi_2}{\partial \alpha} \right] \\ &= -i\rho E \frac{a}{r^2} \frac{\partial}{\partial \alpha} \left[a \frac{\partial}{\partial \alpha} \left(-\frac{GM_2}{2r} b_{1/2}^{(0)}\left(\frac{a}{r}\right) \right) \right] \\ &= -i\rho E \frac{aGM_2}{2r^2} \frac{\partial}{\partial \alpha} \left[\frac{\partial}{\partial \alpha} \left(\frac{a}{r} b_{1/2}^{(0)}(\alpha) \right) \right] \\ &= -i\rho E \frac{aGM_2}{2r^2} \frac{\partial}{\partial \alpha} \left[\frac{\partial}{\partial \alpha} \left(\alpha b_{1/2}^{(0)}(\alpha) \right) \right] \\ &= -i\rho E \frac{aGM_2}{2r^2} \frac{\partial}{\partial \alpha} \left[\frac{\partial b_{1/2}^{(0)}(\alpha)}{\partial \alpha} \alpha + b_{1/2}^{(0)}(\alpha) \right] \\ &= -i\rho E \frac{aGM_2}{2r^2} \left[\frac{\partial^2 b_{1/2}^{(0)}(\alpha)}{\partial \alpha^2} \alpha + \frac{\partial b_{1/2}^{(0)}(\alpha)}{\partial \alpha} + \frac{\partial b_{1/2}^{(0)}(\alpha)}{\partial \alpha} \right]. \end{aligned} \quad (4.57)$$

We apply the Laplace coefficient identity (equation (4.50)) to write:

Gravity induced eccentricity for a circumbinary disk in terms of Laplace coefficients

$$2r^2 \rho \Omega \left. \frac{\partial E}{\partial t} \right|_{\text{grav,p,s}} = \frac{iGM_{\text{p,s}} \rho E a_{\text{p,s}}}{2r^2} \left[b_{3/2}^{(1)} \left(\frac{a_{\text{p,s}}}{r} \right) \right]. \quad (4.58)$$

Equations (4.51) and (4.58) are a compact way to write gravitational eccentricity effects. However, using this form is impractical because the eccentricity equation (2.73), (3.9), (3.14), and (3.15) require us to be able to distinct two lowest orders of the gravitational potential.

Forcing effects

5.1 Eccentricity generation

We define an eccentricity generating function as:

$$\xi = \frac{\partial E}{\partial t} \frac{1}{E}. \quad (5.1)$$

Eccentricity can be generated by orbital resonances. An orbit of a disk ellipse with orbital frequency Ω and apsidal precession Ω_{aps} will experience a resonance if there are two positive integers of k and j for which:

$$k(\Omega - \Omega_{\text{aps}}) = j(\Omega - \Omega_{\text{b}}). \quad (5.2)$$

The axis of a closed (periodic) orbit does not change direction (does not precess) so for period motion, we write:

$$\Omega_{\text{aps}} = 0. \quad (5.3)$$

We can define a new quantity $m \equiv j - k$, and write equation (5.2) in another form:

$$\Omega_{j,k} = \Omega_{\text{b}} \frac{j}{j-k} \Omega_{\text{b}} m, \quad (5.4)$$

to see that the resonance occurs if the frequency of the disk ellipse is a multiple of the binary frequency. These resonances are called $j : m$ Lindblad resonances. Location of these resonances is given by:

$$r_{\text{res}} = a(1+q)^{-1/3} \left(\frac{j-k}{j} \right)^{2/3}, \quad (5.5)$$

so the eccentricity forcing due to $\xi_{j,k}$ will be:

$$\left(\frac{\partial E}{\partial t} \right) \Big|_{\text{Lin}} = E \xi_{j,k} \delta(r - r_{\text{res}}). \quad (5.6)$$

A resonance for $k = 1$ is called co-rotational resonance because it is a resonance at a place where the disk ellipse has the same angular frequency as the binary:

$$\Omega_{j,0} = \Omega_b. \quad (5.7)$$

5.2 Eccentricity damping

We discuss viscosity as a way of causing forcing effects. Shear viscosity does not result in eccentricity forcing, as shown by Ogilvie (2001), but the bulk viscosity does. We quickly show how. The force on a fluid element caused by the bulk viscosity is:

$$f_{b,\nu} = \vec{\nabla}T, \quad (5.8)$$

where the function T is defined as:

$$T = \frac{\alpha_b p}{r\Omega} \left[\frac{\partial(ru)}{\partial r} + \frac{\partial v}{\partial \phi} \right]. \quad (5.9)$$

The change of eccentricity function caused by the bulk viscosity is:

$$\left(\frac{\partial E}{\partial t} \right) \Big|_{b,\nu} = \frac{1}{2r^3\Omega_0\rho_0} \frac{\partial}{\partial r} \left(\alpha p r^3 \frac{\partial E}{\partial r} \right). \quad (5.10)$$

Boundary conditions

A general boundary condition states that the Lagrangian pressure perturbation is zero at both disk boundaries (Muñoz and Lithwick, 2020; Lee *et al.*, 2019):

$$dP = 0. \quad (6.1)$$

In Appendix (G), we show that equation (6.1) is satisfied for a adiabatic disk if:

Boundary condition for a locally isothermal disk

$$\frac{\partial E}{\partial r} = 0, \quad (6.2)$$

and for a locally isothermal disk if:

Boundary condition for a locally isothermal disk

$$\frac{d E}{dr c_s^2} = 0. \quad (6.3)$$

Stationary eccentricity and Schrödinger equation

Stationary eccentricity

A stationary eccentricity solution is a solution $E(r, t)$ whose absolute value does not change in time:

$$\frac{\partial |E(r, t)|}{\partial t} = 0, \quad (7.1)$$

Since $E(r, t)$ is in general a complex function, we write:

$$\frac{\partial E^*(r, t)E(r, t)}{\partial t} = 0. \quad (7.2)$$

For this to be satisfied, we need:

$$E(r, t) = E_r(r)e^{i\omega(r)t}, \quad (7.3)$$

where $\omega(r)$ is a real function. To see why it needs to be real, we check a general case of a complex $\omega(r)$:

$$\omega(r) = i\omega_{Im}(r) + \omega_{Re}(r), \quad (7.4)$$

and:

$$\omega^*(r) = -i\omega_{Im}(r) + \omega_{Re}(r). \quad (7.5)$$

In this case:

$$e^{i\omega(r)t}e^{i\omega^*(r)t} = e^{-2\omega_{Im}(r)t}, \quad (7.6)$$

and:

$$\frac{\partial E^*(r, t)E(r, t)}{\partial t} = |E(r)|^2 e^{-2\omega_{Im}(r)t} \neq 0. \quad (7.7)$$

We use equation (7.3) to write:

$$\frac{\partial E(r, t)}{\partial t} = i\omega(r)E_r(r)e^{i\omega(r)t} = i\omega(r)E(r, t). \quad (7.8)$$

If we use equation (7.8) in any of the eccentricity equations, we see that imaginary parts of the solution are due to $\partial E/\partial t$, pressure and gravitational potential. Real parts of the eccentricity equation are forcing effects. In a stationary eccentricity state, the total sum of all forcing effects has to be zero. In other words, stationary eccentricity is a solution for an unforced eccentricity equation.

We can write any steady eccentricity equation as:

$$f_1(r)E = f_2(r)E'' + f_3(r)E, \quad (7.9)$$

or as:

$$E + P(r)E'' + Q(r)E = 0. \quad (7.10)$$

7.1 Schrödinger form

Every equation of the form:

$$E'' + P(r)E' + Q(r)E = 0 \quad (7.11)$$

can be transformed to a Schrödinger form:

$$y'' + k^2(r)y = 0 \quad (7.12)$$

by using a substitution:

$$\ln E = \ln y - \frac{1}{2} \int P(r)dr. \quad (7.13)$$

Function $q(r)$ is then:

$$k^2(r) = Q(r) - \frac{1}{2}P'(r) - \frac{1}{4}P^2(r). \quad (7.14)$$

Since every unforced eccentricity equation can be written in this form, we can use equations (7.13) and (7.14) to write the eccentricity equation in the form of a Schrödinger equation.

We now illustrate how the Schrodinger form of the eccentricity equation can be used to visualise eccentricity solutions on an example of a potential ω_{pot}

whose value is a constant $\Omega_{\text{pot},1}$ for $r < r_1$, and another constant $\Omega_{\text{pot},2}$ for $r > r_2$, and whose maximum value is reached at $r = r_{\text{max}}$:

$$\omega_{\text{pot}}(r) = \begin{cases} \Omega_{\text{pot},1}, & \text{for } r < r_1 \\ \Omega_{\text{max}}, & \text{for } r = r_{\text{max}} \\ \Omega_{\text{pot},2}, & \text{for } r > r_2 \end{cases} \quad (7.15)$$

In figure (7.1), we plot an example of such potential. We choose three radial points such that $r_1 < r_{\text{max}} < r_2$, and three values of potential such that $\Omega_{\text{pot},1} < \Omega_{\text{pot},2} < \Omega_{\text{pot,max}}$.

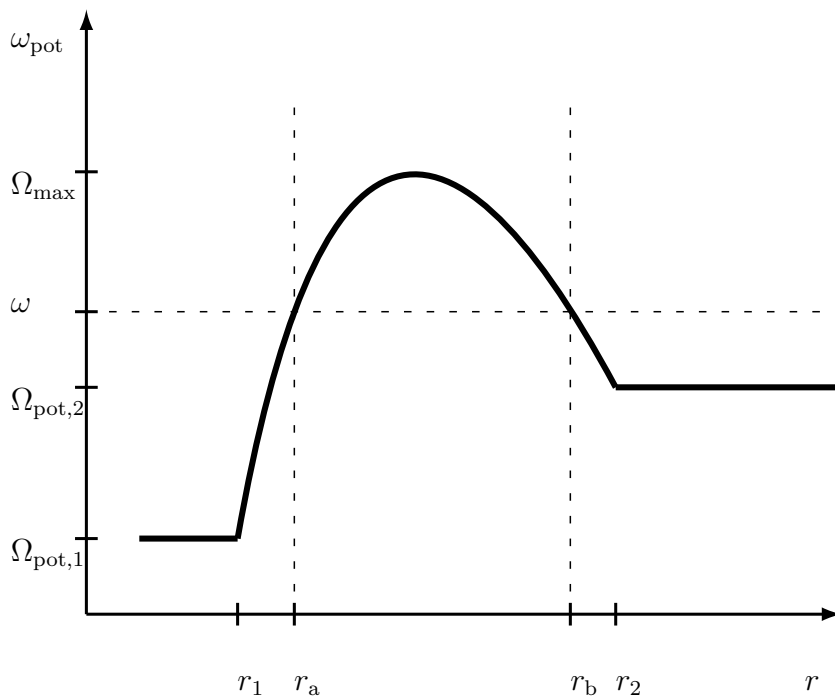


Figure 7.1.: An example of a potential that can trap modes in area between r_1 and r_2 .

A trapped mode is possible only for $\Omega_{\text{pot},2} \leq \omega \leq \Omega_{\text{pot,max}}$. Turning points of the mode are radial points where $\omega_{\text{pot}} = \omega$ ($k = 0$). Function $y(r)$ oscillates in range $r_a \leq r \leq r_b$, and decline from $r = r_a$ to $r = 0$, and from $r = r_b$ to $r = \infty$.

In figure (7.1), we plot one ω value that corresponds to a trapped along with both turning points r_a and r_b .

We can find three properties of the solution to the eccentricity equation by plotting the potential. We will illustrate them using the above example:

- A trapped mode is impossible if the potential does not have a maximum in that range. For a potential in figure (7.1), a trapped mode is not possible in area $2r_2 < r < 10r_2$.
- Next, we can find upper and lower limits on ω . Frequency can not be larger than the maximum value of the potential and can not be lower than values of potential for both $r < R_1$ and $r > R_2$. For a potential in figure (7.1), the frequency has to be in range $\Omega_2 \leq \omega \leq \Omega_{\max}$.
- Finally, the mode is trapped in the area between turning points. Until we calculate ω , we can not know the exact value of turning points. However, we can put limits on those values. For a potential in figure (7.1), we can see that $[r_a, r_b] \in [r_1, r_2]$.

Part III

Locally isothermal circumbinary disk in a stationary state

In chapter (8), we reproduce results from Muñoz and Lithwick (2020).

We then explore locally isothermal circumbinary disks around binaries in more detail. In chapter (9), we look for the lowest eccentricity mode. We first find its frequencies. We then discuss the location and width of those modes. We end by summarizing the most important findings.

In chapter (10), we look for higher order ($n > 0$) modes. We find the number of modes that a disk can support. After that, we illustrate the properties of higher order modes on an example of a disk that supports them. We end by summarizing the most important findings.

In chapter (8), we focus on the disk density profile. We vary the disk density parameters (torque, cavity size, and cavity slope) to show what effect that has on eccentricity solutions. After that, we focus on the choice of the density cutoff function itself to show that it dominates the eccentricity results and explain why that happens. We end by summarizing the most important findings.

Eccentricity equation and solutions

In this chapter, we reproduce results for the eccentricity frequency and radial eccentricity distribution obtained by Muñoz and Lithwick (2020).

8.1 The equation

We use the eccentricity equation for a 2d locally isothermal disk (equation (3.9)), the gravitational eccentricity effects for a circumbinary disk (equation (4.39)), and the definition of the stationary eccentricity (equation (7.8)), to write:

Eccentricity equation for a circumbinary locally isothermal disk.

$$2\Sigma r^2 \Omega_0 \omega E(r) = \frac{1}{r} \frac{\partial}{\partial r} \left[\Sigma c_s^2 r^3 \frac{\partial E(r)}{\partial r} \right] + r \frac{d}{dr} (\Sigma c_s^2) E(r) - \frac{1}{r} \frac{\partial}{\partial r} \left[\Sigma \frac{dc_s^2}{dr} r^3 E(r) \right] + \Sigma \Omega_0^2 E(r) \frac{3q}{2(1+q)^2} a^2. \quad (8.1)$$

According to equation (6.3), boundary conditions for a 2d locally isothermal disk with an inner radius r_{in} and an outer radius r_{out} are:

Boundary conditions for the eccentricity equation.

$$\left. \frac{d}{dR} \left(\frac{E}{c_s^2} \right) \right|_{r_{\text{in}}} = \left. \frac{d}{dR} \left(\frac{E}{c_s^2} \right) \right|_{r_{\text{out}}} = 0. \quad (8.2)$$

Differential equation (8.1), together with boundary conditions (8.2) defines a boundary value problem for eccentricity. The solutions of this problem is defined by a radial eccentricity profile of the disk $E(r)$, and the frequency

profile $\omega(r)$ it precesses with. We are interested in eccentricity modes, solutions for an eccentricity profile that precesses uniformly ($\omega \neq \omega(r)$).

Ω_0 is the lowest order unperturbed orbital frequency (Keplerian frequency):

$$\Omega_0 = \sqrt{\frac{GM}{r^3}}. \quad (8.3)$$

We want to express all eccentricity solutions in terms of binary parameters so we use:

$$\Omega_b = \sqrt{\frac{GM}{a^3}}, \quad (8.4)$$

to write Ω_0 as a function of the binary orbital frequency Ω_b , binary separation a and radius r :

$$\Omega_0(r) = \Omega_b \frac{a^{3/2}}{r^{3/2}}. \quad (8.5)$$

The disk height is:

$$H(r) = \frac{\Omega_0}{c_s}, \quad (8.6)$$

and we assume that the disk aspect ratio h :

$$h = \frac{H}{r} \quad (8.7)$$

is a constant to write:

$$c_s^2(r) = h^2 r^2 \Omega_0^2(r) = h^2 \Omega_b^2 \frac{a^3}{r}. \quad (8.8)$$

The positive direction of precession is the direction of the secondary around the primary. If the eccentricity precesses in the same direction as the binary, the mode is called a prograde mode. If the eccentricity precesses in the opposite direction, the mode is called a retrograde mode.

8.2 Pressure and binary quadrupole effects

We make a short analysis of the eccentricity equation for two extreme cases; one where the motion of the disk is governed solely by pressure and one when the disk is affected only by the gravitational potential of the binary.

8.2.1 Binary quadrupole effects

We set the pressure to zero:

$$c_s = 0, \quad (8.9)$$

to write the eccentricity equation (equation (8.1)) as:

$$2\Sigma r^2 \Omega \omega E(r) = \Sigma \Omega^2 E(r) \frac{3q}{2(1+q^2)} a^2. \quad (8.10)$$

Equation (8.10) can only be satisfied if the frequency is dependent on radius:

$$\omega(r) = \Omega \frac{3q}{4(1+q^2)} \left(\frac{a}{r}\right)^2 = \Omega_b \frac{3q}{4(1+q^2)} \left(\frac{r}{a}\right)^{-7/2}. \quad (8.11)$$

This frequency is called quadrupole precession frequency. We can see that binary quadrupole effects always cause prograde motion ($\Omega_b > 0$). The frequency is largest at $r = a$, and decreases with r . Radial dependence tells us that if only binary quadrupole effect is present, the eccentricity profile will not precess with a uniform frequency.

We define the cavity quadrupole frequency ω_Q as the quadrupole induced frequency (equation (8.11)) at $r = R_{\text{cav}}$:

$$\omega_Q \equiv \Omega_b \frac{3q}{4(1+q^2)} \left(\frac{a}{R_{\text{cav}}}\right)^{7/2}. \quad (8.12)$$

8.2.2 Pressure effects

We set quadrupole effects to zero:

$$q = 0, \quad (8.13)$$

to write the eccentricity equation (equation (8.1)) as:

$$\begin{aligned} 2\Sigma r^2 \Omega \omega E(r) = & \frac{1}{r} \frac{\partial}{\partial r} \left[\Sigma c_s^2 r^3 \frac{\partial E(r)}{\partial r} \right] + r \left[\frac{d}{dr} (\Sigma c_s^2) \right] E(r) \\ & - \frac{1}{r} \frac{\partial}{\partial r} \left[\Sigma \frac{dc_s^2}{dr} r^3 E(r) \right]. \end{aligned} \quad (8.14)$$

This frequency depends on the density profile. Instead of finding an exact solution for the frequency in this case, we perform a dimensional analysis of equation (8.14) to find an expression that we can use for any density profile:

$$2\Sigma r^2 \Omega \omega E(r) = K_1 \frac{1}{r} \frac{1}{r} \left(\Sigma c_s^2 r^3 \frac{E}{r} \right) + K_2 r \frac{1}{r} \Sigma c_s^2 E + K_3 \frac{1}{r} \frac{1}{r} \Sigma \frac{c_s^2}{r} r^3 E, \quad (8.15)$$

where K_1 , K_2 and K_3 are unknown constants. All right hand side terms are proportional to the same combination of functions:

$$2\Sigma r^2 \Omega \omega E(r) \propto c_s^2 \Sigma E = h^2 \Omega_b^2 \frac{a^3}{r} \Sigma E. \quad (8.16)$$

This frequency is also dependent on the radius:

$$\omega \propto \frac{h^2 \Omega_b^2 \frac{a^3}{r}}{r^2 \Omega} = \frac{h^2 \Omega_b^2 \frac{a^3}{r}}{r^2 \Omega_b (r/a)^{-3/2}} = h^2 \Omega_b \left(\frac{r}{a} \right)^{-3/2}. \quad (8.17)$$

We see that the pressure effect scales with h^2 . Compared to the binary quadrupole effect, the pressure effect drops off less steeply.

We define the cavity pressure frequency ω_P as the pressure induced frequency (equation (8.17)) at $r = R_{\text{cav}}$:

$$\omega_P \equiv h^2 \Omega_b \left(\frac{a}{R_{\text{cav}}} \right)^{3/2}. \quad (8.18)$$

8.3 Schrödinger equation for eccentricity

We write the eccentricity equation in the form of equation (7.11):

$$E'' + E' \left[3r^{-1} - \frac{\Sigma'}{\Sigma} \right] + E \left[2 \frac{\Sigma'}{\Sigma} r^{-1} + \frac{3q}{2a^6 h^2 (1+q)^2} r^{-4} - \frac{2\omega}{\Omega_b a^{9/2} h^2} r^{-1/2} \right] = 0, \quad (8.19)$$

so that we can use equation (7.13) to find:

$$E = y(\Sigma r^3)^{-1/2}, \quad (8.20)$$

and equation (7.14) to find:

$$k^2(r) = \frac{2\Omega}{c_s^2} [\omega_{\text{pot}}(r) - \omega], \quad (8.21)$$

where the eccentricity potential is:

Eccentricity potential for the eccentricity Schrödinger equation.

$$\omega_{\text{pot}}(r) = \omega_Q \left(\frac{r}{R_{\text{cav}}} \right)^{-7/2} + \frac{\omega_P}{2} \left(\frac{r}{R_{\text{cav}}} \right)^{-3/2} \left[\frac{r\Sigma'}{2\Sigma} + \left(\frac{r\Sigma'}{2\Sigma} \right)^2 - \frac{r^2\Sigma''}{2\Sigma} - \frac{3}{4} \right]. \quad (8.22)$$

We can now write the eccentricity equation in a Schrodinger form:

$$\frac{d^2y}{dr^2} + k^2y = 0. \quad (8.23)$$

We divide the potential into two parts:

$$\omega_{\text{pot}}(r) = \omega_{\text{pot,Q}}(r) + \omega_{\text{pot,P}}(r), \quad (8.24)$$

where $\omega_{\text{pot,Q}}$ is the quadrupole eccentricity potential:

$$\omega_{\text{pot,Q}}(r) \equiv \omega_Q \left(\frac{r}{R_{\text{cav}}} \right)^{-7/2}, \quad (8.25)$$

and $\omega_{\text{pot,P}}$ is the pressure eccentricity potential:

$$\omega_{\text{pot,P}}(r) = \frac{\omega_P}{2} \left(\frac{r}{R_{\text{cav}}} \right)^{-3/2} \left[\frac{r\Sigma'}{2\Sigma} + \left(\frac{r\Sigma'}{2\Sigma} \right)^2 - \frac{r^2\Sigma''}{2\Sigma} - \frac{3}{4} \right]. \quad (8.26)$$

8.4 The density profile

We formulate a density profile by requiring that the density distribution satisfies three requirements (Muñoz and Lithwick, 2020).

First, we require that there is no net torque on the outer area of the disk. For viscosity $\nu \propto r^{-1/2}$, the zero net torque condition is:

$$\Sigma \propto r^{-1/2}. \quad (8.27)$$

Next, we require the density function to produce a net torque L at the binary separation radius so we modify the density as:

$$\Sigma \rightarrow \Sigma \left(1 - \frac{L}{a\Omega_b^2} \sqrt{\frac{a}{r}} \right). \quad (8.28)$$

Finally, we want to describe a disk with a central cavity of radius R_{cav} . One way to impose this condition is:

$$\Sigma \rightarrow \Sigma e^{-(R_{\text{cav}}/r)^2}. \quad (8.29)$$

We set $R_{\text{cav}} = 2.5a$ and $L = 0.7a\Omega_b^2$. The resulting density profile is:

$$\Sigma(r) = \Sigma_0 \left(\frac{r}{a} \right)^{-1/2} \left[1 - 0.7 \sqrt{\frac{a}{r}} \right] e^{-(2.5a/r)^2}. \quad (8.30)$$

In figure (8.1), we plot the density profile (8.30).

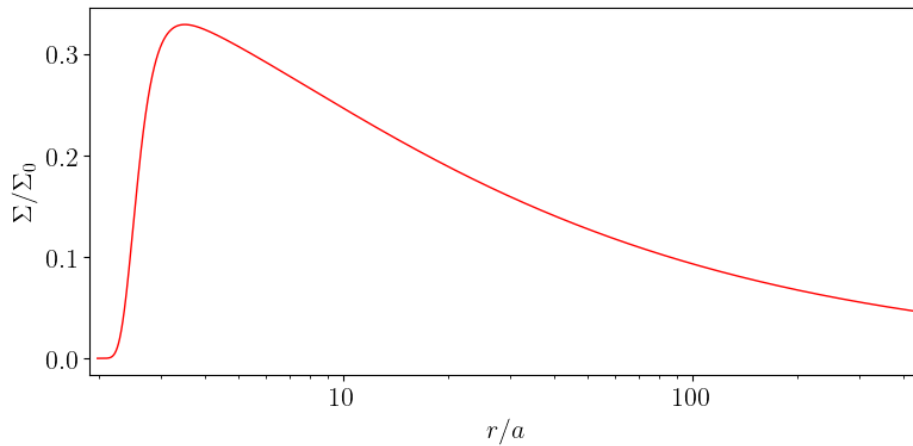


Figure 8.1.: The density profile for a disk with a central cavity.

The scaling constant Σ_0 is irrelevant for eccentricity solutions; eccentricity equation (8.1) is linear in Σ , and the Schrodinger form (equation (8.22)) depends only on ratios Σ'/Σ and Σ''/Σ .

In figure (8.2), we plot the pressure eccentricity potential (equation 8.26) for $h = 0.2$, the quadrupole eccentricity potential (equation (8.25)) for $q = 1$ and the total eccentricity potential (equation (8.22)).

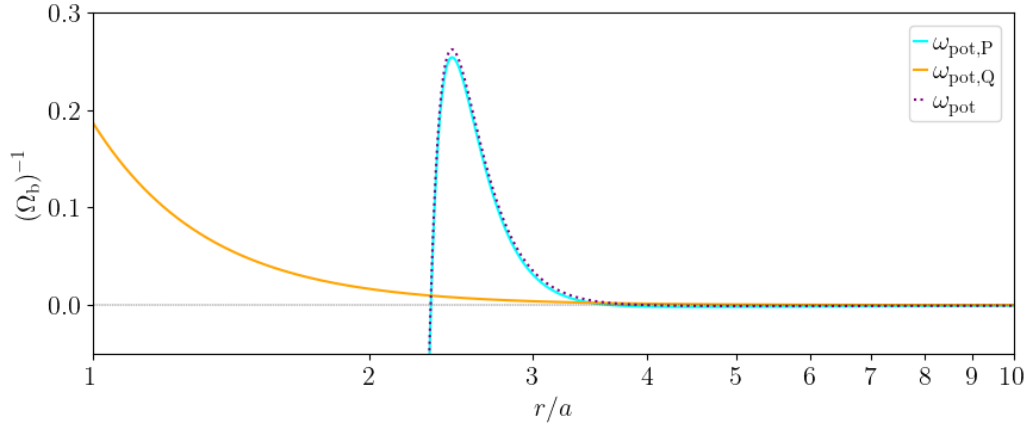


Figure 8.2.: Potentials in units of the binary precession frequency as a function of radius in unites of binary separation. Quadrupole eccentricity potential (orange) for $q = 1$. Pressure eccentricity potential (cyan) for $h = 0.2$). Eccentricity potential for $q = 1$ and $h = 0.2$ (dotted black).

Only a prograde modes with a frequency in range $0 < \omega \leq \frac{1}{3}\Omega_b$ are possible.

8.5 The quantization condition

The first method we use for finding the frequency is the quantization condition. In general, a quantization condition restricts the eigenvalue through physical reasoning. Since we are assuming a steady-state, the wave phase ωt at each radius r has to be the same at all times t . Nevertheless, a wave reflects off each barrier, and that reflection causes a phase change. Therefore, in a steady state, the total sum of all phase changes has to be a multiple of 2π . There is no exact formula for a quantization condition for a potential of arbitrary form. However, approximate quantization conditions exist. One of them is the WKB quantization condition, derived assuming that:

$$\left| \frac{1}{k(r)} \frac{dk(r)}{dr} \right| \ll k(r). \quad (8.31)$$

For a potential with two turning points r_a and r_b , the WKB condition is:

$$\int_{r_a}^{r_b} k(\omega_n, r) dr = \frac{2n + N_s + N_h}{2} \pi, \quad (8.32)$$

where $n \in \mathbb{N}_0$ is the order of the mode. N_s is the number of turning points for a potential with finite value at the turning point. This type of scattering of a wave is called smooth scattering. N_h is the number of turning points for a potential with infinite value at the turning point. This type of potential is called a hard wall. From figure (8.2), we can see that $N_s = 2$ and $N_h = 0$, so we can write:

$$\int_{r_a}^{r_b} k(\omega_n, r) dr = \frac{2n + 1}{2} \pi \quad (8.33)$$

If there is a trapped mode inside this potential, its frequency ω has to satisfy the equation (8.33). It is important to stress that this condition can not be satisfied for every n . In other words, different potentials allow different numbers of modes. We can borrow other results from QM to analyze solutions. The lowest (0-th) mode corresponds to the highest frequency (ω_0). Every higher mode has a frequency lower than all the lower modes. In range $r_a < r < r_b$, n -th mode has n nodes (radial points where $y(r) = 0$).

We will apply this formula on two examples.

WKB frequencies and dispersion relation maps

We find frequencies that satisfy the WKB quantization condition for two binary-disk settings: $[q, h] = [0.9, 0.1]$, and $[q, h] = [0.9, 0.03]$. For $[q, h] = [0.9, 0.1]$, the WKB quantization condition can be satisfied for only one frequency (only $n = 0$ mode is possible). For $[q, h] = [0.9, 0.03]$, the WKB quantization condition can be satisfied for two frequencies ($n = 0$ and $n = 1$ modes are possible).

In left panels of figure (8.3), we plot eccentricity potentials and allowed frequencies for $[q, h] = [0.9, 0.1]$, and $[q, h] = [0.9, 0.03]$. In right panels of figure (8.3), we plot dispersion relation maps (DRMs) for allowed modes and for several frequencies that do not correspond to allowed modes. In a DRM, frequencies that correspond to trapped states are closed lines, and frequencies that correspond to free states are open lines. A state can be trapped, but not steady, in which case, it is presented as a closed line on a DRM, but does not satisfy the quantization condition.

Negative frequencies (light brown lines) correspond to waves approaching for $r \gg 1$, reflecting on $r \approx 2.2a$ (the only barrier for a wave of negative frequencies), and go back to $r \gg 1$. These states are not trapped.

Positive frequencies (dark brown lines) that do not satisfy the quantization condition correspond to closed lines. These states are trapped but are not steady.

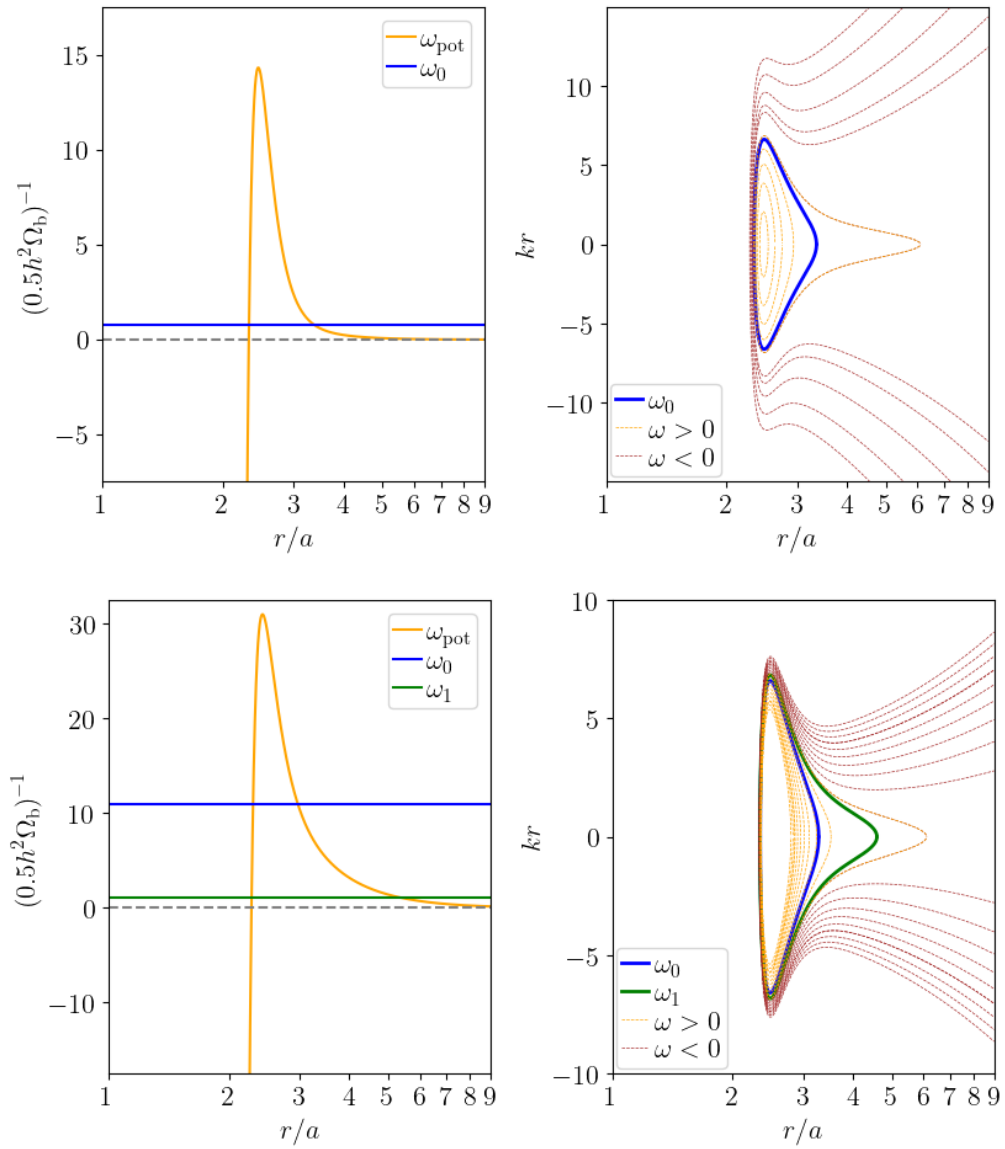


Figure 8.3.: Eccentricity potentials and allowed frequencies (left) and dispersion relation maps (right) for $[q, h] = [0.9, 0.1]$ (upper panels) and $[q, h] = [0.9, 0.03]$ (lower panels).

8.6 Numerical results for the eccentricity boundary value problem

Differential equation (8.1), along with the boundary condition (6.3)) defines a boundary value problem. To find $E(r)$ and $E'(r)$, we need to integrate equation (8.1). Values of those two function at the boundaries need to satisfy equation (6.3)). The only unknown in the eccentricity equation is ω . Once we know ω , integrating the eccentricity equation is easy: an ordinary differential equation such as (8.1) can be integrated from the inner boundary outwards, and this is known as the initial value problem.

To find ω , we integrate equation (8.1) as an initial value problem for a wide range of guesses for ω . Then we see which of those guessed values results in $E(r)$ and $E'(r)$ that satisfy the boundary conditions. This method is called the shooting method.

In figure (8.4), we plot frequencies of the lowest mode (ω_0) for five different values of disk's thickness $h \in 0.01, 0.02, 0.05, 0.1, 0.2$ and for the binary mass ratio in range $0.01 \leq q \leq 1$. We obtain these values by implementing a numerical shooting method. We refer to solutions obtained by numerically solving the boundary value problem as numerical BVP solutions.

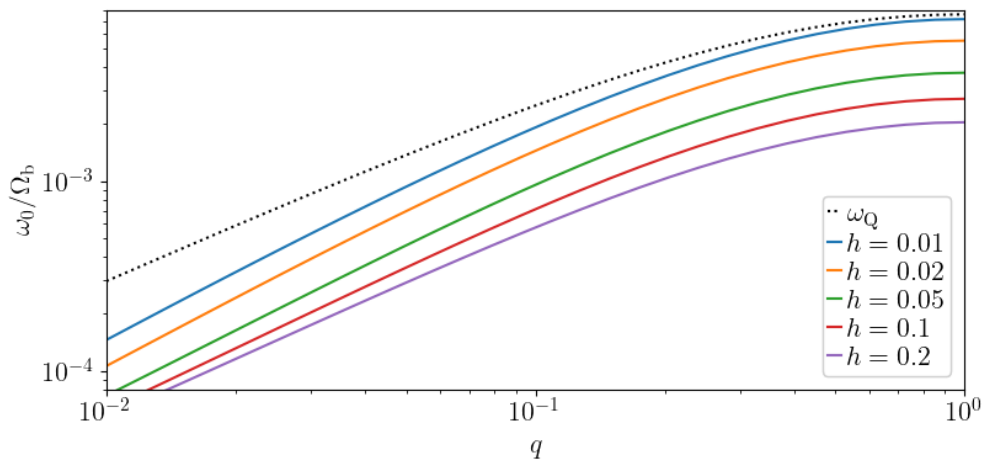


Figure 8.4.: Lowest mode frequencies ω_0 in units of the binary orbital frequency Ω_b , as a function of the binary mass ratio q for $h = [0.01, 0.02, 0.05, 0.1, 0.2]$.

We find values of ω_0 using both the WKB and the shooting method for three different values of the cavity size $R_{\text{cav}} \in [2.5a, 3.5a, 5a]$ and $0.01 \leq h \leq 0.2$,

$0.03 \leq q \leq 1$. Result in figure (8.5). From figure (8.5), we see that the WKB

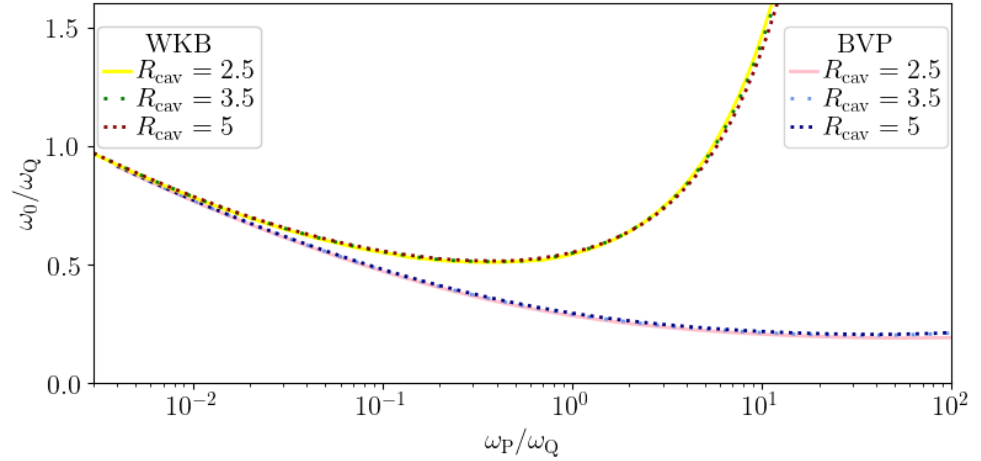


Figure 8.5.: WKB and numerical BVP frequencies of the lowest mode in units of the cavity quadrupole frequency as a function of the ratio of the cavity pressure and the cavity quadrupole frequency.

quantization condition gives correct solutions only for $\omega_P/\omega_Q \lesssim 0.1$. We also see that solutions collapse into a single line, indicating that the ratio ω_P/ω_Q is the determining factor in solutions for ω_0 . We also see that the cavity size does not affect results.

We use the shooting method to confirm that the frequency solution for $[q, h] = [1, 0.03]$ found using the WKB method are correct and, in figure (8.6), we plot eccentricity profiles $E(r)$ for the two allowed modes. From it, we see that the $n = 1$ mode is spread further out than the $n = 0$ mode.

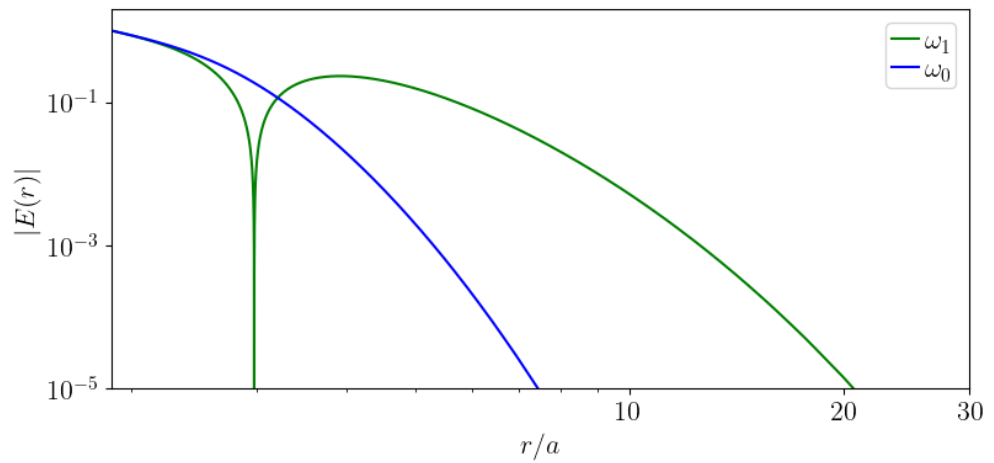


Figure 8.6.: Eccentricity profiles $E(r)$ for $[q, h] = [0.9, 0.03]$.

In figure (8.7), we plot eccentricity profiles $E(r)$ and scaled eccentricity profiles $y(r)$ for $\omega_P/\omega_Q = 0.05$ and for $\omega_P/\omega_Q = 50$. From it, we see that eccentricity profile spreads further out in the disk for larger ω_P/ω_Q .

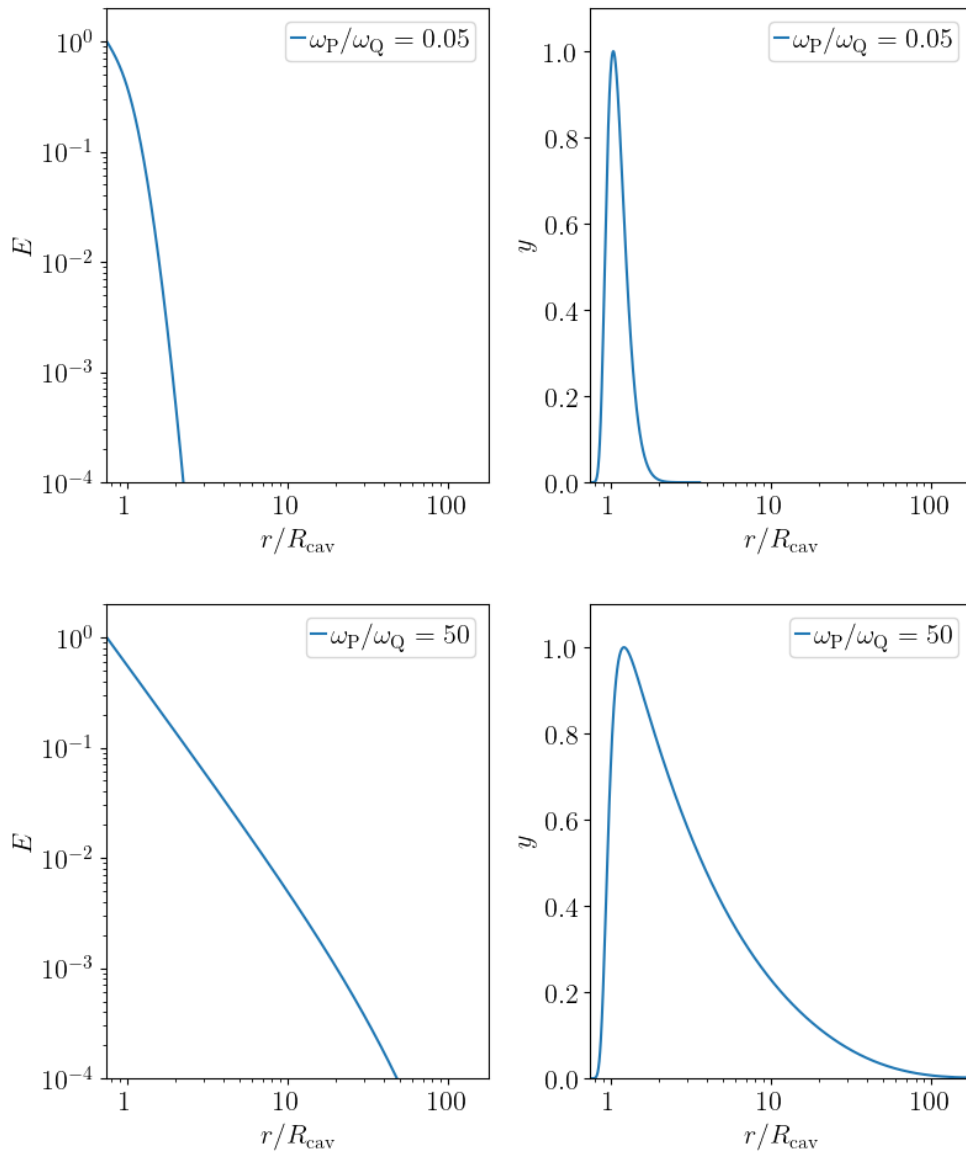


Figure 8.7.: Eccentricity profiles (left) and scaled eccentricity profiles (right) for $\omega_P/\omega_Q = 0.05$ (upper panels) and $\omega_P/\omega_Q = 50$ (lower panels). The radius is scaled with the size of the cavity, and the eccentricity is scaled to $E = 1$ at the inner disk boundary.

The lowest mode

In this chapter, we allow the disk to be thinner, so we set $10^{-4} \leq h \leq 0.2$, as opposed to $10^{-4} \leq h \leq 0.2$ used in chapter (8). We also allow the the binary mass ratio to be smaller, so we set $10^{-6} \leq q \leq 1$, instead of $0.03 \leq q \leq 1$ used in chapter (8).

In figure (8.5), we saw that ω_0 solutions for independent values of h and q collapse into a single line if we plot them in a $\omega/\omega_Q - \omega_P/\omega_Q$ plot, where:

$$\omega_P = h^2 R_{\text{cav}}^{-3/2}, \quad (9.1)$$

is the cavity pressure frequency, and:

$$\omega_Q = \frac{3q}{4(1+q)^2} R_{\text{cav}}^{-7/2}, \quad (9.2)$$

is the cavity quadrupole frequency. We call the ratio ω_P/ω_Q the cavity frequency ratio (CFR). To show why ω_0/ω_Q solutions depend only on the CFR, we write the eccentricity equation again:

$$\begin{aligned} 2\Sigma r^2 \Omega \omega E(r) &= \frac{1}{r} \frac{\partial}{\partial r} \left[\Sigma c_s^2 r^3 \frac{\partial E(r)}{\partial r} \right] + r \frac{d(\Sigma c_s^2)}{dr} E(r) \\ &- \frac{1}{r} \frac{\partial}{\partial r} \left[\Sigma \frac{dc_s^2}{dr} r^3 E(r) \right] + \Sigma \Omega^2 E(r) \frac{3q}{2(1+q)^2}. \end{aligned} \quad (9.3)$$

We use $c_s^2 = h^2/r$, and equations (9.1) and (9.2) to write (9.3) as:

$$\begin{aligned} 2\Sigma r^2 \Omega \frac{\omega}{\omega_Q} E(r) &= \frac{\omega_P}{\omega_Q} \frac{1}{r} \frac{\partial}{\partial r} \left[\Sigma r^2 \frac{\partial E(r)}{\partial r} \right] R_{\text{cav}}^{3/2} + \frac{\omega_P}{\omega_Q} r \frac{d(\Sigma r^{-1})}{dr} E(r) R_{\text{cav}}^{3/2} \\ &+ \frac{\omega_P}{\omega_Q} \frac{1}{r} \frac{\partial}{\partial r} [\Sigma r E(r)] R_{\text{cav}}^{3/2} + 2\Sigma \Omega^2 E(r) R_{\text{cav}}^{7/2}. \end{aligned} \quad (9.4)$$

Equation (9.4) depends on ω , q and h only in terms of ω/ω_Q and ω_P/ω_Q . In addition to equation (9.4), solutions also depend on boundary conditions, so we write a general frequency solution as:

$$\frac{\omega}{\omega_Q} = f\left(r_{\text{in}}, r_{\text{out}}, \Sigma, R_{\text{cav}}, \frac{\omega_P}{\omega_Q}\right). \quad (9.5)$$

For a fixed density profile (Σ, R_{cav}), and a fixed disk size ($r_{\text{in}}, r_{\text{out}}$), we write:

$$\frac{\omega}{\omega_Q} = f\left(\frac{\omega_P}{\omega_Q}\right). \quad (9.6)$$

We use equation (9.6) as a standard representation of frequency results; we present results as functions of the CFR throughout this part. New ranges of h and q set the CFR range as $10^{-6} \lesssim \omega_P/\omega_Q \lesssim 10^6$. In figure (9.1), we show values of h and q that correspond to $CFR = [10^{-6}, 10^{-4}, 10^{-2}, 10^0, 10^2, 10^4]$. In pink, we mark the area of $h - q$ that we explored in part 8.

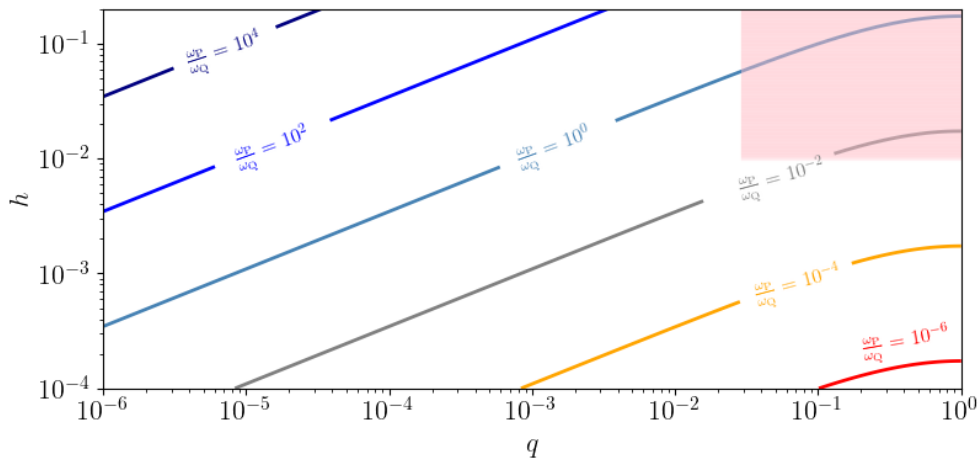


Figure 9.1.: CFR as a function of h and q .

In this chapter we look for the lowest $n = 0$ mode. In section (9.1), we use the WKB quantization condition to find the frequency of the lowest mode. We do it for two reasons. First, to see if the agreement between WKB and numerical BVP frequency values is true for even thinner disks (lower CFRs). Second, unlike numerical BVP solutions, the WKB approximation can be used to gain intuitive understanding of solutions. In section (9.2), we find numerical solutions for the eccentricity boundary value problem. In section (9.3), we discuss the location of the mode.

9.1 WKB frequency

We use the WKB quantization condition (equation (8.33)) to find ω_0 . In the left panel of figure (9.2), we plot solutions ω_0/ω_Q as a function of ω_P/ω_Q . In it, we see that the function $\omega_0/\omega_Q = f(\omega_P/\omega_Q)$ has a minimum at $\omega_P/\omega_Q \approx 0.1$. This suggest that something interesting might be happening with the eccentricity potential. To examine this further, in the right panel of figure (9.2), we plot the eccentricity potential (ω_{pot}) in same units (ω_Q). We do this for $\omega_P/\omega_Q \approx 0.1$, which is the value that we approximate as the critical CFR, and for four values below and above the critical CFR. We see that $\omega_{\text{pot}}/\omega_Q$ also has a minimum at $\omega_P/\omega_Q \approx 0.1$. We use this fact to divide the CFR range into 2 parts; the low CFR range ($0 < \omega_P/\omega_Q \lesssim 0.1$) and the high CFR range ($0.1 \lesssim \omega_P/\omega_Q < \infty$). We discuss each part separately.

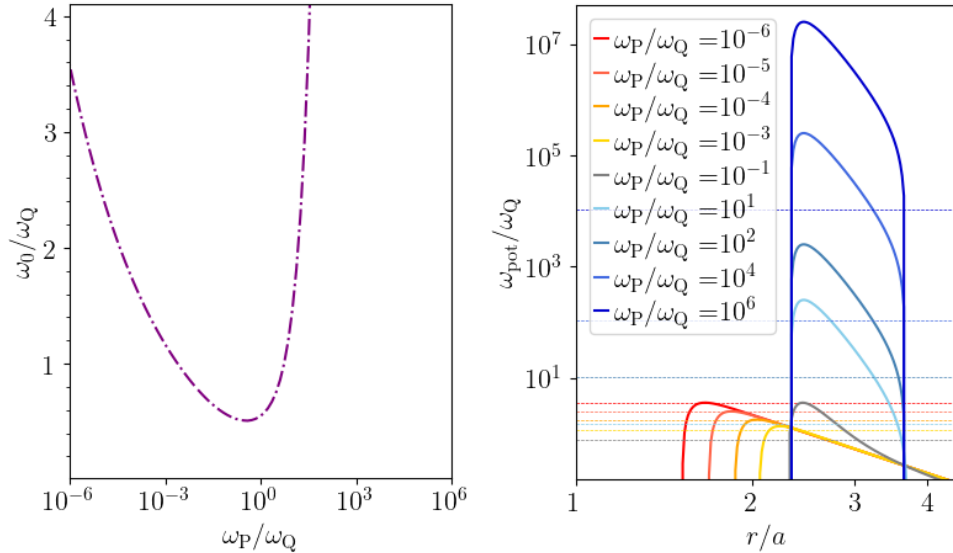


Figure 9.2.: Left: The frequency of the lowest mode (ω_0) in units of the cavity quadrupole frequency (ω_Q), as a function of the cavity frequency ratio (ω_P/ω_Q) Right: eccentricity potential ($\omega_{\text{pot}}/\omega_Q$) in units of the cavity quadrupole frequency (ω_Q) as a function of radius in units of the binary separation (a). Eccentricity potentials corresponding to CFRs larger than the critical one are in blue, and those corresponding to CFRs lower than the critical one are in red. The critical CFR is in grey. Lowest mode frequencies (ω_0/ω_Q) are in thin dashed lines in the same colors as the corresponding eccentricity potentials.

9.1.1 Low CFR range

We discuss the frequency value. From the right panel of figure (9.2), we see that in the low CFR range, ω_0 is near the maximum of the eccentricity potential. The frequency ω_0 is higher for binaries with larger mass ratio and for thinner disks. In the left panel of figure (9.2), we see that for $\omega_P/\omega_Q \lesssim 10^{-3}$, the solution is:

$$\frac{\omega_0}{\omega_Q} > 1, \quad (9.7)$$

meaning that the lowest mode frequency can grow above the cavity quadrupole frequency ω_Q . We expect that a lower pressure influence causes a lower frequency because the total potential is lower (equation 4.40). Therefore, it seems counter intuitive that lowering ω_P increases ω_0 past ω_Q .

We now explain how lowering the pressure eccentricity potential can increase the frequency. First, we see that a binary mass ratio of $q = 1$ results in a low range CFR for $h \lesssim 0.1$:

$$\begin{aligned} [q, h] = [1, 10^{-4}] &\rightarrow \frac{\omega_P}{\omega_Q} \approx 10^{-7}, \\ [q, h] = [1, 0.1] &\rightarrow \frac{\omega_P}{\omega_Q} \approx 10^{-1}. \end{aligned} \quad (9.8)$$

We change the CFR in a way that we fix the binary mass ratio to $q = 1$ and change the value of the disk's thickness h . In the left panel of figure (9.3), we plot the eccentricity potential $\omega_{\text{pot}}(r)$ for $q = 1$ and $h = [0.0001, 0.0005, 0.001, 0.005, 0.01]$. In the right panel of figure (9.3), we plot pressure eccentricity potential $\omega_{\text{pot,P}}(r)$ for $h = [0.0001, 0.0005, 0.001, 0.005, 0.01]$. In both figures we plot quadrupole eccentricity potential $\omega_{\text{pot,Q}}(r)$ for $q = 1$.

From the left panel of figure (9.3), we see that even though ω_0 grows above the cavity quadrupole frequency (black dot), it does not grow above the maximum quadrupole frequency (black dotted line). From the right panel of figure (9.3), we see that the pressure eccentricity potential in the low range CFR is effectively:

$$\omega_{\text{pot,P}}(r) \approx \begin{cases} -\infty, & \text{if } r < a_P \\ 0, & \text{otherwise,} \end{cases} \quad (9.9)$$

where the value of a_P depend on h . In other words, in low range CFR, the pressure will simply cut off the quadrupole eccentricity potential, creating a potential well. Lowering h moves the location of the cutoff to the left (inwards in the disk), where the quadrupole frequency is larger.

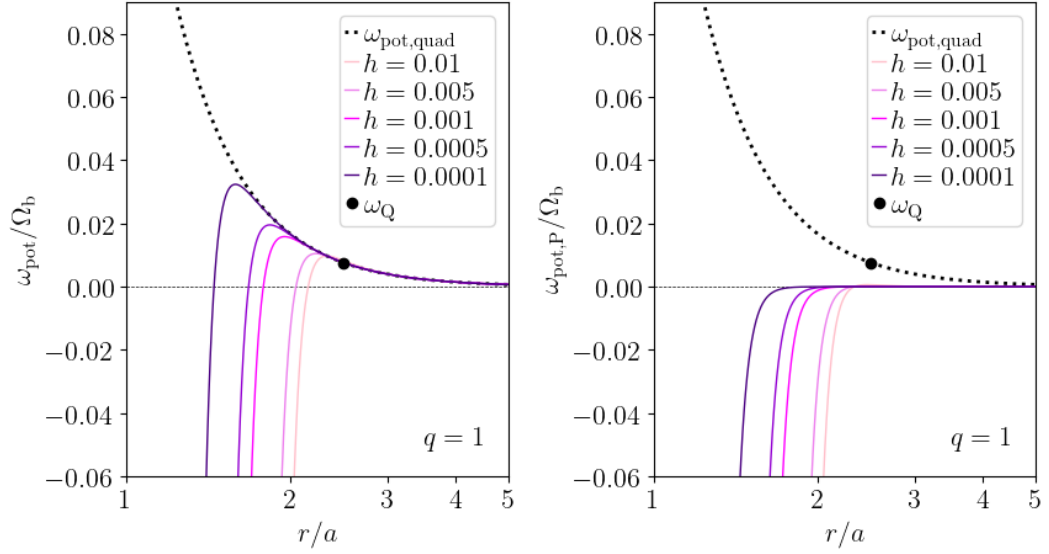


Figure 9.3.: Eccentricity potentials and potential contributions for an equal mass binary ($q = 1$) and five different values of the disks thickness h . All plot in units of binary precession frequency (Ω_b), and as a function of radius in units of the binary separation (r/a). Left: quadrupole eccentricity potential to eccentricity potential in dotted black, total eccentricity potential in solid lines. Right: quadrupole eccentricity potential in dotted black, pressure eccentricity potential in solid lines. In both plots, the cavity quadrupole frequency ω_Q is in a black dotted line for reference.

9.1.2 High CFR range

Now we turn to the high CFR range represented by the blue curves with $\omega_P/\omega_Q > 0.1$ in the right panel of figure (9.2).

A short WKB analysis

From figure (9.2), we see that the lowest mode is trapped far from the potential maximum, and that the lowest mode will be located in the same place and have the same width for all high CFRs. We use this fact to preform a short analysis of the WKB quantization condition. We use $c_s^2 \propto h^2/2 \propto \omega_P/r$ and $\Omega \propto r^{-3/2}$ to write equation (8.21) as:

$$\begin{aligned} k_0^2(\omega_0, r) &= \frac{K_1 r^{-1/2}}{\omega_P} [\omega_{\text{pot}}(r, \Sigma) - \omega_0] \\ &= \frac{K_1 r^{-1/2}}{\omega_P} \left[K_2 r^{-7/2} \omega_Q + r^{-3/2} f(r, \Sigma) \omega_P - \omega_0 \right] \\ &= K_1 r^{-1/2} \left[K_2 r^{-7/2} \frac{\omega_Q}{\omega_P} + f(r, \Sigma) r^{-3/2} - \frac{\omega_0}{\omega_P} \right], \end{aligned} \quad (9.10)$$

where K_1 and K_2 are some constants, and f is a function of the radius and the density profile. In the high CFR range ($\omega_Q/\omega_P \ll 1$), we can approximate the WKB quantization condition as:

$$\int_{r_a}^{r_b} k_0(\omega_0, r) dr = \int_{r_a}^{r_b} K_1 r^{-1} \sqrt{f(r, \Sigma) - \frac{\omega_0}{\omega_P}} dr = \frac{1}{2} \pi. \quad (9.11)$$

The turning points (r_a and r_b) are fixed in this regime. The density profile does not depend on the CFR either. Therefore, when we change the CFR, the only part of equation (9.11) that changes is ω_0/ω_P . So, equation (9.11) is satisfied when we change the CFR only if:

$$\frac{\omega_0}{\omega_P} = C, \quad (9.12)$$

where C is an undetermined constant. Equation (9.12) tells us that in this range, the frequency of the lowest mode is not dependent on the cavity quadrupole frequency. To explain how this relates to results from figure (9.2), we write equation (9.12) in another form:

$$\frac{\omega_0}{\omega_Q} = C \frac{\omega_P}{\omega_Q}. \quad (9.13)$$

Equation (9.13) shows that even if the value of the lowest mode frequency ω_0 is a small finite value, the ratio ω_0/ω_Q will be large if ω_Q is small enough. In other words, the apparent infinite growth of ω_0 in the left panel of figure (9.2) is a consequence of scaling ω_0 with ω_Q .

Another way to represent eccentricity results

If we multiply equation (9.4) by ω_Q/ω_P , we can write it as:

$$2\Sigma r^2 \Omega \frac{\omega}{\omega_P} E(r) = \frac{1}{r} \frac{\partial}{\partial r} \left[\Sigma r^2 \frac{\partial E(r)}{\partial r} \right] R_{\text{cav}}^{3/2} + r \frac{d}{dr} (\Sigma r^{-1}) E(r) R_{\text{cav}}^{3/2} + \frac{1}{r} \frac{\partial}{\partial r} [\Sigma r E(r)] R_{\text{cav}}^{3/2} + 2\Sigma \Omega^2 E(r) R_{\text{cav}}^{7/2} \left(\frac{\omega_P}{\omega_Q} \right)^{-1}, \quad (9.14)$$

which shows that we can write the eccentricity frequency solution as:

$$\frac{\omega_0}{\omega_P} = f \left(\frac{\omega_P}{\omega_Q} \right). \quad (9.15)$$

We now show that equation (9.15) is a more suitable way to examine the high CFR range. In figure (9.4), we plot solutions from figure (9.2) in units of ω_P , instead of ω_Q . From it, we see that in the high CFR range, the frequency and the eccentricity potential settle on constant values. Just like ω_0 , the eccentricity potential seemed to infinitely grow in figure (9.2) because it was scaled with ω_Q .

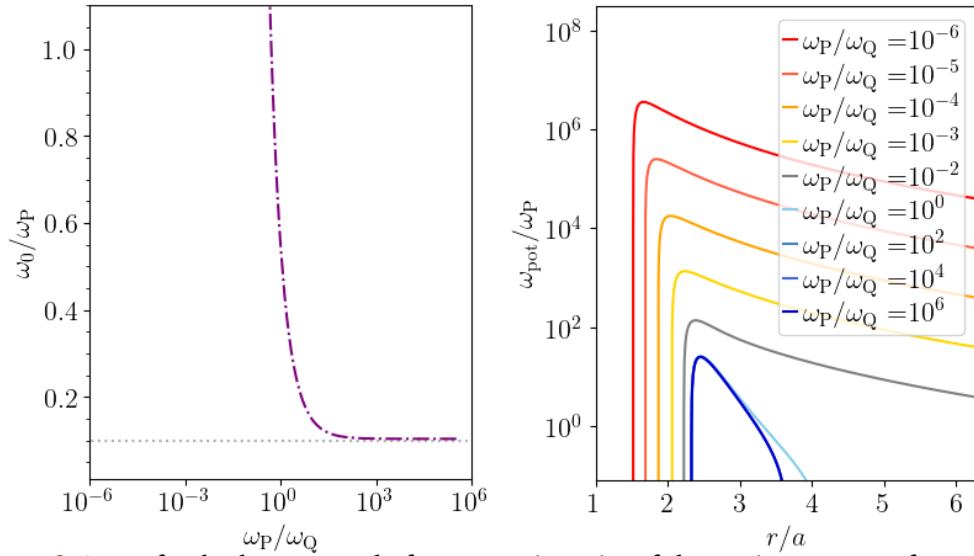


Figure 9.4.: Left: the lowest mode frequency in units of the cavity pressure frequency, as a function of the CFR. Right: eccentricity potential in units of the cavity pressure frequency, as a function of radius in units of binary separation.

From the left panel, we see that that (as predicted by equation (9.12)) ω_0/ω_P settles on a constant value:

$$\lim_{\omega_P/\omega_Q \gg 1} \frac{\omega_0}{\omega_P} = 0.1. \quad (9.16)$$

We show why ω_0 comes to be independent on ω_Q in the high CFR range. First, we see that a thick disk will be in the high CFR range for $q \in [0.1, 1]$:

$$\begin{aligned} [q, h] = [10^{-4}, 0.2] &\rightarrow \frac{\omega_P}{\omega_Q} \approx 10^7, \\ [q, h] = [0.1, 0.2] &\rightarrow \frac{\omega_P}{\omega_Q} \approx 10^0 \end{aligned} \quad (9.17)$$

We fix $h = 0.2$ and change the CFR by changing q . In figure (9.5), we plot a high CFR equivalent of figure (9.3). From it, we see that the quadrupole eccentricity potential is negligible compared to the pressure eccentricity potential:

$$\omega_{\text{pot},Q} \approx 0. \quad (9.18)$$

In the low CFR range, even though the pressure was low, it still affected the eccentricity potential by causing a cutoff. But here, a low quadrupole value causes no change in the eccentricity potential. Since the eccentricity potential in units of ω_P does not change with the CFR, neither do eccentricity solutions:

$$\frac{\omega_{\text{pot}}}{\omega_P} \neq f\left(\frac{\omega_P}{\omega_Q}\right) \rightarrow \frac{\omega_0}{\omega_P} \neq f\left(\frac{\omega_P}{\omega_Q}\right) \quad (9.19)$$

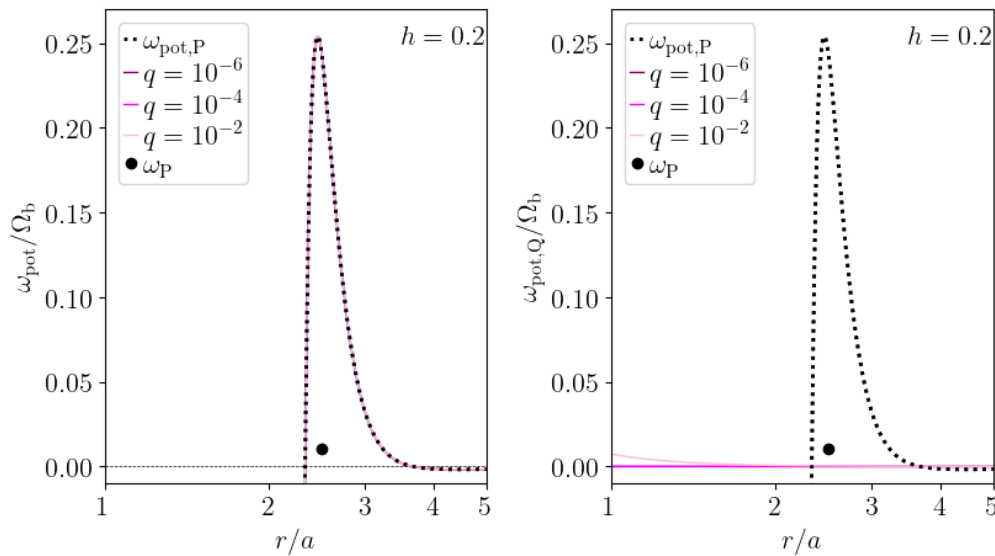


Figure 9.5.: Eccentricity potentials in units of the binary precession frequency as a function of radius scaled with the binary separation (r/a) for $h = 2$ and $q = [10^{-6}, 10^{-4}, 10^{-2}]$. Left: pressure eccentricity potential (dotted black line) and total eccentricity potentials (solid lines). Right: pressure eccentricity potential (dotted black line) and quadrupole eccentricity potentials (solid lines).

9.1.3 The entire CFR range

We saw that we can write eccentricity frequencies scaled with cavity quadrupole frequency (ω/ω_Q) as a function of the CFR, and we saw that this representation is more suitable for the low CFR range. Then, in section (9.1.2) we saw that we can write eccentricity frequencies scaled with cavity pressure frequency (ω/ω_P) as a function of the CFR, and that this representation is more suitable for the high CFR range.

Now, we want to represent the lowest mode frequency solutions for the entire CFR range. From equation (9.4), we see that it is not possible to write ω_0 (or ω/Ω_b) as a function of the CFR only. This means that we can not represent solutions with a single line. Therefore, in figure (9.6), we plot frequency solutions in another way. We plot ω/Ω_b as a function of q ($10^{-6} \leq q \leq 1$) for each h in $h \in [0.2, 0.1, 0.01, 0.001, 0.0001]$.

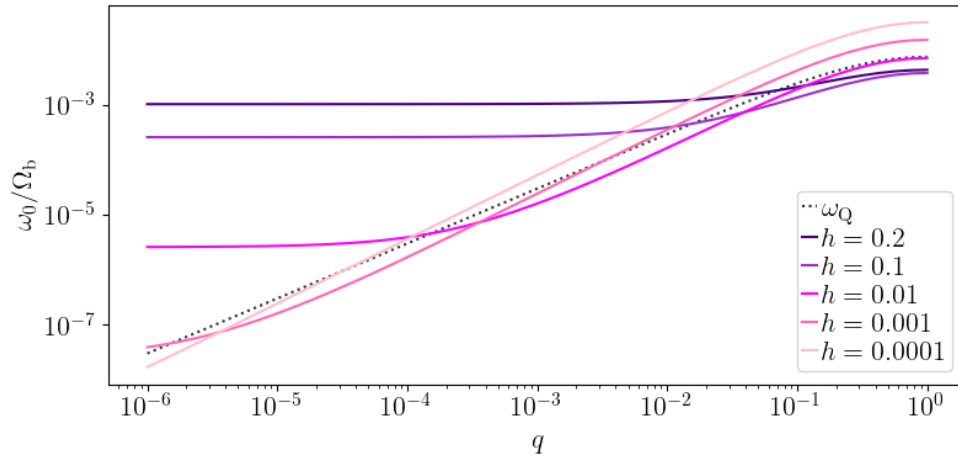


Figure 9.6.: ω_0 in units of Ω_b as a function of q for five different values of h (solid lines). Cavity quadrupole frequency (dotted black line).

We use figure (9.6) to point out the results that we found in this section. First, ω_0 of a thick disk is less sensitive to changes in the binary mass ratio. We see how the constant we found before (equation (9.16)) presents itself in this plot; for $h \gg q$, $\omega_0/\omega_P = 0.1$, and $R_{\text{cav}} = 2.5$, we write:

$$\frac{\omega_0}{\Omega_b} \approx \frac{1}{40} h^2. \quad (9.20)$$

For $h = 0.2$, $\omega_0/\Omega_b \approx 10^{-3}$, just like we see in figure (9.6) for $q \lesssim 0.01$.

9.2 Numerical BVP frequency

We use numerical methods to solve the boundary value problem defined by the differential equation (8.1) and the boundary condition (8.2). Again, we search for frequency solutions in terms of the CFR.

9.2.1 Low CFR range

We lower the thickness of the disk to $10^{-4} \leq h \leq 0.2$, and keep the binary mass ratio in range $0.001 \leq q \leq 1$. This puts the CFR in range $10^{-6} \lesssim \omega_P/\omega_Q \lesssim 10^2$. In figure (9.7), we plot ω_0/ω_Q (left panel) and ω_0/ω_P (right panel) solutions as functions of ω_P/ω_Q . In both panels, we plot WKB solutions for comparison. From both panels of figure (9.4), we see that the agreement between the two method is excellent for $\omega_P/\omega_Q \lesssim 0.1$.

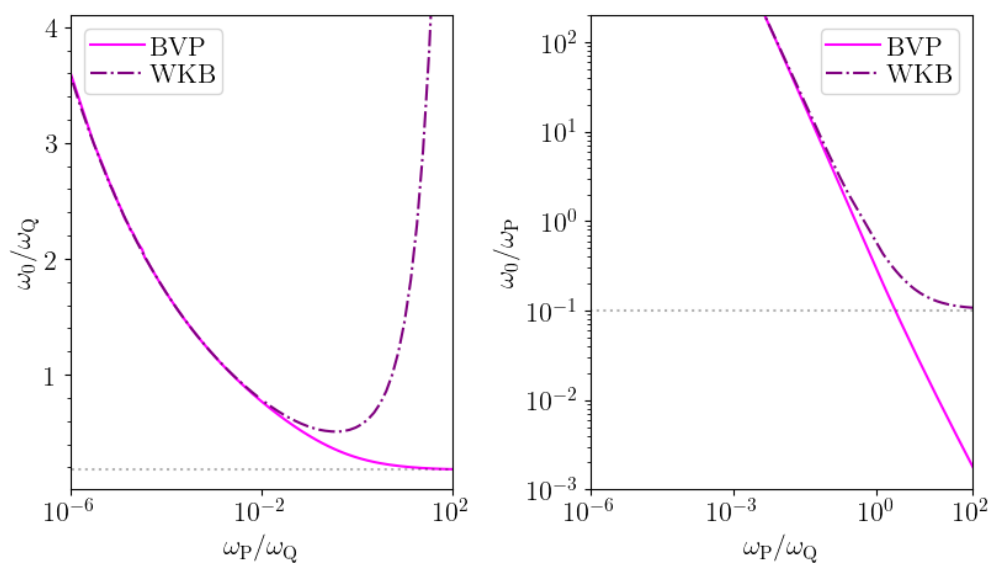


Figure 9.7.: Comparison of WKB and BVP frequencies as a function of CFR. Left: lowest mode frequency in units of the cavity quadrupole frequency. Right: lowest mode frequency in units of the cavity pressure frequency.

9.2.2 High CFR range

We use figure (9.7) to point out the main difference between the WKB and the numerical BVP solutions for higher values of the CFR. Numerical BVP solutions show that, for $\omega_P/\omega_Q \gtrsim 10$, ω_0 are not dependent on ω_P (depends only on ω_Q). This is why in units of ω_Q , numerical BVP solutions converge to a constant value of $\omega_0 \approx 0.18\omega_Q$. The WKB solutions state the exact opposite; for $\omega_P/\omega_Q \gtrsim 10$, ω_0 is not dependent on ω_Q (depends only on ω_P). This is why in units of ω_P , the WKB solutions converge to a constant value of $\omega_0 \approx 0.1\omega_P$.

While discussing the WKB solutions, we showed two important properties of the high CFR range. First, the pressure eccentricity potential alone leads to a potential with a local maximum, which is a necessary condition for trapping modes (right panel of figure (9.3)). Second, WKB frequencies do not grow infinitely like figure (9.2) suggests. Instead, they settle on a constant value that is proportional to h and not dependent on q (left panel of figure (9.4) and figure (9.6)). Knowing this, even if we do not expect WKB frequencies to be exact, we do expect their general behaviour to be true. Meaning, we expect that in the limit of small binary mass ratio, the mode frequency will be a function of the disk's thickness, and independent of the binary mass ratio:

$$\lim_{q \rightarrow 0} \omega_0 = f(h) \neq f(q). \quad (9.21)$$

First, we find numerical BVP solutions for a limit of infinite CFR. Then, we gradually increase the CFR to see if we reach the same limit.

The limit of an infinite CFR

We find numerical BVP frequencies for a nonexistent quadrupole potential:

$$q = 0 \rightarrow \frac{\omega_P}{\omega_Q} \rightarrow \infty, \quad (9.22)$$

and plot an equivalent to figure (9.7). In the left panel of figure (9.8), we plot frequency solutions ω_0/ω_b as a function of h . In the right panel of figure (9.8), we plot frequency solutions ω_0/ω_P as a function of h .

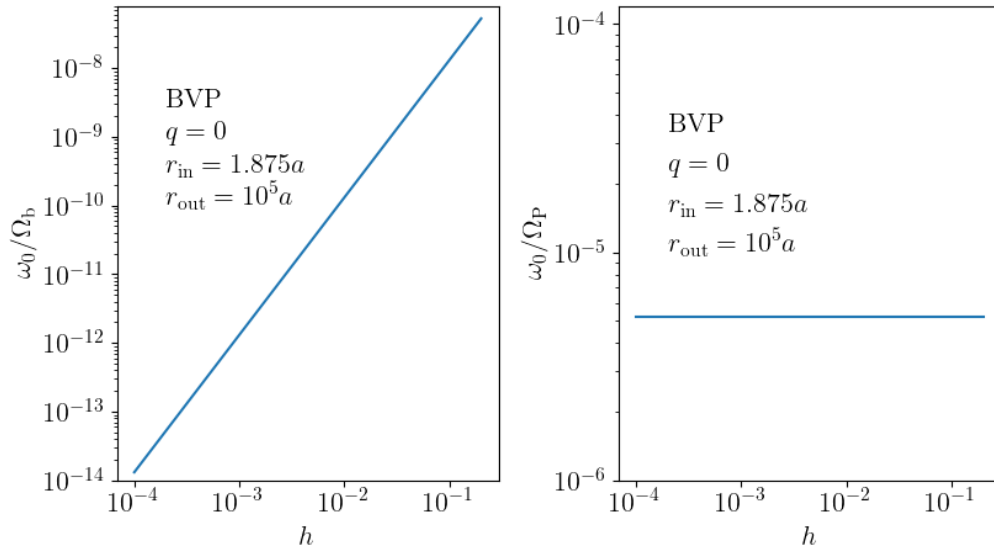


Figure 9.8.: Numerical BVP ω_0 frequencies for $q = 0$ and $0.001 \leq h \leq 0.2$. Disk boundaries are $r_{in} = 1.875a$ and $r_{out} = 10^5a$. Left: ω_0 in units of the binary precession frequency, as a function of the disk's thickness. Right: ω_0 in units of the cavity pressure frequency, as a function of the disk's thickness.

From it, we see that ω_0 is some function of h , which is in agreement with equation (9.21). In the right panel, we plot frequencies in units of ω_P . In these units, the frequency is a constant:

$$\frac{\omega_0}{\omega_P}(q = 0) = 5.2 \cdot 10^{-6}. \quad (9.23)$$

Equation (9.23) is the equation we predicted in the short quantization condition analysis (equation (9.12)), and tells us the value of the undetermined constant: $C = 5.2 \cdot 10^{-6}$. This is also the behaviour that the WKB method predicted (equation (9.16)), but with a different value for the constant C .

Since the numerical BVP solutions (figure (8.5)) predicted that:

$$\frac{\omega_0}{\omega_Q} = 0.18 \rightarrow \frac{\omega_0}{\omega_P} = 0.18 \frac{\omega_P}{\omega_P}, \quad (9.24)$$

if we set $q = 0$, we get:

$$\frac{\omega_0}{\omega_P} = 0. \quad (9.25)$$

This is at odds with what we found for $q = 0$ (equation (9.23)). This indicates that maybe the CFR of 10^2 is not high enough to properly observe the pressure dominant range. Another possible explanation is the dependence on the disk radius. To examine this further, we find numerical BVP solutions for large CFRs, and for several values of the disk outer radius.

High, but finite CFR and the dependence on the outer disk radius

The WKB quantization condition is not a function of the boundary conditions, so WKB solutions do not depend on them. In general, BVP solutions depend on the boundary location. Since numerical BVP and WKB solutions are in agreement for low CFR, and WKB solutions are not dependent on the boundary conditions, we expect that BVP solutions for low CFRs are not dependent on the boundary conditions either.

In figure (9.9), we plot numerical BVP solutions for ω_0/ω_Q (upper panel), and for ω_0/ω_P (lower panel). We do it for 8 different values of the outer disk radius $r_{\text{out}} = [10a, 20a, 30a, 40a, 50a, 100a, 500a, 1000a]$, and for $10^{-1}\omega_P/\omega_Q < 10^6$. As expected, the change of the disk outer radius affects solutions in CFR ranges where the WKB method is completely invalid ($\omega_P/\omega_Q > 10$). We see that ω_0/ω_Q solutions get lower with larger r_{out} . However, they do not settle on a constant value like in figure (8.5). Instead, they reach $\omega_0/\omega_Q = 0.18$ at $\omega_P/\omega_Q \approx 10$, but they start growing again at $\omega_P/\omega_Q \approx 10^3$. In it, we see a behaviour similar to WKB solutions (figures (9.2), (9.4)). We also plot the numerical BVP frequencies that we found for $q = 0$ and we see that this frequency is exactly the limiting frequency that we found here.

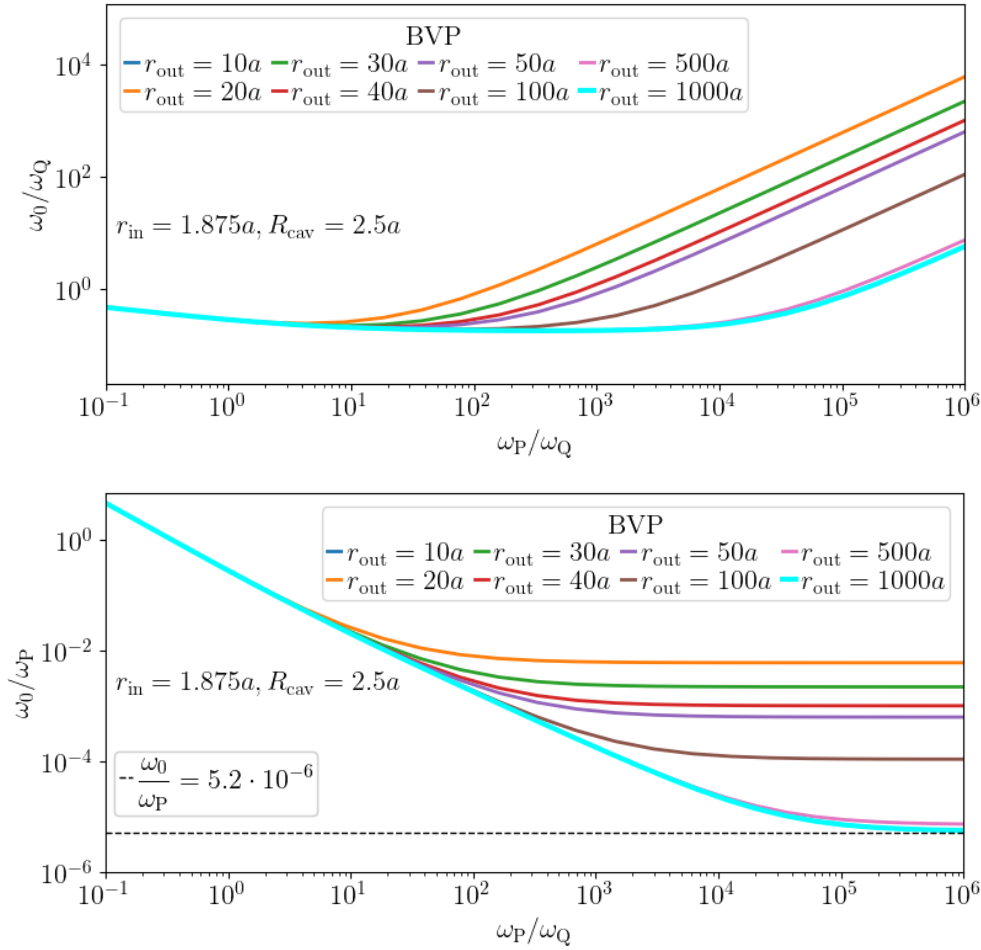


Figure 9.9.: Frequency dependence as a function of ω_P/ω_Q for eight values of the outer disk radius. Upper panel: frequencies in units of the quadrupole cavity frequency. For larger outer radii, frequencies are smaller, but they diverge to a cyan line for $r_{\text{out}} > 500a$. We see that $\omega_0/\omega_Q = 0.18$ behaviour stops for sufficiently large CFR. Lower panel: frequencies in units of the pressure cavity frequency. We plot the numerical BVP solution for $q = 0$ (equation 9.23) in a dashed black line. We see that this value is in agreement with numerical BVP solutions for $\omega_Q/\omega_P > 10^5$.

We can use figure (9.9) to explain why the outer radius dependence was not noticed before (Muñoz and Lithwick, 2020); for $\omega_Q/\omega_P \lesssim 10^2$, the solutions are not dependent on outer radius, as long as $r_{\text{out}} \gtrsim 100a$.

9.2.3 The entire CFR range

Just like in section (9.1.3), we want to visualise the frequency value without scaling it with pressure or quadrupole effects.

In figure (9.10), we set $r_{\text{out}} = 450a$ for two reasons. First, so that we can compare it directly to figure (8.4). Second, the solutions converge (figure 9.9) at approximately this value of the outer disk radius so this shows the limiting (large outer disk radius) behaviour as well.

In it, we see that the converging behaviour of ω_0 to $\omega_0 = 0.18\omega_Q$ for all h predicted by Muñoz and Lithwick (2020) lasts only up to $q \approx 10^{-4}$. For $q < 10^{-4}$, the frequency solutions diverge.

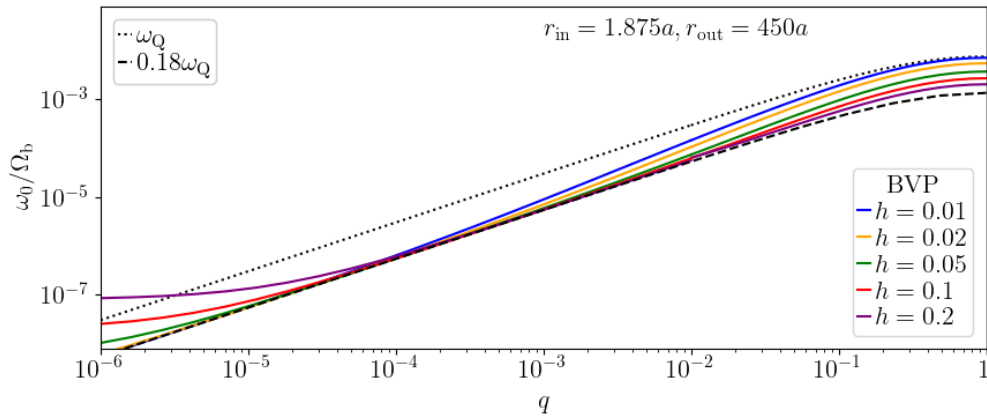


Figure 9.10.: Numerical BVP lowest mode frequency in units of the binary precession frequency, as a function of the binary mass ratio.

9.3 Mode location and width

A mode is trapped in area where $\omega \leq \omega_{\text{pot}}$, i.e. in between the two radial points where $k(r) = 0$. Therefore, a standard dispersion relation map ($kr - r$ plot) can be used to read the location and the width of a mode. In figure (9.11), we plot the dispersion map for WKB solutions for ω_0 .

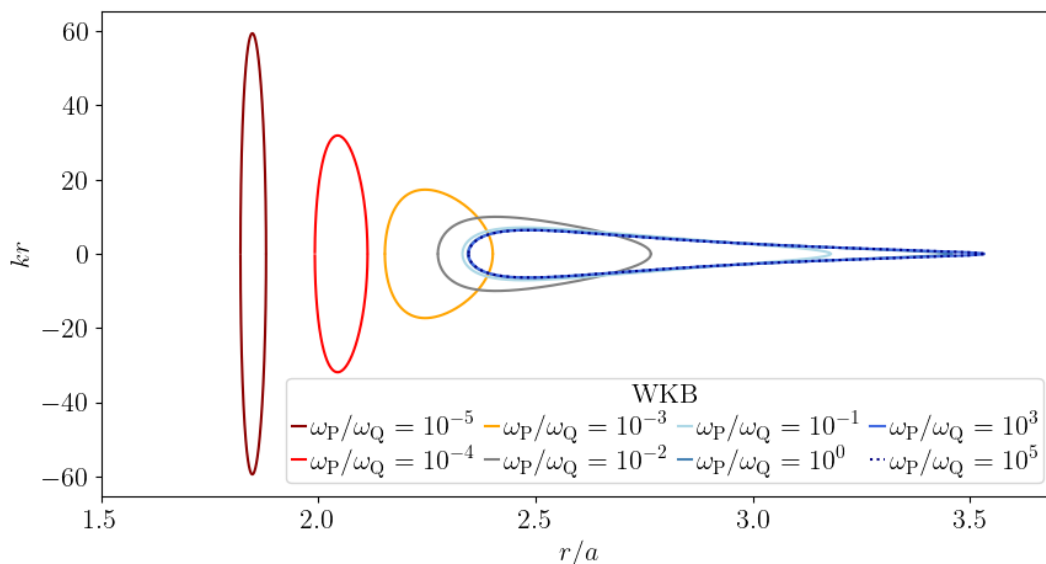


Figure 9.11.: Dispersion relation maps.

In figure (9.12), we plot the dispersion map for numerical BVP solutions for ω_0 .

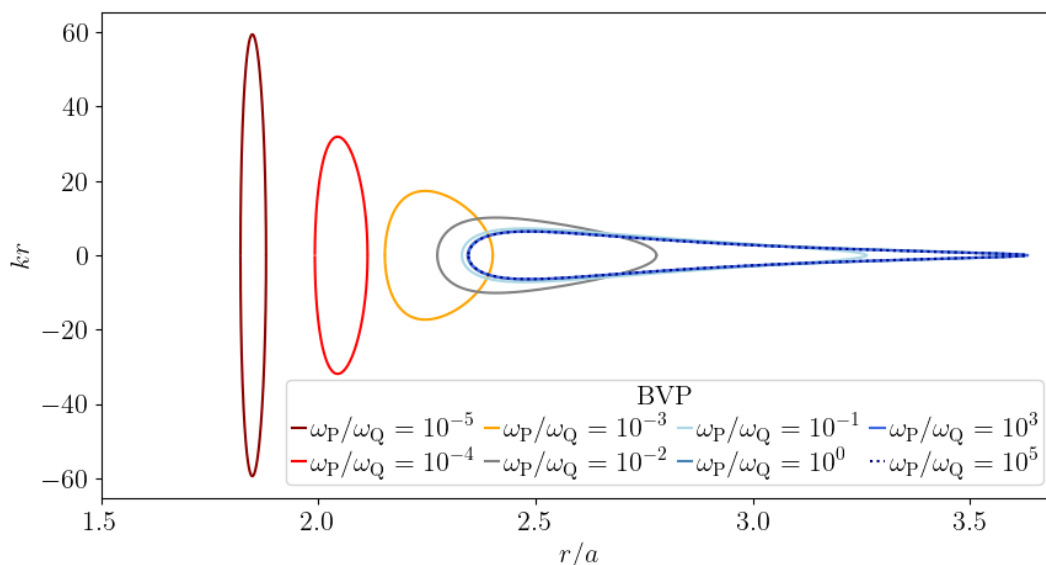


Figure 9.12.: Dispersion relation maps.

As expected, $kr - r$ lines for low CFR range frequencies are identical.

For high CFR range frequencies, where the BVP and the WKB solution are not in agreement, $kr - r$ lines still barely differ. To explain this, we turn to the right panel of figure (9.2). From it, we see that WKB frequencies are such that the potential below them (as low as $\omega_{\text{pot}} = 10^{-2}\omega_Q$) is basically a vertical line. Because of this, lower frequencies are still localised in the same area. Since BVP solutions are always lower than WKB solutions, they correspond to a mode with same turning points as the WKB frequencies.

We can show that in the high CFR range, a mode has to be trapped somewhere in area between $r \approx 2.2a$ and $r \approx 3.8a$. From the left panel of figure (9.5), we see that the eccentricity potential is positive at $2a \lesssim r \lesssim 3.8a$, and negative elsewhere. Therefore, if a mode exists, it has to be located within this area.

From figures (9.11) and (9.12), we see that increasing the CFR pushes the $n = 0$ mode to larger radius and increases its width. We also see that for higher CFRs, the 0-th mode location and width get more and more insensitive to changes in the CFR. No $n = 0$ mode is wider than $2a$, or located at $r > 4a$.

The width of area where the eccentricity has non-zero value is harder to estimate. In general, the eccentricity radial profile decays for $r > r_b$, where $r > r_b$ is the right turning point, that we can read from (9.12). But, figure (9.11) we can not say how fast it decays.

9.4 Summary

With respect to the mode location and width, we can divide the CFR range in two areas. For $\omega_P/\omega_Q < 0.1$, the location and the width of a mode depend on the CFR. For $\omega_P/\omega_Q > 0.1$, the location and the width of a mode are not dependent on the CFR. The modes are located in the area between $r \approx 2.2a$ and $r \approx 3.8a$.

WKB approximation is invalid for $\omega_P/\omega_Q > 0.1$. Numerical BVP solutions depend on the outer disk radius for $\omega_P/\omega_Q > 10$, but converge for a large outer radius ($r_{\text{out}} \gtrsim 500a$).

With respect to what effect the change of pressure and quadrupole influence has on eccentricity results, we can divide the CFR range of a large disk ($r_{\text{out}} \gtrsim 10^2a$) into three areas.

The CFR range $\omega_P/\omega_Q < 10$ is the area where frequency solutions sensitively depend on both h and q ; we can not write $\omega_0 \propto \omega_Q$ nor $\omega_0 \propto \omega_P$.

The CFR range $10 < \omega_P/\omega_Q < 10^5$ is the area of quadrupole dominance and frequency solutions depend only on q : $\omega_0 \approx 0.2\omega_Q$. The CFR range $\omega_P/\omega_Q > 10^5$ is the area of pressure dominance and frequency solutions depend only on h : $\omega_0 \approx 10^5\omega_P$.

Higher order modes

In the two examples we discussed in part (8) (figure (8.3)), we saw that one disk ($h = 0.1$, $q = 0.9$) supported just one mode, and the other one ($h = 0.03$, $q = 0.9$) supported two modes. In those two cases, we changed only the thickness of the disk. Muñoz and Lithwick (2020) state that a quantization condition can be satisfied by more than one frequency for a thin disk with $h \lesssim 0.05$.

In this chapter, we explore the number of possible modes in more detail. We want to know exactly how many modes a disk can support, and see more precisely how the disk thickness affects that number. Furthermore, we want to see if the number of modes can also be changed by changing the binary mass ratio q .

We are interested in higher modes because their existence means that disks in identical binary-disk systems can evolve in different ways. They can have different eccentricity profiles, and those profiles can be localized in different areas of the disk. In addition, the eccentricity profiles can precess with different frequencies. Therefore, if we want to find the full set of solutions for the eccentricity equation, we need to discuss higher order modes as well.

First, in section (10.1), we find the maximum number of possible modes as a function of h and q . Then, in section (10.2), we do an analysis of higher order mode frequencies and eccentricity profiles. Finally, in section (10.3), we summarize the main findings.

10.1 The number of modes

To find the maximum number of modes in terms of h and q , we use the WKB quantization condition.

There are two reasons for choosing the WKB quantization condition instead of numerically solving the BVP. First, the shooting method tends to give the lowest mode frequency. If we carefully choose several different initial guesses, we can obtain several different frequencies (if higher order modes are possible). However, this requires making an estimate of the frequency values for every combination of h and q . In addition to that, even if the shooting method provides us with different frequencies, we can not that those frequencies are all possible frequencies. For example, if we get 5 different frequency values using the shooting method, we can not know if those five are in order ($\omega_0, \omega_1, \omega_2, \omega_3$, and ω_4). If the frequency levels are dense, the shooting method can find some of the frequencies (for example $\omega_0, \omega_1, \omega_2, \omega_{10}$, and ω_{11}), in which case the ones in between get 'lost'. Unless we plot eccentricity profiles $E(r)$ for each ω , we can not know the order of the mode with that frequency. Again, this problem can in theory be solved by choosing a wide variety of initial guesses, but the method would still be impractical and unreliable.

On the other hand, using the WKB approximation condition (equation (8.33)) requires a choice of the mode order, so we always know which mode order we are working with. The second reason for choosing the WKB quantization is the fact that, in this section, we are only looking for the number of possible modes, and not their frequencies. In other words, the difference in the BVP and WKB solutions is irrelevant at the moment because we are not searching for values of ω , but only for the number of all possible ω -s.

We also want to see what $h - q$ areas are areas of the WKB approximation validity ($CFR < 0.1$). We use:

$$\frac{\omega_P}{\omega_Q} = \frac{h^2 \Omega_{cav}}{\frac{3q}{4(1+q)^2} (R_{cav}/a)^2 \Omega_{cav}} = \frac{h^2}{\frac{3q}{4(1+q)^2} (R_{cav}/a)^2} \quad (10.1)$$

to write $\omega_P/\omega_Q = 0.1$ as:

$$h = \sqrt{0.1 \frac{3q}{4(1+q)^2} \left(\frac{R_{\text{cav}}}{a}\right)^2}. \quad (10.2)$$

Equation (10.2) depends on the cavity size R_{cav} because we defined ω_P and ω_Q as the pressure and quadrupole frequencies at the cavity radius. Since the quadrupole and pressure influence are different power laws, their ratio is dependent on the cavity size. Like in most of this work, we set $R_{\text{cav}} = 2.5a$.

In figure (10.1), we plot the maximum number of allowed modes for $10^{-6} \leq q \leq 1$ and $10^{-4} \leq h \leq 0.2$. We highlight $q-h$ areas that support a maximum of 5, 10, 20, 40, or 80 modes. We plot the $\omega_P/\omega_Q = 0.1$ line; the area above it is the area where the WKB approximation breaks down, the area below it is the area where the WKB frequencies are exact.

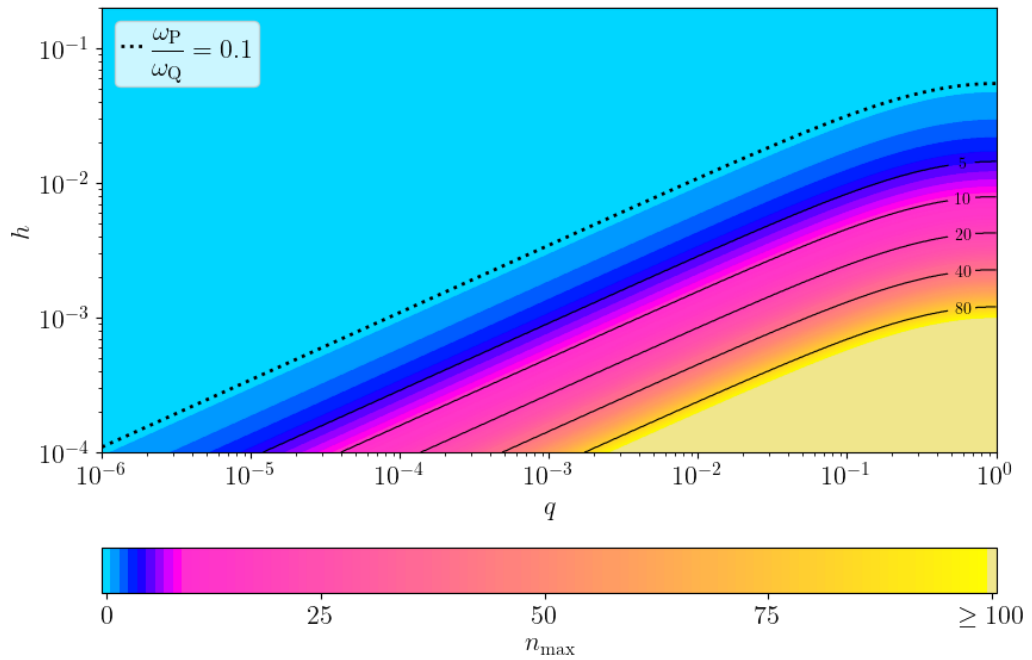


Figure 10.1.: The highest possible mode order as a function of the binary mass ratio and the thickness of the disk (colored lines). Lines $n_{\text{max}} = [5, 10, 20, 40, 80]$ is solid black lines for reference. The area where the WKB approximation gives correct ω_0 values is below the dotted black line. The cavity size of the disk is taken to be $R_{\text{cav}} = 2.5a$

In figure (10.2), we plot the same results as in figure (figure (10.1)), but in linear h and q scales.

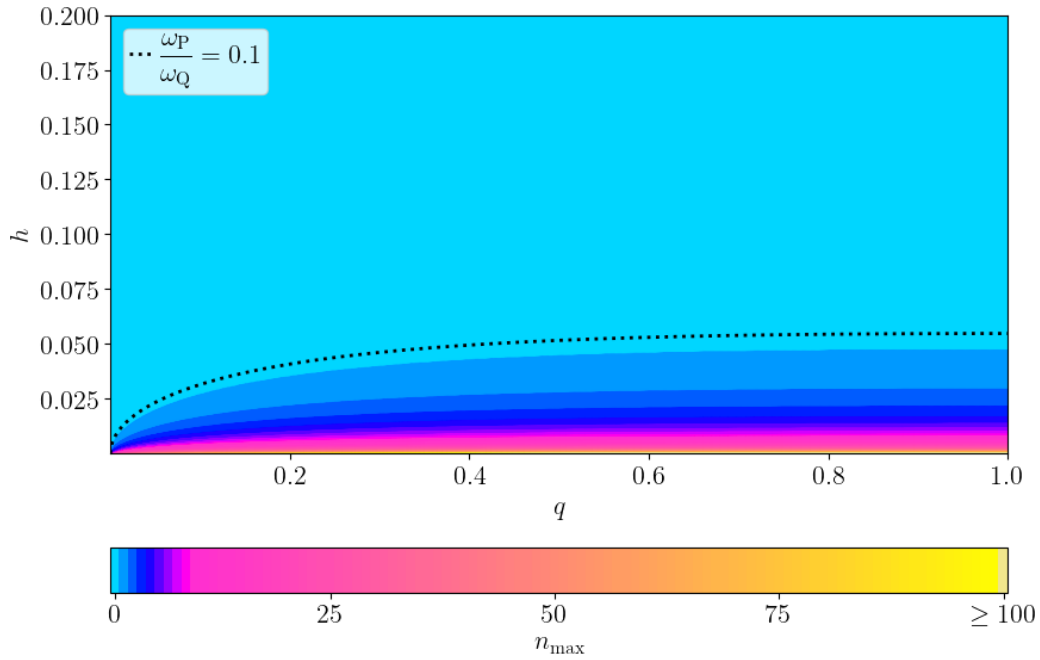


Figure 10.2.: Maximum number of possible modes as a function of binary mass ratio and the thickness of the disk for a disk with a cavity size $R_{\text{cav}} = 2.5a$. Same as figure (10.1), but in a linear scale.

We quickly check that these solutions are consistent with the ones from part 8. From figure (10.2), we see that for $h = 0.1$ and $q = 0.9$, $n_{\text{max}} = 0$, which is agreement with what we see in figure (8.3). Similarly, we see that for $h = 0.03$ and $q = 0.9$, $n_{\text{max}} = 1$, which is agreement with what we see in figure (8.3). We now use figures (10.1) and (10.2) to show important properties.

From figure (10.2), we see that roughly 4/5 of explored $q - h$ area supports only a single mode. We also see that higher order modes are impossible for $h \gtrsim 0.05$. However, this is only partly in agreement with a statement that higher modes are possible for $h \lesssim 0.05$ (Muñoz and Lithwick, 2020). Instead, from figure (10.1), we see that for $h \lesssim 0.05$, the possibility of a higher order mode depends on the binary mass ratio. We use figure (10.2) to show why the dependence on q is not visible in the $h - q$ range used in part 8. We see that for thick disks and near equal mass binaries, n_{max} areas are almost horizontal lines and n_{max} is a function of h only.

From figure (10.1), we see that every higher mode is supported by a smaller $q - h$ area. For $n_{\text{max}} \gtrsim 10$, areas of constant n_{max} become thin lines. This allows us to comment the stability of n_{max} on changes of h and q . For example, for $h = 0.1$, we see that $n_{\text{max}} = 0$ for every $q \in [10^{-6}, 1]$. On the other hand,

for $h = 10^{-3}$, n_{\max} depends on q and can be $0 < n_{\max} < 100$. We conclude that the number of possible modes depend on q more for smaller h . Similarly, the number of possible modes depend on h more for higher q .

To observe how n_{\max} grows with h , we focus on $q = 1$ part of the figure (10.1). We see that the maximum number of possible modes doubles in equal spacing of h (in a log-log graph). If this behaviour continues, n_{\max} would grow indefinitely. This indicates that the frequency spectrum becomes quasi-continuous. We show one example of this behaviour in section (10.2).

Stability of the disk radial eccentricity profile and frequency

We make an estimate of how an increased number of possible modes affects the stability of eccentricity solutions. A thick ($h = 0.1$) disk around an equal mass binary $q = 1$ can support only one mode. If the eccentricity profile or frequency are perturbed, it can reach a steady state again only by going back to that one mode. A thinner ($h = 0.04$) disk around an equal mass binary $q = 1$ can support two modes. If that disk is perturbed, it can reach a steady state by going to any of the two modes or to any of linear combinations of those two modes. A thin mode ($h = 0.0001$) around an equal mass binary ($q = 1$) can support modes of virtually continuous frequency spectrum $\omega \in [0, \max(\omega_{\text{pot}})]$ (figure (10.3)). A minor perturbation of such a disk in a steady state is most likely still a steady state, and the disk will stay in that state.

10.2 Higher mode frequencies, eccentricity profiles and the location of higher order modes

We saw in figure (10.1) that the entire $q - h$ space that supports higher order modes is located in the area where the WKB quantization condition gives the correct lowest mode frequency (ω_0). Now, we convince ourselves that it gives correct higher mode frequencies (ω_n) as well. To do so, we turn to quantum mechanics results by Ma and Xu (2005). They show how an exact quantization condition for a function $\Psi(r)$ that is a solution of a Schrodinger equation:

$$\frac{d^2\Psi}{dr^2} = k(r)^2\Psi \quad (10.3)$$

can be written as:

$$\int_{r_a}^{r_b} k(\omega_n, r) dr = (n + 1)\pi + Q, \quad (10.4)$$

where Q is called the quantum correction and has the same value for all n . In the WKB quantization condition, the correction is taken to be:

$$Q_{\text{WKB}} = -\frac{\pi}{2}. \quad (10.5)$$

Since we saw that for $\omega_P/\omega_Q \leq 0.1$, the WKB quantization condition gives correct values of ω_0 , we conclude that the WKB quantum correction is exact for $n = 0$. This, combined with the upper discussion, tells us that this correction is then exact for all $n \geq 0$. Therefore, we expect the WKB frequencies to be exact for all order modes as long as $\omega_P/\omega_Q \leq 0.1$.

A thin disk around an equal mass binary.

We set $q = 1$ and $h = 0.001$, and use it as an example to visualise higher order modes. We are interested in the mode frequency, location, width and the eccentricity profile. We use the WKB quantization condition to find all possible modes. In left panel in figure (10.5), we plot the eccentricity potential and frequencies of all possible modes. Next, we choose five different modes $n \in [0, 1, 10, 20, 90]$ that we will discuss in more detail and plot them in the right panel of figure (10.5).

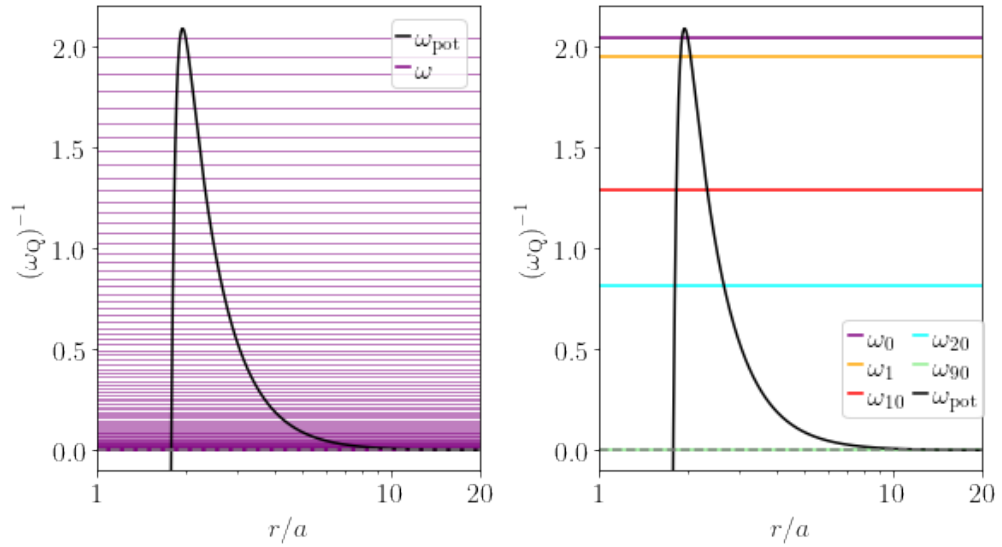


Figure 10.3.: Left panel: eccentricity potential (black) as a function of radius scaled with binary separation in units of the quadrupole frequency at the cavity radius. Frequencies of all possible modes ω_n (purple). Right panel: same as left, with five highlighted modes ($n \in [0, 1, 10, 20, 90]$).

We first use these 5 modes to verify the accuracy of WKB results. We use two numerical methods of solving the BVP: the shooting method and a python BVP solver. Both of these are sensitive to initial guesses so we use several values close to the WKB results as initial guesses. All three methods give same results:

$$\begin{aligned}
 \omega_0 &= 2.04\omega_Q = 0.0155\Omega_b \\
 \omega_1 &= 1.95\omega_Q = 0.0148\Omega_b \\
 \omega_{10} &= 1.29\omega_Q = 0.00979\Omega_b \\
 \omega_{20} &= 0.811\omega_Q = 0.00615\Omega_b \\
 \omega_{90} &= 0.00192\omega_Q = 0.0000146\Omega_b.
 \end{aligned} \tag{10.6}$$

All eccentricity profiles presses with a frequency much smaller than the binary precession frequency: $\omega_n \lesssim 10^{-2}\Omega_b$. The frequencies can differ by several orders of magnitude ($\omega_{90}/\omega_0 = 10^{-3}$).

From figure (10.3), we see that the left turning point of every order mode is at the approximately same location. We also see that the right turning point of every $n = m$ mode is further out than all $n < m$ modes. So we expect every higher order mode to be less localised. In figure (10.4), we plot the frequency dispersion map.

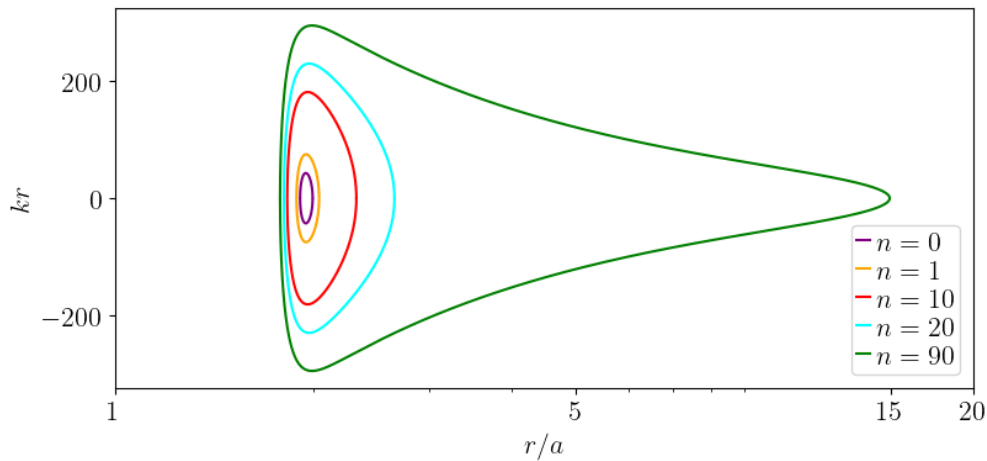


Figure 10.4.: Frequency dispersion maps for 0-th (purple), 1 – st (orange), 10-th (red), 20-th (cyan), and 90-th (green) mode in a disk of thickness $h = 0.001$ around an equal mass binary ($q = 1$).

In figure (10.5), we plot eccentricity profiles $E(r)$ for modes $n = [0, 1, 10, 20, 90]$. These profiles allow us to do a consistency check. The n -th mode should have n nodes within area where $\omega \leq \omega_{\text{pot}}$, and decay for $\omega > \omega_{\text{pot}}$. Comparing figures (10.3) and (10.5), we see that this is true.

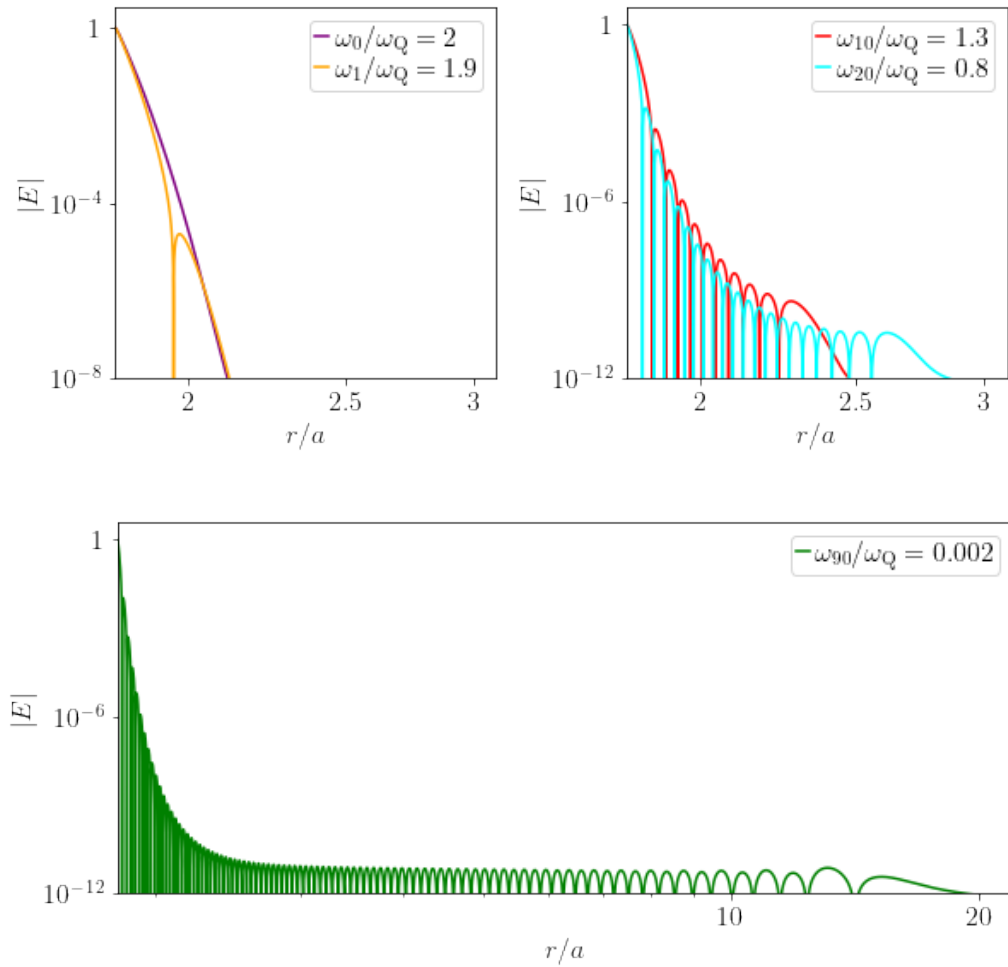


Figure 10.5.: Absolute values of eccentricity profiles as functions of radius in units of the binary separation (a) for five modes in a thin disk ($h = 10^{-3}$) around an equal mass binary ($q = 1$). All five eccentricity profiles are scaled to $E = 1$ at the inner boundary. Upper left: eccentricity profiles of the 0-th mode (purple) and the 1-st mode (orange). Upper right: eccentricity profiles of the 10-th mode (red) and the 20-th mode (cyan). Lower panel: eccentricity profiles of the 90-th mode (green).

10.3 Summary

Higher order modes are possible only in the range where the WKB approximation gives exact solutions. This fact can simplify finding eccentricity solutions, because for higher and/or densely spaced modes, numerical BVP methods are impractical.

The number of possible modes depends on both the disk thickness h and the binary mass ratio q . We can write three general rules concerning n_{\max} . One, thinner disks around binaries of a more equal mass can support higher modes. Two, the number of possible modes in a disk is more sensitive to changes of q if the disk is thin. Three, the number of possible modes in a disk around a binary is more sensitive to changes of h if the binary components are near-equal mass.

Possible precession frequencies of an eccentric circumbinary disk with $\text{CFR} \ll 1$ are almost continuous and can take any positive value of the eccentricity potential.

Every m -th mode is less localized than every $n < m$ mode. In areas of the disk further away from the binary, the eccentricity will be non-zero only if the disk is in a higher order mode.

Since the eccentricity of a disk can be any linear combination of possible modes, the time evolution of a thin disk can be far more complicated than the evolution of a thick ($h > 0.05$) disk.

Eccentricity solutions as a function of density

Up to now, we used the density profile:

$$\Sigma = \Sigma_0 \left(r^{-0.5} - Lr^{-1} \right) e^{-(R_{\text{cav}}/r)^Z}, \quad (11.1)$$

with $L = 0.7$, $R_{\text{cav}} = 2.5a$, and $Z = 12$.

In this chapter we wish to see how much this density profile affects eccentricity results and in what way. In section (11.1), we keep $R_{\text{cav}} = 2.5a$ and $Z = 12$, and we change L . In section (11.2), we keep $L = 0.7$ and $Z = 12$, and we change the value of R_{cav} . In section (11.3), we keep $L = 0.7$ and $R_{\text{cav}} = 2.5a$, and we change the value of Z .

11.1 The torque exerted on the binary by the disk

In part 8, we found eccentricity solutions for one value of the torque exerted on the binary by the disk (L). Now we see how L affects ω/ω_Q solutions. Duffell *et al.* (2020b) showed that the value of L depends on the binary mass ratio. Since only the pressure eccentricity contributions depend on the density, we expect L to make a difference only for higher CFRs, and in that range, (Duffell *et al.*, 2020b), $0 \lesssim L \lesssim 1$. We can not draw a parallel between that binary-disk set up and ours, but we use $L = [0, 0.5, 0.7, 0.9, 1]$ as a very rough idea of what the value of L might be. In figure (11.1), we plot density profiles (equation (11.1)) for $R_{\text{cav}} = 2.5a$ and $L = 0.7$.

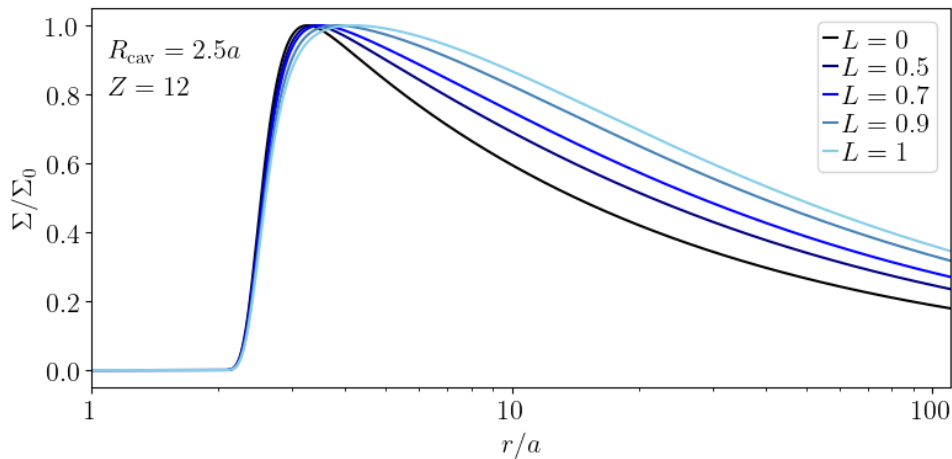


Figure 11.1.: Radial density profiles of a disk with a cavity of size $R_{\text{cav}} = 2.5a$ and cavity slope $Z = 12$ for $L = [0, 0.5, 0.7, 0.9, 1]$.

For a fixed disk size, cavity size, and the cavity slope, we can write (equation (11.3)):

$$\frac{\omega}{\omega_Q} = f\left(L, \frac{\omega_Q}{\omega_Q}\right). \quad (11.2)$$

In figure (11.2), we plot frequency solutions represented by equation (11.2). From it, we see that the change of L does not change solutions for $\omega_P/\omega_Q \lesssim 0.1$. For $\omega_P/\omega_Q \gtrsim 0.1$, the frequency is larger for smaller L .

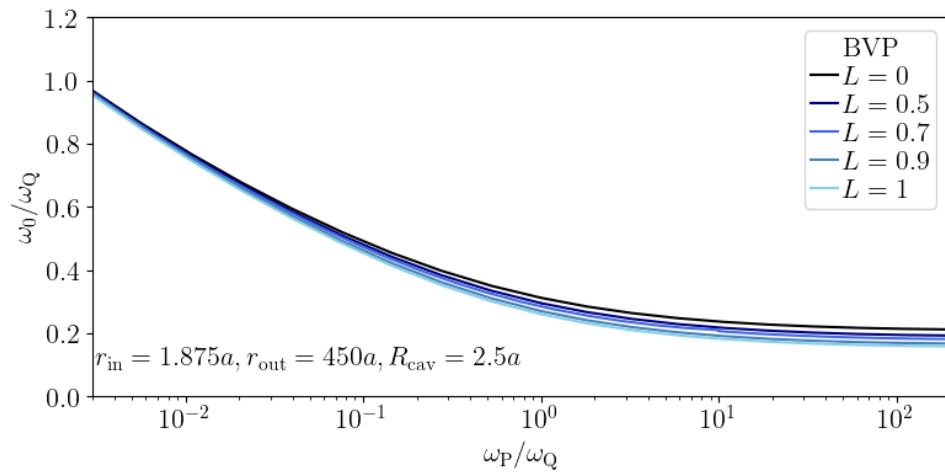


Figure 11.2.: The lowest mode frequency in units of the cavity quadrupole frequency as a function of the CFR for $L = [0, 0.5, 0.7, 0.9, 1]$.

11.2 The size of the disk cavity

In figure (8.5), we saw that the cavity size in range $2.5a \leq R_{\text{cav}} \leq 5a$ does not change solutions. However, in section (11.1), we saw that a change in L can cause a slight change for large CFRs. In Appendix I, we show that, for the density profile (11.1), frequency solutions depend on R_{cav} and L only as a product $LR_{\text{cav}}^{-1/2}$. Therefore, we write:

$$\frac{\omega}{\omega_Q} = f\left(LR_{\text{cav}}^{-1/2}, Z, \frac{\omega_P}{\omega_Q}\right). \quad (11.3)$$

Since solutions depend on the product $LR_{\text{cav}}^{-1/2}$, we expect that a wider range of cavity sizes can make the difference in eccentricity solutions visible. Therefore, we widen the cavity size range to $R_{\text{cav}} = [1.5a, 4a, 6a, 10a]$. In figure (11.3), we plot density profiles (equation (11.1)) for $L = 0.7$ and $Z = 12$.

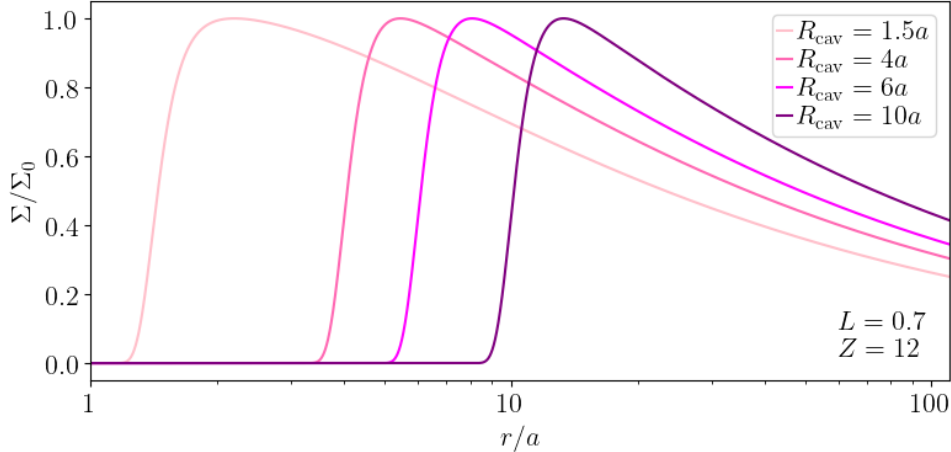


Figure 11.3.: Radial density profiles of a disk with $Z = 12$ and $L = 0.7$ for cavity sizes $R_{\text{cav}} = [1.5a, 4a, 6a, 10a]$.

In figure (11.4), we plot. From it, we see that the cavity size can change solutions only for $\omega_P/\omega_Q \gtrsim 0.1$.

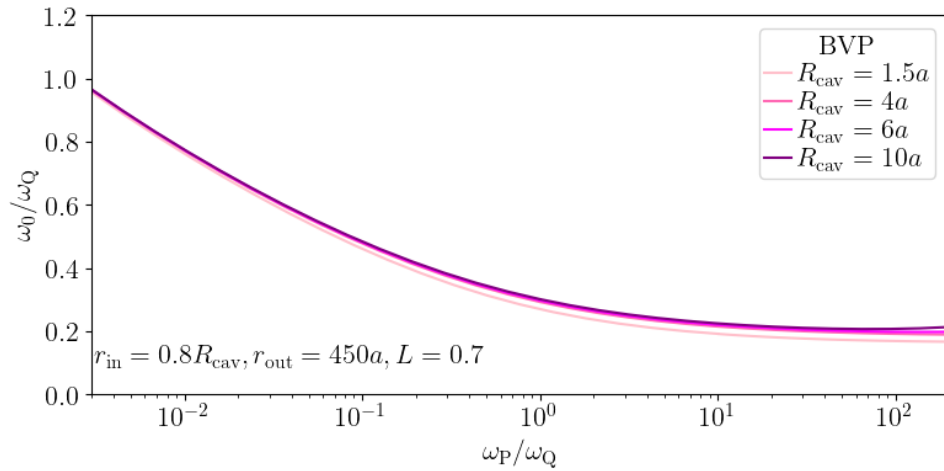


Figure 11.4.: The lowest mode frequency in units of the cavity quadrupole frequency, as a function of the CFR. $L = 0.7$ and $r_{\text{out}} = 450a$. The disk cavity size is $R_{\text{cav}} = [1.5a, 4a, 6a, 10a]$, and the inner disk radius is taken to be $r_{\text{out}} = 0.8r_{\text{cav}}$.

Here, we discuss the choice of the density cutoff function. First, in section (11.4), we show that the cutoff function we used to create a cavity greatly influences all eccentricity solutions. Next, in section (11.5), we explain why the cutoff function dominates eccentricity results. Then, in section (11.3), we change the cutoff exponent and see how that changes solutions for lowest mode frequencies. Finally, in section (11.6), we use the findings of this chapter to write the eccentricity equation in a simplified form and to explain some of the results from earlier chapters.

11.3 The cutoff exponent

Now we want to see how the change of the cutoff exponent Z influences eccentricity results. In figure (11.6), we plot density profiles (equation (11.1)) for $R_{\text{cav}} = 2.5a$, $L = 0.7$, and $Z = [4, 6, 12, 18]$.

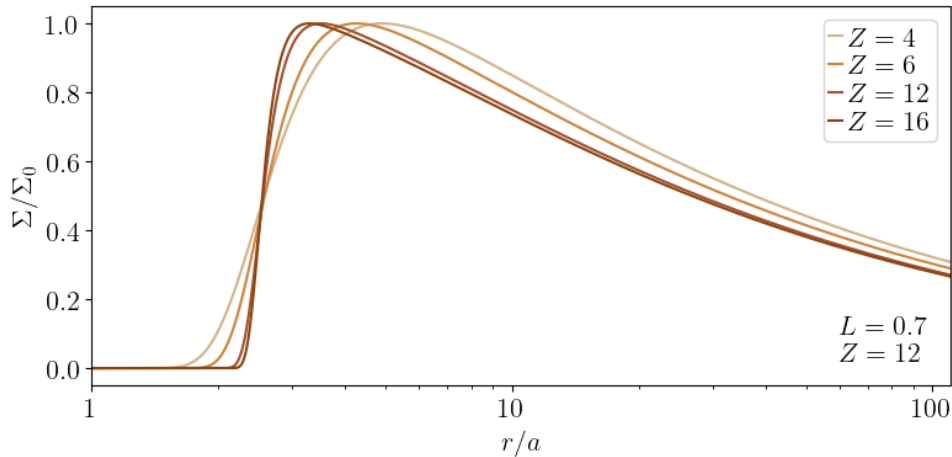


Figure 11.5.: Radial density profiles of a disk with $R_{\text{cav}} = 2.5a$ and $L = 0.7$ for $Z = [4, 6, 12, 18]$.

In figure (11.6), we plot numerical BVP solutions for ω_0 .

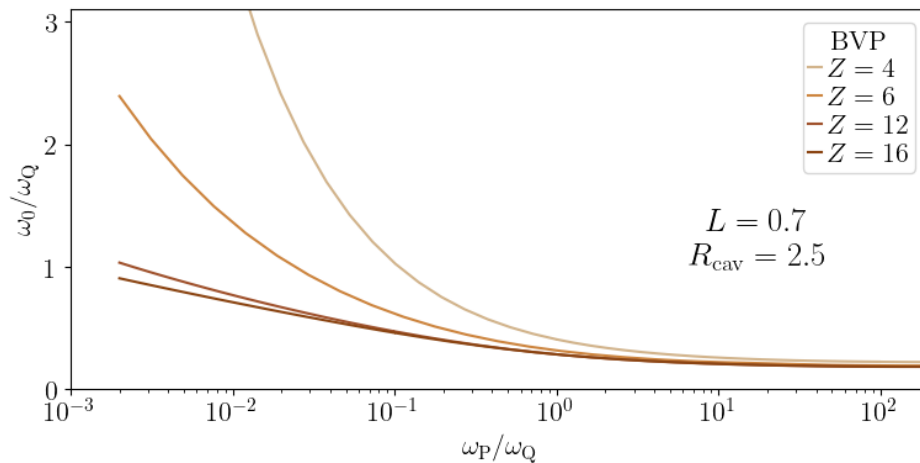


Figure 11.6.: Caption

The change of the cutoff exponent significantly changes frequencies in the low CFR range. It does not change results in the high CFR range. Because we a

change in solutions, we explore the change of the cutoff exponent a bit more. In figure (11.7), we plot numerical BVP and WKB solutions for each Z

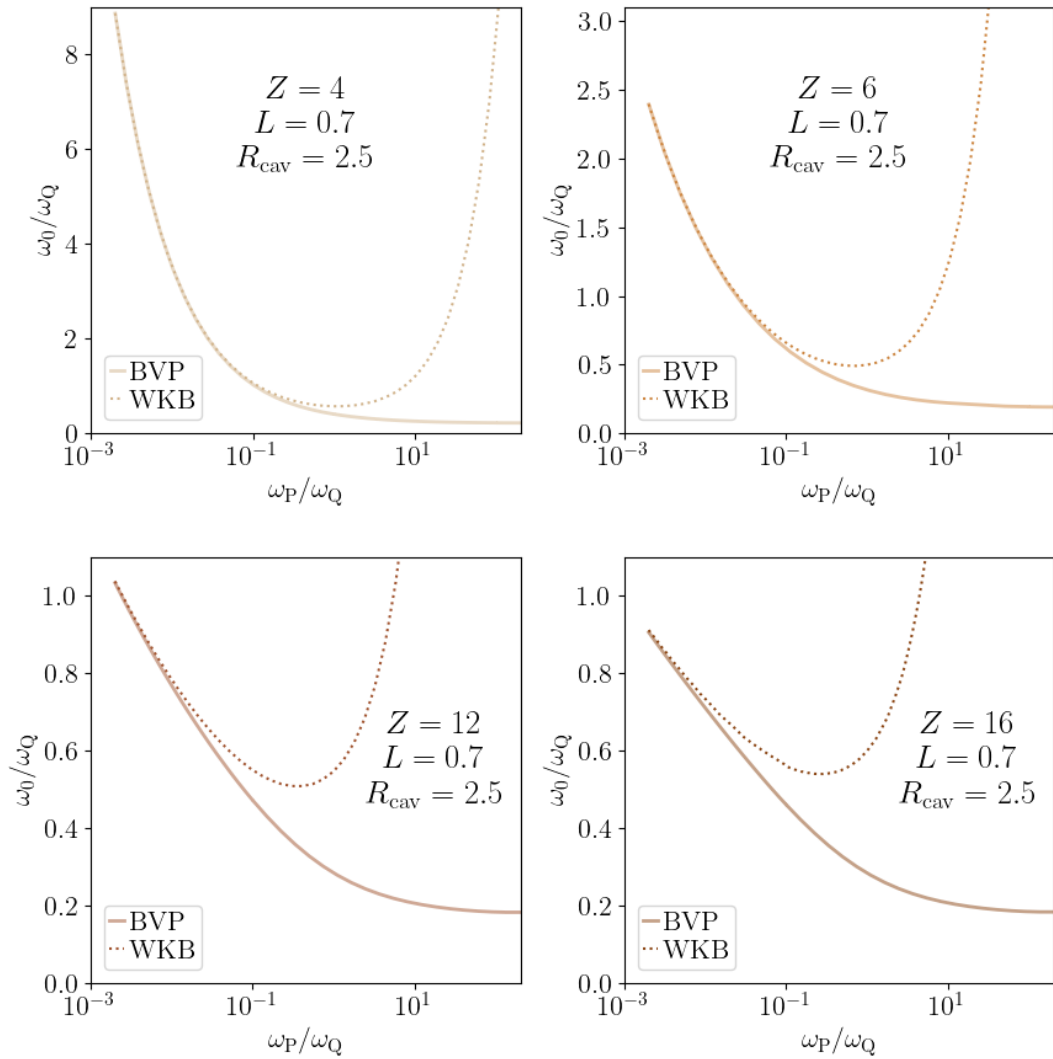


Figure 11.7.: Comparison of WKB and numerical BVP frequencies ω_0 for each Z .

From figure (11.7), we see that the agreement between WKB and numerical BVP solutions is better for lower Z .

11.4 Illustration of the importance of the cutoff function.

We saw that the only density parameter that caused eccentricity solutions to change was the cutoff exponent, and it influenced solutions greatly. That motivates us to see just how much eccentricity solutions are determined by the cutoff function.

To illustrate this, we solve the eccentricity equation in same ways as in part (8). This time, we do it for a density profile described by just the cutoff function:

$$\Sigma = e^{-(2.5/r)^{12}}. \quad (11.4)$$

We plot these results, along with results for the density profile:

$$\Sigma = \Sigma_0 (r^{-0.5} - Lr^{-1}) e^{-(R_{\text{cav}}/r)^2}, \quad (11.5)$$

that we found in part 8.

We start by comparing frequency results. In figure (11.8), we plot ω_0 WKB and numerical BVP solutions. The agreement between solutions for both density profiles is worse for higher CFRs, but is not significant.

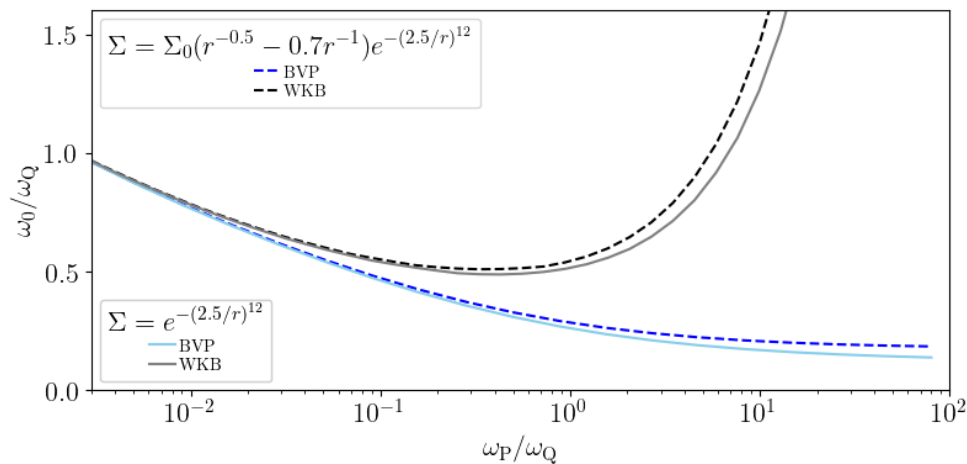


Figure 11.8.: Frequency solutions ω_0/ω_Q as a function of the CFR. Comparison of results obtained using just the cutoff function (solid lines) and results obtained using the full density profile (dashed lines).

Now that we know that the frequency solutions are determined by the cutoff function, we see if the same is true for the eccentricity profile. In figure (11.9), we plot eccentricity profiles for $h = 0.1$ and $q = [0.1, 0.2, 0.4, 0.6, 1]$.

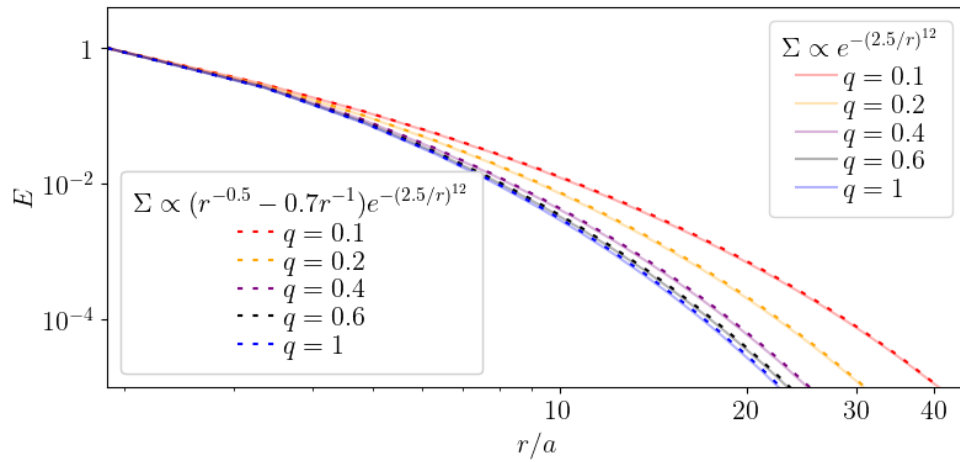


Figure 11.9.: Radial eccentricity profiles for $h = 1$ and $q = [0.1, 0.2, 0.4, 0.6, 1]$. Comparison of results obtained using just the cutoff function (solid lines) and results obtained using the full density profile (dashed lines).

Next, we compare scaled eccentricity solutions. In figure (11.10), we plot; eccentricity profiles $E(r)$ and scaled eccentricity profiles $y(r)$ profiles for $\omega_P/\omega_Q = 0.05$ and $\omega_P/\omega_Q = 50$. From it, we can see that the agreement is worse for larger CFRs, but even then, the agreement is great.

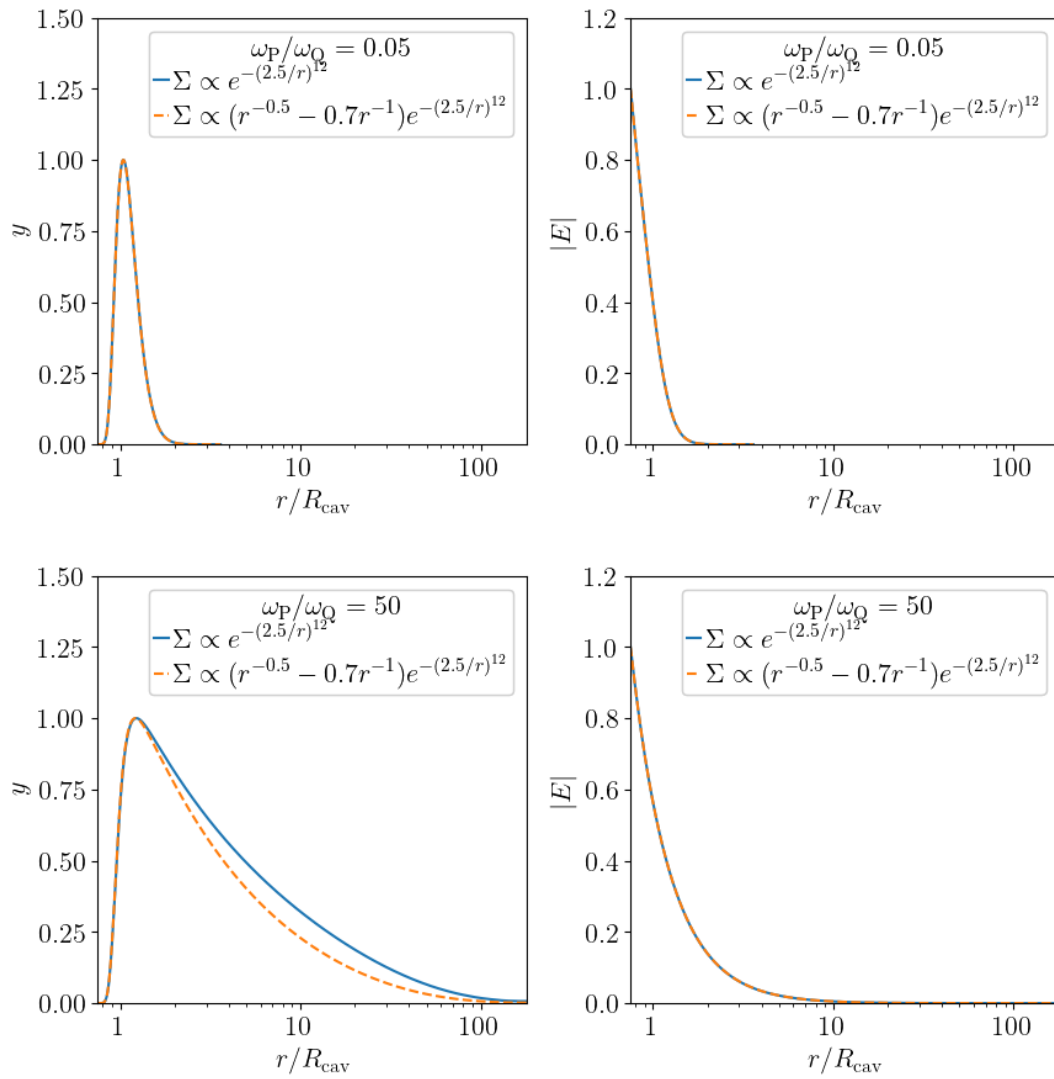


Figure 11.10.: Scaled eccentricity profiles (left panels) and eccentricity profiles (right panels) for $\omega_P/\omega_Q = 0.05$ (upper panels) and $\omega_P/\omega_Q = 50$ (lower panels). Comparison of results obtained using just the cutoff function (solid lines) and results obtained using the full density profile (dashed lines).

11.5 Explanation of the dominance of the density cutoff function on all eccentricity results

We saw in figures (11.9), (11.10), and (11.8) that results from part (8) can be reproduced by taking the density profile to be equal to just the cutoff function. To explain why the cutoff function dominates results, we discuss the differences between a cut disk (11.4), a combined disk (11.5), and an the extended disk:

$$\Sigma = \Sigma_0 \left(\left(\frac{r}{a} \right)^{-0.5} - 0.7 \left(\frac{r}{a} \right)^{-1} \right). \quad (11.6)$$

In figure (11.11), we plot all three density profiles.

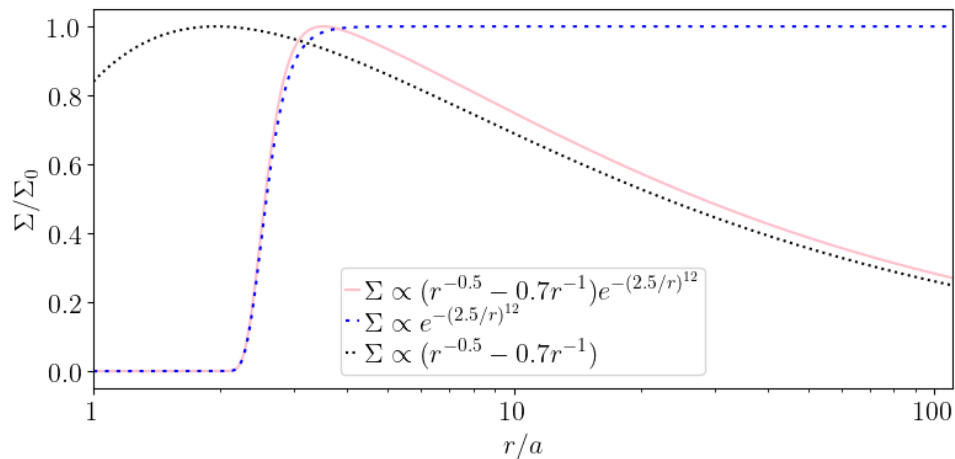


Figure 11.11.: Density profiles of cut, extended and combined disks.

From figure (11.11), we see that for $r < 3a$, the agreement between the cut and the combined density profile is excellent. For $r > 3a$, the agreement between the extended and the combined density profile is excellent.

In figure (11.12), we plot the pressure eccentricity potential. We see that the general shape of the potential well is determined by the cutoff function. In addition, the well is entirely located at $r < 4a$, which is the area where (figure (11.11)) the combined density shows no dependence on the extended density. In other words, when we model a cavity in an extended disk with an exponential cutoff function, a potential well is created entirely in the area where the information on the original density is lost.

Since modes are trapped inside the well, we conclude that all eccentricity results will be determined by the cutoff function.

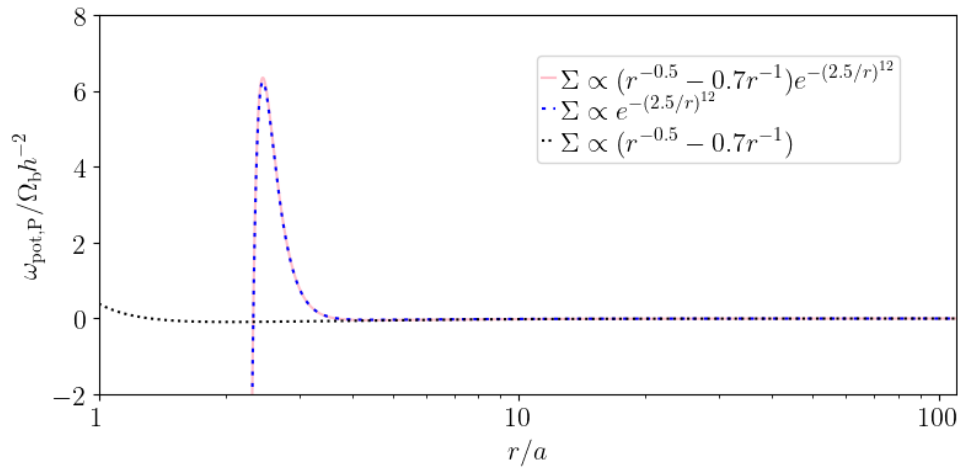


Figure 11.12.: Pressure eccentricity potentials for a cut, extended, and a combined disk.

We write the pressure potential eccentricity potential as:

$$\frac{\omega_{\text{pot,P}}(r)}{h^2 \Omega_b} = \frac{r^{-1/2} \Sigma'}{4\Sigma} + \frac{r^{1/2} \Sigma'^2}{8\Sigma^2} - \frac{r^{1/2} \Sigma''}{4\Sigma} - \frac{3r^{-3/2}}{4}. \quad (11.7)$$

In figure (11.13), we plot all terms of equation (11.7) for density profiles of a cut, extended and a combined disk.

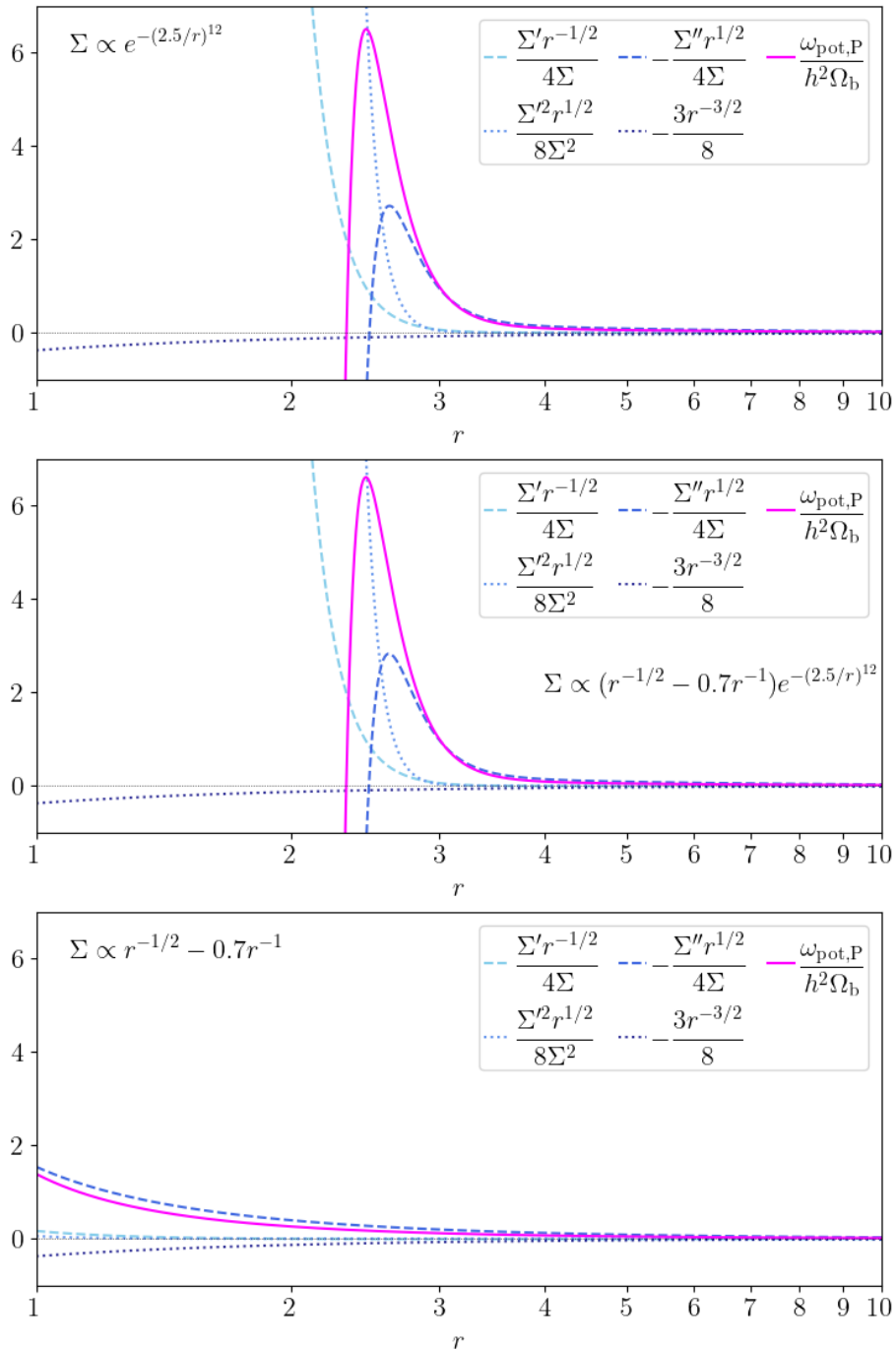


Figure 11.13.: Total pressure eccentricity potential in pink. Each of the four terms contributing to this potential (equation (11.7)) in blue.

In the eccentricity potential (equation (11.7)), the density appears only in ratios Σ , $\partial\Sigma/\partial r$, and $\partial^2\Sigma/\partial r^2$, so for a combined disk, the exponential function gets canceled out. We explain why the exponential cutoff dominates eccentricity solutions anyway. A first derivative of a function $f(r)$ that is a product of two other functions $h(r)$ and $g(r)$:

$$f(r) = h(r)g(r), \tag{11.8}$$

is:

$$\frac{f'}{f} = \frac{h'g + hg'}{fg} = \frac{h'}{h} + \frac{g'}{g}, \quad (11.9)$$

and its second derivative is:

$$\frac{f''}{f} = \frac{h''g + h'g' + h'g' + hg''}{fg} = \frac{h''}{h} + \frac{g''}{g} + 2\frac{h'g'}{hg}. \quad (11.10)$$

We conclude that if the derivative of one function (h or g) is a lot larger than the derivative of the other function (h or g), then the derivative of the product of those two functions (f) will be approximately equal to just the derivative of that one function.

The combined density profile density profile (11.5) is a product of two functions (11.6) and (11.4), so we set:

$$h(r) = r^{-1/2} - Lr^{-1}, \quad (11.11)$$

and:

$$g(r) = e^{-(R_{\text{cav}}/r)^Z}. \quad (11.12)$$

We find derivatives as:

$$\frac{h'}{h} = \frac{-\frac{1}{2}r^{-3/2} + Lr^{-2}}{r^{-1/2} - Lr^{-1}} \propto r^{-1}, \quad (11.13)$$

and:

$$\frac{h''}{h} = \frac{\frac{3}{4}r^{-5/2} - 2Lr^{-3}}{r^{-1/2} - Lr^{-1}} \propto r^{-2}, \quad (11.14)$$

$$\frac{g'}{g} = \frac{Zr^{-1} \left(\frac{R_{\text{cav}}}{r}\right)^Z e^{-(R_{\text{cav}}/r)^Z}}{e^{-(R_{\text{cav}}/r)^Z}} = Zr^{-1} \left(\frac{R_{\text{cav}}}{r}\right)^Z \propto r^{-Z-1}, \quad (11.15)$$

and:

$$\frac{g''}{g} = Zr^{-2} \left(\frac{R_{\text{cav}}}{r}\right)^{2Z} + (Z^2 - Z)r^{-2} \left(\frac{R_{\text{cav}}}{r}\right)^Z \propto r^{-2Z-2}. \quad (11.16)$$

Ratios Σ'/Σ and Σ''/Σ are power laws for both h and g . But, the former power law is so much greater than the latter one that the total density derivatives can be approximated with the derivative values of g .

11.6 Summary

Eccentricity results do not depend on L and R_{cav} for low CFRs. Eccentricity results weakly depend on L and R_{cav} for high CFRs.

Eccentricity results are very dependant on the steepness of the cavity slope for low CFRs. Eccentricity results are independents on the steepness of the cavity slope for higher CFRs.

Results from part 8 can be entirely reproduced by taking the density profile:

$$\Sigma = \Sigma_0 e^{-(R_{\text{cav}}/r)^Z}, \quad (11.17)$$

instead of:

$$\Sigma = \Sigma_0 \left(r^{-0.5} - Lr^{-1} \right) e^{-(R_{\text{cav}}/r)^Z}. \quad (11.18)$$

The cutoff function not only allows for modes to exist, but also completely determines the eccentricity results.

The findings of this chapter can be used to simplify the eccentricity problem for all CFRs; we can use the cutoff density profile to write the eccentricity differential equation as:

Simplified eccentricity equation for a locally isothermal circumbinary disk

$$E''(r) = E'(r) \left[-Z \left(\frac{R_{\text{cav}}}{r} \right)^Z r^{-1} - 3r^{-1} \right] + E(r) \left[-2Z \left(\frac{R_{\text{cav}}}{r} \right)^Z r^{-2} + \frac{2}{h^2} \frac{\omega}{\Omega_b} r^{-1/2} - \frac{1}{h^2} \frac{3q}{2(1+q)^2} r^{-4} \right], \quad (11.19)$$

or, in terms of $R \equiv r/R_{\text{cav}}$, as:

Simplified eccentricity equation for a locally isothermal circumbinary disk as a function of a scaled radius R

$$\frac{d^2 E}{dR^2} = \frac{dE}{dR} \left[-ZR^{-Z-1} - 3R^{-1} \right] + E \left[-2ZR^{-Z-2} + 2\frac{\omega}{\omega_P} R^{-1/2} - \frac{\omega_Q}{\omega_P} R^{-4} \right]. \quad (11.20)$$

We can use equation (11.20) to find eccentricity solutions for any density profile (11.18), and still obtain results that are highly accurate or exact regardless of L and R_{cav} . Solving the simplified eccentricity equation numerically is faster compared to solving it for a profile (11.18).

To conclude, to solve the eccentricity equation for a general density profile (11.18), all we need is the cavity slope Z . For larger CFRs, we do not even need to know the exact slope, and any value of the slope (at least in the range $4 \leq Z \leq 16$ that we explored) will give correct results.

Summary and conclusion

In chapter 8, we showed how to use the recipes from part II on a locally isothermal disk in a stationary state. We then found known solutions (Muñoz and Lithwick, 2020) for a disk of a relatively high thickness ($h \geq 0.01$) around binaries with a higher mass ratio ($q \geq 0.03$). We reproduced most results from Muñoz and Lithwick (2020) to verify that our understanding of methods for solving the eccentricity equation is correct. Those results showed that the frequency of the lowest mode is in range $0.2\omega_Q \leq \omega_0 \leq \omega_Q$, and that quadrupole effects always dominate the eccentricity. Solutions were independent of the outer disk radius and pointed out a possibility of at least two disk eccentricity modes, with the number of modes being determined by the disk thickness. In addition, modes were located at $r > 2a$.

In chapters (III), (10.1), and (11), we turned to thinner disks ($10^{-4} \leq h \leq 0.2$), and disks around binaries of a more unequal mass ratio ($10^{-6} \leq q \leq 1$). We presented results as functions of the CFR.

In the low CFR range, the mode frequency can grow above $\omega_0 = \omega_Q$. The location and width of the 0-th mode depend on the CFR's exact value. The number of modes can grow up to at least a hundred. Different modes have different widths and can spread over significant portions of the disk. Solutions are not dependent on the outer disk radius, and the WKB and numerical BVP results are in perfect agreement. Solutions do not depend on L or R_{cav} and depend significantly on Z .

In the high CFR range, the location and the width of the lowest mode are not dependent on the CFR. There can only be one mode, and its location and width are fixed. Solutions depend on the outer disk radius, and the WKB approximation is invalid. Solutions weakly depend on L and R_{cav} , and are not dependent on Z .

We found that we can divide the CFR spectrum into two regions, each dependent on one set of parameters (density profile away from the cavity, the exact value of the CFR) and not on the other set of parameters (cavity slope, outer disk radius). Interestingly, disks from part 8 fall between those two regions.

Our results for thin disks are especially important as they make predictions for the disk behavior in a regime that we expect to be relevant astrophysical, and which has yet to be simulated. Accretion disks, such as disks in AGN (Bellovary *et al.*, 2016), are as thin as $10^{-4} \lesssim h$. However, these disks are hard to simulate, so simulations are only available for thicker disks. We showed that eccentricity results found by either solving the eccentricity equation or by simulating a thick disk should not be used to estimate the eccentricity solution for a thin disk.

Future prospects

We found that higher modes are possible, but we do not know how each of them is excited, nor the amplitude of different modes. To understand how different modes are excited and if the disk is more likely to settle on specific modes and not the others, we need to look at the time-dependent eccentricity equation. In other words, we need to set a forcing effect, such as resonance (chapter (5)), and solve the time-dependent equation.

It could also prove interesting to examine disks with cavities that are not described with exponential functions. A cutoff function describing a more gradual decay into the cavity might influence the solutions in a way that the information on the density profile away from the cavity is preserved (11.5).

A 3d treatment (section (3.3)) could be a better choice for finding eccentricity solutions for thick disks around binaries with $q \ll 1$. It could explain or counter the results found by treating it as a 2d disk.

Part IV

Appendix

Polar coordinate system

In a polar coordinate system, each point in a plane can be described with 2 coordinates: distance from the origin r , and an angle from the reference direction ϕ . To compare it to (x, y) coordinate system, we put the origin of both systems in the same place, and choose x direction as a reference direction for the polar system. We can then define the angle ϕ as:

$$\tan \phi = \frac{y}{x}, \quad (\text{A.1})$$

and radial distance r as:

$$r^2 = x^2 + y^2. \quad (\text{A.2})$$

This is illustrated in figure (A.1).

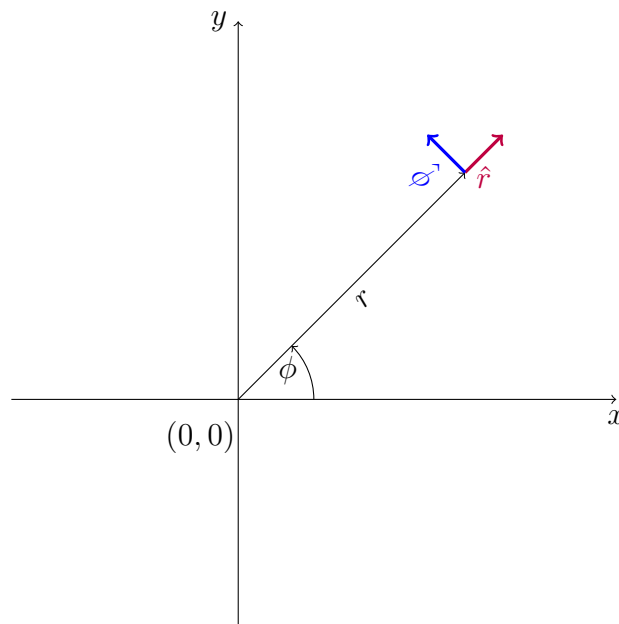


Figure A.1.: Polar coordinate system.

Unit vectors are orthogonal:

$$\hat{r} \cdot \hat{r} = \hat{\phi} \cdot \hat{\phi} = 1, \quad (\text{A.3})$$

$$\hat{r} \cdot \hat{\phi} = 0. \quad (\text{A.4})$$

. Unit vectors do not explicitly depend on time:

$$\frac{\partial \hat{r}}{\partial t} = \frac{\partial \hat{\phi}}{\partial t} = 0. \quad (\text{A.5})$$

Radial motion does not change either unit vectors:

$$\frac{\partial \hat{\phi}}{\partial r} = \frac{\partial \hat{r}}{\partial r} = 0, \quad (\text{A.6})$$

but azimuthal motion changes both:

$$\frac{\partial \hat{\phi}}{\partial \phi} = -\hat{r}, \quad (\text{A.7})$$

$$\frac{\partial \hat{r}}{\partial \phi} = \hat{\phi}. \quad (\text{A.8})$$

In polar coordinates, the gradient of a function $g(r, \phi)$ is:

$$\vec{\nabla} g = \frac{\partial g}{\partial r} \hat{r} + \frac{1}{r} \frac{\partial g}{\partial \phi} \hat{\phi}. \quad (\text{A.9})$$

In polar coordinates is, the divergence of a vector field $\vec{A} = A_r(r, \phi)\hat{r} + A_\phi(r, \phi)\hat{\phi}$ is:

$$\vec{\nabla} \cdot \vec{A} = \vec{\nabla} \cdot (A_r \hat{r} + A_\phi \hat{\phi}) = \frac{1}{r} \frac{\partial (r A_r)}{\partial r} + \frac{1}{r} \frac{\partial A_\phi}{\partial \phi}. \quad (\text{A.10})$$

B.1 Equations of motion

We use equations (1.11) and (A.4) to write equation (2.15) in polar coordinates as:

$$\frac{\partial(u\hat{r} + v\hat{\phi})}{\partial t} + \left(u \frac{\partial}{\partial r} + \frac{v}{r} \frac{\partial}{\partial \phi} \right) (u\hat{r} + v\hat{\phi}) = -\frac{1}{\rho} \vec{\nabla} p - \vec{\nabla} \Phi. \quad (\text{B.1})$$

We write it out as:

$$\frac{\partial(u\hat{r} + v\hat{\phi})}{\partial t} + \left(u \frac{\partial}{\partial r} + \frac{v}{r} \frac{\partial}{\partial \phi} \right) (u\hat{r}) + \left(u \frac{\partial}{\partial r} + \frac{v}{r} \frac{\partial}{\partial \phi} \right) (v\hat{\phi}) = -\frac{1}{\rho} \vec{\nabla} p - \vec{\nabla} \Phi, \quad (\text{B.2})$$

$$\begin{aligned} \frac{\partial u}{\partial t} \hat{r} + u \frac{\partial \hat{r}}{\partial t} + \frac{\partial v}{\partial t} \hat{\phi} + v \frac{\partial \hat{\phi}}{\partial t} + u \hat{r} \frac{\partial u}{\partial r} + u^2 \frac{\partial \hat{r}}{\partial r} + \frac{uv}{r} \frac{\partial \hat{r}}{\partial \phi} + \frac{v \hat{r}}{r} \frac{\partial u}{\partial \phi} \\ + u \hat{\phi} \frac{\partial v}{\partial r} + uv \frac{\partial \hat{\phi}}{\partial r} + \frac{v^2}{r} \frac{\partial \hat{\phi}}{\partial \phi} + \frac{v \hat{\phi}}{r} \frac{\partial v}{\partial \phi} = -\frac{1}{\rho} \frac{\partial p}{\partial r} \hat{r} - \frac{1}{\rho r} \frac{\partial p}{\partial \phi} \hat{\phi} - \frac{\partial \Phi}{\partial r} \hat{r} - \frac{1}{r} \frac{\partial \Phi}{\partial \phi} \hat{\phi}. \end{aligned} \quad (\text{B.3})$$

and use equations (A.6), (A.7) and (A.8) to write:

$$\begin{aligned} \frac{\partial u}{\partial t} \hat{r} + \frac{\partial v}{\partial t} \hat{\phi} + u \hat{r} \frac{\partial u}{\partial r} + \frac{uv}{r} \hat{\phi} + \frac{v \hat{r}}{r} \frac{\partial u}{\partial \phi} \\ + u \hat{\phi} \frac{\partial v}{\partial r} + \frac{v^2}{r} (-\hat{r}) + \frac{v \hat{\phi}}{r} \frac{\partial v}{\partial \phi} = -\frac{1}{\rho} \frac{\partial p}{\partial r} \hat{r} - \frac{1}{\rho r} \frac{\partial p}{\partial \phi} \hat{\phi} - \frac{\partial \Phi}{\partial r} \hat{r} - \frac{1}{r} \frac{\partial \Phi}{\partial \phi} \hat{\phi}. \end{aligned} \quad (\text{B.4})$$

We can now find two independent equations by taking a dot product of equation (B.4) and \hat{r} :

$$\frac{\partial u}{\partial t} + u \frac{\partial u}{\partial r} + \frac{v}{r} \frac{\partial u}{\partial \phi} - \frac{v^2}{r} = -\frac{1}{\rho} \frac{\partial p}{\partial r} - \frac{\partial \Phi}{\partial r}, \quad (\text{B.5})$$

and by taking a dot product of equation (B.4) and $\hat{\phi}$:

$$\frac{\partial v}{\partial t} + u \frac{\partial v}{\partial r} + \frac{v}{r} \frac{\partial v}{\partial \phi} + \frac{uv}{r} = -\frac{1}{\rho r} \frac{\partial p}{\partial \phi} - \frac{1}{r} \frac{\partial \Phi}{\partial \phi}. \quad (\text{B.6})$$

Coefficients of expansion of the disk's unperturbed state

We want to expand these quantities up to the lowest two terms. However, we do not know the ratio of magnitudes of all quantities. This means that we do not know if all quantities can be described with terms with same orders of ϵ . We will do a short analysis to see how this should be done. First, we know that radial velocity is zero (equation (2.29)), so we do not need to expand it:

$$u = 0. \quad (\text{C.1})$$

Next, we perform a dimensional analysis on equation (2.32):

$$\frac{v^2}{r} \propto \frac{1}{\rho r} p + \frac{\Phi}{r}. \quad (\text{C.2})$$

We write these values as expansion of unknown orders. We call lowest terms of every expansion X_0 and X_2 .

$$\begin{aligned} v &= v_0 + v_2\epsilon^2 + v_4\epsilon^4 + v_6\epsilon^6 + \dots \\ \Phi &= \Phi_0 + \Phi_2\epsilon^2 + \Phi_4\epsilon^4 + \Phi_6\epsilon^6 \\ p &= p_0 + p_2\epsilon^2 + p_4\epsilon^4 + p_6\epsilon^6 \\ \rho &= \rho_0 + \rho_2\epsilon^2 + \rho_4\epsilon^4 + \rho_6\epsilon^6 \end{aligned} \quad (\text{C.3})$$

In equation (2.32), pressure and density appear only as ratio p/ρ so we can choose the lowest non vanishing term of density series to be ϵ^0 :

$$\rho = \rho_0 + \rho_2\epsilon^2, \quad (\text{C.4})$$

and we know that the ratio needs to be of order ϵ^2 so we write:

$$p = p_4\epsilon^4 + p_6\epsilon^6. \quad (\text{C.5})$$

Now we can write equation (C.2) as:

$$\begin{aligned}
v^2 &\propto \frac{p}{\rho} + \Phi \\
(v_0 + v_2\epsilon^2 + v_4\epsilon^4 + v_6\epsilon^6)^2 &\propto \frac{p_4\epsilon^4 + p_6\epsilon^6}{\rho_0 + \rho_2\epsilon^2} + \Phi_0 + \Phi_2\epsilon^2 + \Phi_4\epsilon^4 + \Phi_6\epsilon^6 \\
v_0^2 + 2v_0v_2\epsilon^2 + 2v_0v_4\epsilon^4 + 2v_0v_6\epsilon^6 + v_2x^4 + 2v_2v_4\epsilon^6 + 2v_2v_6\epsilon^8 + v_4\epsilon^8 \\
+ 2v_4v_6\epsilon^{10} + v_6\epsilon^{12} &\propto \frac{p_2}{\rho_0}\epsilon^2 + \frac{\rho_0 p_4 - \rho_2 p_2}{\rho_0^2}\epsilon^4 + \Phi_0 + \Phi_2\epsilon^2 + \Phi_4\epsilon^4 + \Phi_6\epsilon^6
\end{aligned} \tag{C.6}$$

Equation (C.6) can be satisfied for two different orders of ϵ only if the lowest non vanishing terms of density and gravitational potential are v_0 , v_2 , Φ_0 , and Φ_2 . So, quantities expanded up to lowest two non vanishing terms are:

$$\begin{aligned}
v &= v_0 + v_2\epsilon^2 \\
\rho &= \rho_0 + \rho_2\epsilon^2 \\
\Phi &= \Phi_0 + \Phi_2\epsilon^2 \\
p &= p_2\epsilon^2 + p_4\epsilon^4.
\end{aligned} \tag{C.7}$$

Now we put equations (2.37) in the steady state equation that we have obtained (equation (2.32)):

$$-\frac{(v_0 + \epsilon^2 v_2)^2}{r} = -\frac{1}{\rho_0 + \epsilon^2 \rho_2} \frac{\partial (p_2\epsilon^2 + p_4\epsilon^4)}{\partial r} + \frac{\partial (\Phi_0 + \epsilon^2 \Phi_2)}{\partial r} \tag{C.8}$$

$$\begin{aligned}
-\frac{v_0^2 + 2v_0v_2\epsilon^2 + v_2^2\epsilon^4}{r} &= -\frac{1}{\rho_0} \frac{1}{1 + \frac{\epsilon^2 \rho_2}{\rho_0}} \frac{\partial [p_2\epsilon^2 + p_4\epsilon^4]}{\partial r} + \frac{\partial (\Phi_0 + \epsilon^2 \Phi_2)}{\partial r} \\
&= \frac{-1}{\rho_0} \left[1 - \frac{\epsilon^2 \rho_2}{\rho_0} \right] \frac{\partial [p_2\epsilon^2 + p_4\epsilon^4]}{\partial r} + \frac{\partial (\Phi_0 + \epsilon^2 \Phi_2)}{\partial r}
\end{aligned} \tag{C.9}$$

Equation (C.9) up to ϵ^2 is:

$$-\frac{v_0^2 + 2v_0v_2\epsilon^2}{r} = \frac{-1}{\rho_0} \frac{\partial p_2\epsilon^2}{\partial r} + \frac{\partial (\Phi_0 + \epsilon^2 \Phi_2)}{\partial r}. \tag{C.10}$$

Derivation of perturbed equation

In practice, this means that for every two perturbations a' and b' :

$$a'b' = a' \frac{\partial b'}{\partial t} = a' \frac{\partial b'}{\partial r} = a' \frac{\partial b'}{\partial \phi} = 0. \quad (\text{D.1})$$

Equations E.25 and E.33 of order ϵ^2 are:

$$\begin{aligned} \frac{\partial u'_0}{\partial t} - i\Omega_{\text{unp},2}u'_0 - i\Omega_{\text{unp},0}u'_2 - 2\Omega_{\text{unp},2}v'_0 - 2\Omega_{\text{unp},0}v'_2 \\ = -\frac{1}{\rho_{\text{unp},0}} \frac{\partial p'_0}{\partial r} + \frac{\rho'_0}{\rho_{\text{unp},0}^2} \frac{\partial p_{\text{unp},2}}{\partial r} \end{aligned} \quad (\text{D.2})$$

$$\frac{\partial v'_0}{\partial t} - i\Omega_{\text{unp},2}v'_0 - i\Omega_{\text{unp},0}v'_2 + \frac{u'_0}{r} \frac{\partial}{\partial r}(r^2\Omega_{\text{unp},2}) + \frac{u'_2}{r} \frac{\partial}{\partial r}(r^2\Omega_{\text{unp},0}) = \frac{ip'_0}{r\rho_{\text{unp},0}} \quad (\text{D.3})$$

Equation E.38 in 0th order:

$$\frac{\partial \rho'_0}{\partial t} - i\Omega_{\text{unp},0}\rho'_0 + u'_0 \frac{\partial \rho_{\text{unp},0}}{\partial r} = -\frac{\rho_{\text{unp},0}}{r} \left[\frac{\partial(ru'_0)}{\partial r} - iv'_0 \right] \quad (\text{D.4})$$

Equation E.44 in order ϵ^2 (there are no 0th order factors) is:

$$\frac{\partial p'_0}{\partial t} - i\Omega_{\text{unp},0}p'_0 + u'_0 \frac{\partial p_{\text{unp},2}}{\partial r} = -\frac{\gamma p_{\text{unp},2}}{r} \left[\frac{\partial(ru'_0)}{\partial r} - iv'_0 \right] \quad (\text{D.5})$$

Multiplying D.3 by $2i$ and adding it to D.2, we get:

$$\begin{aligned}
\frac{\partial(u'_0 + 2iv'_0)}{\partial t} - i\Omega_{\text{unp},0}(u'_0 + 2iv'_0) - 2\Omega_{\text{unp},2}v'_0 + 2i\frac{u'_0}{r}\frac{\partial}{\partial r}(r^2\Omega_{\text{unp},2}) \\
= -\frac{1}{\rho_{\text{unp},0}}\frac{\partial p'_0}{\partial r} + \frac{\rho'_0}{\rho_{\text{unp},0}^2}\frac{\partial p_{\text{unp},2}}{\partial r} + 2i\frac{ip'_0}{r\rho_{\text{unp},0}}
\end{aligned} \tag{D.6}$$

$$\underbrace{\frac{\partial}{\partial t}[u'_0 + 2iv'_0]}_A \underbrace{-i\Omega_2 u'_0 + 2i\frac{u'_0}{r}\frac{\partial}{\partial r}(r^2\Omega_2)}_B = \underbrace{-\frac{1}{\rho_0}\frac{\partial p'_0}{\partial r}}_C + \underbrace{\frac{\rho'_0}{\rho_0^2}\frac{\partial p_0}{\partial r}}_D \underbrace{-\frac{2p'_0}{r\rho_0}}_F \tag{D.7}$$

$$\begin{aligned}
A &= \frac{\partial}{\partial t}[u'_0 + 2iv'_0] = \frac{\partial}{\partial t}\left[ir\Omega_0 E + 2i\frac{1}{2}r\Omega_0 E\right] \\
&= \frac{\partial}{\partial t}[i2r\Omega_0 E] = i2r\Omega_0 \frac{\partial E}{\partial t}
\end{aligned} \tag{D.8}$$

$$\begin{aligned}
B &= i\left[-\Omega_2 u'_0 + 2\frac{u'_0}{r}\frac{\partial}{\partial r}(r^2\Omega_2)\right] \\
&= i\left[-\frac{1}{2r\Omega_0}\left[\frac{\partial\Phi_2}{\partial r} + \frac{1}{\rho_0}\frac{\partial p_0}{\partial r}\right]ir\Omega_0 E + \frac{2}{r}ir\Omega_0 E\frac{\partial}{\partial r}\left[\frac{1}{2r\Omega_0}r^2\left(\frac{\partial\Phi_2}{\partial r} + \frac{1}{\rho_0}\frac{\partial p_0}{\partial r}\right)\right]\right] \\
&= \frac{E}{2}\left[\frac{\partial\Phi_2}{\partial r} + \frac{1}{\rho_0}\frac{\partial p_0}{\partial r}\right] - 2\Omega_0 E\left[\frac{\partial\Phi_2}{\partial r} + \frac{1}{\rho_0}\frac{\partial p_0}{\partial r}\right]\frac{\partial}{\partial r}\left(\frac{r}{2\Omega_0}\right) - 2\Omega_0\frac{Er}{2\Omega_0}\frac{\partial}{\partial r}\left[\frac{\partial\Phi_2}{\partial r} + \frac{1}{\rho_0}\frac{\partial p_0}{\partial r}\right] \\
&= \frac{E}{2}\left[\frac{\partial\Phi_2}{\partial r} + \frac{1}{\rho_0}\frac{\partial p_0}{\partial r}\right] - \frac{5}{2}\frac{\Omega_0 E}{\Omega_0}\left[\frac{\partial\Phi_2}{\partial r} + \frac{1}{\rho_0}\frac{\partial p_0}{\partial r}\right] - Er\frac{\partial}{\partial r}\left[\frac{\partial\Phi_2}{\partial r} + \frac{1}{\rho_0}\frac{\partial p_0}{\partial r}\right] \\
&= -2E\left[\frac{\partial\Phi_2}{\partial r} + \frac{1}{\rho_0}\frac{\partial p_0}{\partial r}\right] - Er\frac{\partial}{\partial r}\left[\frac{\partial\Phi_2}{\partial r} + \frac{1}{\rho_0}\frac{\partial p_0}{\partial r}\right] \\
&= -\frac{E}{r}\frac{\partial}{\partial r}\left[r^2\left(\frac{\partial\Phi_2}{\partial r} + \frac{1}{\rho_0}\frac{\partial p_0}{\partial r}\right)\right] \\
&= -\frac{E}{r}\frac{\partial}{\partial r}\left[r^2\frac{\partial\Phi_2}{\partial r}\right] - \frac{E}{r}\frac{\partial}{\partial r}\left[\frac{r^2}{\rho_0}\frac{\partial p_0}{\partial r}\right] \\
&= -\frac{E}{r}\frac{\partial}{\partial r}\left[r^2\frac{\partial\Phi_2}{\partial r}\right] - 2E\frac{1}{\rho_0}\frac{\partial p_0}{\partial r} - \frac{Er}{\rho_0}\frac{\partial^2 p_0}{\partial r^2} + Er\frac{\partial p_0}{\partial r}\frac{1}{\rho_0^2}\frac{\partial \rho_0}{\partial r}
\end{aligned} \tag{D.9}$$

$$\begin{aligned}
\frac{\partial}{\partial r}[ru'_0] - iv_0 &= \frac{\partial}{\partial r}[rir\Omega_0 E] - i\frac{1}{2}r\Omega_0 E = \frac{\partial}{\partial r}[ir^2\Omega_0 E] - i\frac{r\Omega_0 E}{2} \\
&= i\left[E\frac{\partial}{\partial r}(r^2\Omega_0) + r^2\Omega_0\frac{\partial E}{\partial r} - \frac{r\Omega_0 E}{2}\right] = ir^2\Omega_0\frac{\partial E}{\partial r}
\end{aligned} \tag{D.10}$$

$$\begin{aligned}
-i\Omega_0\rho'_0 + u'_0\frac{\partial\rho_0}{\partial r} &= -\frac{\rho_0}{r}ir^2\Omega_0\frac{\partial E}{\partial r} \\
-i\Omega_0\rho'_0 + ir\Omega_0 E\frac{\partial\rho_0}{\partial r} &= -i\rho_0 r\Omega_0\frac{\partial E}{\partial r} \\
-\rho'_0 + rE\frac{\partial\rho_0}{\partial r} &= -\rho_0 r\frac{\partial E}{\partial r} \\
\rho'_0 &= rE\frac{\partial\rho_0}{\partial r} + \rho_0 r\frac{\partial E}{\partial r}
\end{aligned} \tag{D.11}$$

$$\begin{aligned}
-i\Omega_0 p'_0 + u'_0\frac{\partial p_0}{\partial r} &= -\frac{\gamma p_0}{r}ir^2\Omega_0\frac{\partial E}{\partial r} \\
-i\Omega_0 p'_0 + ir\Omega_0 E\frac{\partial p_0}{\partial r} &= -i\gamma p_0 r\Omega_0\frac{\partial E}{\partial r} \\
p'_0 &= rE\frac{\partial p_0}{\partial r} + \gamma p_0 r\frac{\partial E}{\partial r}
\end{aligned} \tag{D.12}$$

$$C = -\frac{1}{\rho_0}\frac{\partial p'_0}{\partial r} = -\frac{1}{\rho_0}\frac{\partial}{\partial r}\left[rE\frac{\partial p_0}{\partial r} + \gamma p_0 r\frac{\partial E}{\partial r}\right] \tag{D.13}$$

$$D = \frac{\partial p_0}{\partial r}\frac{1}{\rho_0^2}\rho'_0 = \frac{\partial p_0}{\partial r}\frac{1}{\rho_0^2}\left[rE\frac{\partial\rho_0}{\partial r} + \rho_0 r\frac{\partial E}{\partial r}\right] \tag{D.14}$$

$$F = -\frac{2}{r\rho_0}p'_0 = -\frac{2}{r\rho_0}\left[rE\frac{\partial p_0}{\partial r} + \gamma p_0 r\frac{\partial E}{\partial r}\right] \tag{D.15}$$

$$A + B = C + D + F$$

$$\begin{aligned}
& i2r\Omega_0 \frac{\partial E}{\partial t} - \frac{E}{r} \frac{\partial}{\partial r} \left(r^2 \frac{\partial \Phi_2}{\partial r} \right) - \frac{2E}{\rho_0} \frac{\partial p_0}{\partial r} - \frac{Er}{\rho_0} \frac{\partial^2 p_0}{\partial r^2} + \frac{Er}{\rho_0^2} \frac{\partial p_0}{\partial r} \frac{\partial \rho_0}{\partial r} \\
&= -\frac{1}{\rho_0} E \frac{\partial p_0}{\partial r} - \frac{r}{\rho_0} \frac{\partial E}{\partial r} \frac{\partial p_0}{\partial r} - \frac{rE}{\rho_0} \frac{\partial^2 p_0}{\partial r^2} - \frac{1}{\rho_0} \frac{\partial}{\partial r} \left[\gamma p_0 r \frac{\partial E}{\partial r} \right] \\
&+ \frac{\partial p_0}{\partial r} \frac{\partial \rho_0}{\partial r} \frac{rE}{\rho_0^2} + \frac{\partial p_0}{\partial r} \frac{r}{\rho_0} \frac{\partial E}{\partial r} - \frac{2rE}{r\rho_0} \frac{\partial p_0}{\partial r} - \frac{2\gamma p_0}{\rho_0} \frac{\partial E}{\partial r} \\
& i2r\Omega_0 \frac{\partial E}{\partial t} - \frac{E}{r} \frac{\partial}{\partial r} \left(r^2 \frac{\partial \Phi_2}{\partial r} \right) = -\frac{E}{\rho_0} \frac{\partial p_0}{\partial r} - \frac{1}{\rho_0} \frac{\partial}{\partial r} \left[\gamma p_0 r^3 \frac{\partial E}{\partial r} \right]
\end{aligned} \tag{D.16}$$

$$-\frac{1}{r^2 \rho_0} \frac{\partial}{\partial r} \left[\gamma p_0 r^3 \frac{\partial E}{\partial r} \right] = -\frac{1}{r^2 \rho_0} \frac{\partial}{\partial r} \left[r^2 \gamma p_0 r \frac{\partial E}{\partial r} \right] = -\frac{1}{\rho_0} \frac{\partial}{\partial r} \left[\gamma p_0 r \frac{\partial E}{\partial r} \right] - \frac{2}{r\rho_0} \gamma p_0 r \frac{\partial E}{\partial r} \tag{D.17}$$

$$2r\Omega_0 \frac{\partial E}{\partial t} = -\frac{iE}{r} \frac{\partial}{\partial r} \left(r^2 \frac{\partial \Phi_2}{\partial r} \right) + \frac{iE}{\rho} \frac{\partial p_0}{\partial r} + \frac{i}{r^2 \rho_0} \frac{\partial}{\partial r} \left[\gamma p_0 r^3 \frac{\partial E}{\partial r} \right] \tag{D.18}$$

Eccentricity equation derivation for a locally isothermal disk

The lowest order (ϵ^0) of equation (3.6) is:

$$-i\rho'_0\Omega_0 + u'_0\frac{\partial\rho_0}{\partial r} = -\frac{\rho_0}{r}\left[\frac{\partial(ru'_0)}{\partial r} - iw'_0\right] \quad (\text{E.1})$$

Now we use equation(3.8) to write is as:

$$-i\rho'_0\Omega_0 + ir\Omega_0E\frac{\partial\rho_{\text{ump}}}{\partial r} = -\frac{\rho_{\text{ump}}}{r}\left[\frac{\partial(ir^2\Omega_0E(r,t))}{\partial r} - i\frac{1}{2}r\Omega_0E\right] \quad (\text{E.2})$$

$$-i\rho'_0\Omega_0 = -ir\Omega_0E\frac{\partial\rho_0}{\partial r} - i\frac{\rho_0}{r}r^2\Omega_0\frac{\partial E}{\partial r} - i\frac{\rho_0}{r}E\frac{\partial(r^2\Omega_0)}{\partial r} + i\frac{\rho_0}{r}\frac{1}{2}r\Omega_0E \quad (\text{E.3})$$

Using equation (2.61), and dividing upper equation by $-i\Omega_0$, we get;

$$\rho'_0 = rE\frac{\partial\rho_0}{\partial r} + \frac{\rho_0}{r}r^2\frac{\partial E}{\partial r} = r\frac{\partial(E\rho_0)}{\partial r}. \quad (\text{E.4})$$

Just like for adiabatic disc, we find what the next (ϵ^2) order of equations (3.6a) and (3.6b) looks like:

$$\frac{\partial u'_0}{\partial t} - i\Omega_2u'_0 - i\Omega_0u'_2 - 2\Omega_2v'_0 - 2\Omega_0v'_2 = -c_s^2\frac{\partial}{\partial r}\left(\frac{\rho'_0}{\rho_0}\right) \quad (\text{E.5})$$

$$\frac{\partial v'_0}{\partial t} - i\Omega_2v'_0 - i\Omega_0v'_2 + \frac{u'_0}{r}\frac{\partial}{\partial r}(r^2\Omega_2) + \frac{u'_2}{r}\frac{\partial}{\partial r}(r^2\Omega_0) = \frac{ic_s^2\rho'_0}{r\rho_0} \quad (\text{E.6})$$

By multiplying equation (E.6) by $2i$, adding it to equation (E.5), and using equation 2.61 we get:

$$\frac{\partial(u'_0 + 2iv'_0)}{\partial t} - 2\Omega_2v'_0 + 2i\frac{u'_0}{r}\frac{\partial}{\partial r}(r^2\Omega_2) = -c_s^2\frac{\partial}{\partial r}\left(\frac{\rho'_0}{\rho_0}\right) - 2\frac{c_s^2\rho'_0}{r\rho_0} \quad (\text{E.7})$$

Now we can use equation (E.4):

$$\underbrace{\frac{\partial(u'_0 + 2iv'_0)}{\partial t}}_A - 2\Omega_2 v'_0 + \underbrace{2i \frac{u'_0}{r} \frac{\partial}{\partial r} (r^2 \Omega_2)}_B = \underbrace{-c_s^2 \frac{\partial}{\partial r} \left(\frac{r}{\rho_0} \frac{\partial(E\rho_0)}{\partial r} \right)}_C - \underbrace{\frac{2c_s^2}{r\rho_0} r \frac{\partial(\rho_0 E)}{\partial r}}_D \quad (\text{E.8})$$

In previous section, A was found to be:

$$A = i2r\Omega \frac{\partial E}{\partial t} \quad (\text{E.9})$$

In the last section, we showed that B can be written as:

$$B = -\frac{E}{r} \frac{\partial}{\partial r} \left[r^2 \frac{\partial \Phi_2}{\partial r} \right] - \frac{E}{r} \frac{\partial}{\partial r} \left[\frac{r^2}{\rho} \frac{\partial(c_s^2 \rho)}{\partial r} \right]. \quad (\text{E.10})$$

We will expand this as:

$$\begin{aligned} B &= -\frac{E}{r} \frac{\partial}{\partial r} \left[r^2 \frac{\partial \Phi_2}{\partial r} \right] - \frac{E}{r} \frac{\partial}{\partial r} \left(r^2 \frac{\partial c_s^2}{\partial r} + \frac{r^2 c_s^2}{\rho} \frac{\partial \rho}{\partial r} \right) \\ &= -\frac{E}{r} \frac{\partial}{\partial r} \left[r^2 \frac{\partial \Phi_2}{\partial r} \right] - 2E \frac{\partial c_s^2}{\partial r} - Er \frac{\partial^2 c_s^2}{\partial r^2} - 2E \frac{c_s^2}{\rho} \frac{\partial \rho}{\partial r} \\ &\quad - \frac{Er}{\rho} \frac{\partial c_s^2}{\partial r} \frac{\partial \rho}{\partial r} + \frac{Er c_s^2}{\rho^2} \left(\frac{\partial \rho}{\partial r} \right)^2 - \frac{Er c_s^2}{\rho} \frac{\partial^2 \rho}{\partial r^2} \end{aligned} \quad (\text{E.11})$$

$$\begin{aligned} C &= -c_s^2 \frac{\partial}{\partial r} \left(\frac{r}{\rho} \frac{\partial(E\rho)}{\partial r} \right) = -c_s^2 \frac{\partial}{\partial r} \left(r \frac{\partial E}{\partial r} + \frac{rE}{\rho} \frac{\partial \rho}{\partial r} \right) \\ &= -c_s^2 r \frac{\partial^2 E}{\partial r^2} - c_s^2 \frac{\partial E}{\partial r} - c_s^2 \frac{rE}{\rho} \frac{\partial^2 \rho}{\partial r^2} - c_s^2 \frac{r}{\rho} \frac{\partial \rho}{\partial r} \frac{\partial E}{\partial r} + c_s^2 \frac{rE}{\rho^2} \left(\frac{\partial \rho}{\partial r} \right)^2 - c_s^2 \frac{E}{\rho} \frac{\partial \rho}{\partial r} \end{aligned} \quad (\text{E.12})$$

$$D = -\frac{2c_s^2}{\rho_0} \frac{\partial(\rho_0 E)}{\partial r} = -\frac{2c_s^2 E}{\rho_0} \frac{\partial \rho_0}{\partial r} - 2c_s^2 \frac{\partial E}{\partial r} \quad (\text{E.13})$$

Finally:

$$A + B = C + D \quad (\text{E.14})$$

$$\begin{aligned}
i2r\Omega \frac{\partial E}{\partial t} - \frac{E}{r} \frac{\partial}{\partial r} \left[r^2 \frac{\partial \Phi_2}{\partial r} \right] - 2E \frac{\partial c_s^2}{\partial r} - Er \frac{\partial^2 c_s^2}{\partial r^2} - \frac{Er}{\rho} \frac{\partial c_s^2}{\partial r} \frac{\partial \rho}{\partial r} \\
= -c_s^2 r \frac{\partial^2 E}{\partial r^2} - 3c_s^2 \frac{\partial E}{\partial r} - c_s^2 r \frac{\partial \rho}{\rho} \frac{\partial E}{\partial r} - c_s^2 \frac{E}{\rho} \frac{\partial \rho}{\partial r}
\end{aligned} \tag{E.15}$$

We will multiply it by $-ir\rho$ and rearrange it a bit:

$$\begin{aligned}
2r^2\rho\Omega \frac{\partial E}{\partial t} + i\rho E \frac{\partial}{\partial r} \left[r^2 \frac{\partial \Phi_2}{\partial r} \right] = -2iEr\rho \frac{\partial c_s^2}{\partial r} - iEr^2\rho \frac{\partial^2 c_s^2}{\partial r^2} - iEr^2 \frac{\partial c_s^2}{\partial r} \frac{\partial \rho}{\partial r} + ic_s^2 r^2 \rho \frac{\partial^2 E}{\partial r^2} \\
+ 3ir\rho c_s^2 \frac{\partial E}{\partial r} + ic_s^2 r^2 \frac{\partial \rho}{\partial r} \frac{\partial E}{\partial r} + irc_s^2 E \frac{\partial \rho}{\partial r}
\end{aligned} \tag{E.16}$$

Now we will show that the right hand side equation (E.16) can be written as:

$$\begin{aligned}
\text{RHS} &= \frac{i}{r} \frac{\partial}{\partial r} \left(\rho c_s^2 r^3 \frac{\partial E}{\partial r} \right) + irE \frac{\partial(\rho c_s^2)}{\partial r} - \frac{i}{r} \frac{\partial}{\partial r} \left(\rho Er^3 \frac{\partial c_s^2}{\partial r} \right) \\
&= ic_s^2 r^2 \frac{\partial \rho}{\partial r} \frac{\partial E}{\partial r} + \frac{i\rho r^2}{r} \frac{\partial c_s^2}{\partial r} \frac{\partial E}{\partial r} + 3ir\rho c_s^2 \frac{\partial E}{\partial r} + \frac{i}{r} \rho c_s^2 r^3 \frac{\partial^2 E}{\partial r^2} + irE\rho \frac{\partial c_s^2}{\partial r} \\
&+ irEc_s^2 \frac{\partial \rho}{\partial r} - ir^2 E \frac{\partial \rho}{\partial r} \frac{\partial c_s^2}{\partial r} - i\rho r^2 \frac{\partial E}{\partial r} \frac{\partial c_s^2}{\partial r} - i3r\rho E \frac{\partial c_s^2}{\partial r} - i\rho Er^2 \frac{\partial^2 c_s^2}{\partial r^2} \\
&= ic_s^2 r^2 \frac{\partial \rho}{\partial r} \frac{\partial E}{\partial r} + 3ir\rho c_s^2 \frac{\partial E}{\partial r} + \frac{i}{r} \rho c_s^2 r^3 \frac{\partial^2 E}{\partial r^2} + irE\rho \frac{\partial c_s^2}{\partial r} \\
&+ irEc_s^2 \frac{\partial \rho}{\partial r} - ir^2 E \frac{\partial \rho}{\partial r} \frac{\partial c_s^2}{\partial r} - i3r\rho E \frac{\partial c_s^2}{\partial r} - i\rho Er^2 \frac{\partial^2 c_s^2}{\partial r^2}.
\end{aligned} \tag{E.17}$$

in order to write it as:

$$2r^2\rho\Omega \frac{\partial E}{\partial t} + i\rho E \frac{\partial}{\partial r} \left[r^2 \frac{\partial \Phi_2}{\partial r} \right] = \frac{i}{r} \frac{\partial}{\partial r} \left(\rho c_s^2 r^3 \frac{\partial E}{\partial r} \right) + irE \frac{\partial(\rho c_s^2)}{\partial r} - \frac{i}{r} \frac{\partial}{\partial r} \left(\rho Er^3 \frac{\partial c_s^2}{\partial r} \right) \tag{E.18}$$

E.0.1 Radial equation of motion

The first equation we will use is equation 2.26b:

$$\underbrace{\frac{\partial u}{\partial t} + u \frac{\partial u}{\partial r} + \frac{v}{r} \frac{\partial u}{\partial \phi} - \frac{v^2}{r}}_{\text{LHS1}} = \underbrace{-\frac{1}{\rho} \frac{\partial p}{\partial r} - \frac{\partial \Phi}{\partial r}}_{\text{RHS1}}.$$

$$\begin{aligned}
LHS1 &= \frac{\partial(u'e^{-i\phi})}{\partial t} + (u'e^{-i\phi})\frac{\partial(u'e^{-i\phi})}{\partial r} + \frac{v_{\text{unp}} + v'e^{-i\phi}}{r} \frac{\partial(u'e^{-i\phi})}{\partial \phi} \\
&\quad - \frac{(v_{\text{unp}} + v'e^{-i\phi})^2}{r} \\
&= \frac{\partial u'}{\partial t} e^{-i\phi} + u' e^{-i\phi} \frac{\partial u'}{\partial r} e^{-i\phi} + \frac{v_{\text{unp}} + v'e^{-i\phi}}{r} (-iu' e^{-i\phi}) \\
&\quad - \frac{v_{\text{unp}}^2 + 2v_{\text{unp}}v'e^{-i\phi} + (v'e^{-i\phi})^2}{r}
\end{aligned} \tag{E.19}$$

$$\begin{aligned}
&= \frac{\partial u'}{\partial t} e^{-i\phi} + u' \frac{\partial u'}{\partial r} e^{-2i\phi} - \frac{iu'v_{\text{unp}}}{r} e^{-i\phi} - \frac{u'v'e^{-2i\phi}}{r} \\
&\quad + \frac{v_{\text{unp}}^2}{r} + \frac{2v_{\text{unp}}v'e^{-i\phi}}{r} + \frac{v'^2 e^{-2i\phi}}{r} \\
LHS1 &= \frac{\partial u'}{\partial t} e^{-i\phi} - \frac{iu'v_{\text{unp}}}{r} e^{-i\phi} + \frac{v_{\text{unp}}^2}{r} + \frac{2v_{\text{unp}}v'e^{-i\phi}}{r}
\end{aligned} \tag{E.20}$$

$$\begin{aligned}
RHS1 &= -\frac{1}{\rho_{\text{unp}} + \rho'e^{-i\phi}} \frac{\partial(p_{\text{unp}} + p'e^{-i\phi})}{\partial r} - \frac{\partial\Phi_{\text{unp}}}{\partial r} \\
&= -\frac{1}{\rho_{\text{unp}}} \left[1 - \frac{\rho'}{\rho_{\text{unp}}} e^{-i\phi} \right] \frac{\partial}{\partial r} \left[p_{\text{unp}} + p'e^{-i\phi} \right] - \frac{\partial\Phi_{\text{unp}}}{\partial r} \\
&= \left[-\frac{1}{\rho_{\text{unp}}} + \frac{\rho'}{\rho_{\text{unp}}^2} e^{-i\phi} \right] \left[\frac{\partial p_{\text{unp}}}{\partial r} + \frac{\partial p'}{\partial r} e^{-i\phi} \right] - \frac{\partial\Phi_{\text{unp}}}{\partial r}
\end{aligned} \tag{E.21}$$

We again use equations (D.1) to approximate this as:

$$RHS1 = -\frac{1}{\rho_{\text{unp}}} \frac{\partial p_{\text{unp}}}{\partial r} + \frac{\rho'}{\rho_{\text{unp}}^2} e^{-i\phi} \frac{\partial p_{\text{unp}}}{\partial r} - \frac{1}{\rho_{\text{unp}}} \frac{\partial p'}{\partial r} e^{-i\phi} - \frac{\partial\Phi_{\text{unp}}}{\partial r} \tag{E.22}$$

Now we can use equations (E.20) and (E.20) to write:

$$\begin{aligned}
\frac{\partial u'}{\partial t} e^{-i\phi} - \frac{iu'v_{\text{unp}}}{r} e^{-i\phi} + \frac{v_{\text{unp}}^2}{r} + \frac{2v_{\text{unp}}v'e^{-i\phi}}{r} &= \\
= -\frac{1}{\rho_{\text{unp}}} \frac{\partial p_{\text{unp}}}{\partial r} + \frac{\rho'}{\rho_{\text{unp}}^2} e^{-i\phi} \frac{\partial p_{\text{unp}}}{\partial r} - \frac{1}{\rho_{\text{unp}}} \frac{\partial p'}{\partial r} e^{-i\phi} - \frac{\partial\Phi_{\text{unp}}}{\partial r}.
\end{aligned} \tag{E.23}$$

Now we can use equation (2.32) to see that the third factor on the left hand side and the first and last factor on the right hand side cancel each other out. What's left is:

$$\frac{\partial u'}{\partial t} e^{-i\phi} - \frac{iu'v_{\text{unp}}}{r} e^{-i\phi} + \frac{2v_{\text{unp}}v'e^{-i\phi}}{r} = \frac{\rho'}{\rho_{\text{unp}}^2} e^{-i\phi} \frac{\partial p_{\text{unp}}}{\partial r} - \frac{1}{\rho_{\text{unp}}} \frac{\partial p'}{\partial r} e^{-i\phi} \tag{E.24}$$

When divided by $e^{-i\phi}$ and using $\Omega = v_{\text{unp}}/r$:

$$\boxed{\frac{\partial u'}{\partial t} - iu'\Omega + 2\Omega v' = -\frac{1}{\rho_{\text{unp}}} \frac{\partial p'}{\partial r} + \frac{\rho'}{\rho_{\text{unp}}^2} \frac{\partial p_{\text{unp}}}{\partial r}} \quad (\text{E.25})$$

E.0.2 Newton's law of motion - angular equation

The next equation we will use is equation 2.26c:

$$\underbrace{\frac{\partial v}{\partial t} + u \frac{\partial v}{\partial r} + \frac{v}{r} \frac{\partial v}{\partial \phi} + \frac{uv}{r}}_{\text{LHS}} = \underbrace{-\frac{1}{\rho r} \frac{\partial p}{\partial \phi} - \frac{1}{r} \frac{\partial \Phi}{\partial \phi}}_{\text{RHS}}$$

$$\begin{aligned} LHS &= \frac{\partial(v_{\text{unp}} + v'e^{-i\phi})}{\partial t} + \frac{v_{\text{unp}} + v'e^{-i\phi}}{r} \frac{\partial(v_{\text{unp}} + v'e^{-i\phi})}{\partial \phi} \\ &\quad - \frac{(v_{\text{unp}} + v'e^{-i\phi})(u'e^{-i\phi})}{r} + (u'e^{-i\phi}) \frac{\partial(v_{\text{unp}} + v'e^{-i\phi})}{\partial r} \\ &= \frac{\partial v_{\text{unp}}}{\partial t} + \frac{\partial(v')}{\partial t} e^{-i\phi} + \frac{v_{\text{unp}} + v'e^{-i\phi}}{r} \left[\frac{\partial v_{\text{unp}}}{\partial \phi} - iv'e^{-i\phi} \right] \\ &\quad - \frac{(v_{\text{unp}} + v'e^{-i\phi})(u'e^{-i\phi})}{r} + (u'e^{-i\phi}) \left[\frac{\partial v_{\text{unp}}}{\partial r} + \frac{\partial v'}{\partial r} e^{-i\phi} \right] \end{aligned} \quad (\text{E.26})$$

Now we use equations (D.1) to approximate this as:

$$\begin{aligned} LHS &\approx \frac{\partial v_{\text{unp}}}{\partial t} + \frac{\partial(v')}{\partial t} e^{-i\phi} + \frac{v_{\text{unp}}}{r} \frac{\partial v_{\text{unp}}}{\partial \phi} - \frac{iv'v_{\text{unp}}e^{-i\phi}}{r} \\ &\quad + \frac{v'e^{-i\phi}}{r} \frac{\partial v_{\text{unp}}}{\partial \phi} - \frac{v_{\text{unp}}u'e^{-i\phi}}{r} + (u'e^{-i\phi}) \frac{\partial v_{\text{unp}}}{\partial r} \end{aligned} \quad (\text{E.27})$$

Now we use assumption that a unp state solution does not depend on ϕ (equation (2.28)):

$$\begin{aligned} LHS &= \frac{\partial v'}{\partial t} e^{-i\phi} - \frac{iv'v_{\text{unp}}e^{-i\phi}}{r} - \frac{v_{\text{unp}}u'e^{-i\phi}}{r} + (u'e^{-i\phi}) \frac{\partial v_{\text{unp}}}{\partial r} \\ &= e^{-i\phi} \left[\frac{\partial v'}{\partial t} - \frac{iv'v_{\text{unp}}}{r} - \frac{v_{\text{unp}}u'}{r} + u' \frac{\partial v_{\text{unp}}}{\partial r} \right] \end{aligned} \quad (\text{E.28})$$

Now we will use a result:

$$\frac{u'}{r} \frac{\partial}{\partial r} (r^2 \Omega) = \frac{u'}{r} \frac{\partial}{\partial r} (rv') = \frac{u'}{r} \left(v' + \frac{\partial v'}{\partial r} \right), \quad (\text{E.29})$$

to finally get:

$$LHS = e^{-i\phi} \left[\frac{\partial v'}{\partial t} - iw'\Omega + \frac{u'}{r} \frac{\partial}{\partial r} (r^2\Omega) \right]. \quad (\text{E.30})$$

$$\begin{aligned} RHS &= -\frac{1}{\rho_{\text{unp}} + \rho'e^{-i\phi}} \frac{1}{r} \frac{\partial(\rho_{\text{unp}} + \rho'e^{-i\phi})}{\partial\phi} - \frac{1}{r} \frac{\partial\Phi_{\text{unp}}}{\partial\phi} \\ &= -\frac{1}{\rho_{\text{unp}}r} \left[1 - \frac{\rho'}{\rho_{\text{unp}}} e^{-i\phi} \right] \frac{\partial}{\partial\phi} \left[\rho_{\text{unp}} + \rho'e^{-i\phi} \right] - \frac{1}{r} \frac{\partial\Phi_{\text{unp}}}{\partial\phi} \\ &= \frac{1}{r} \left[-\frac{1}{\rho_{\text{unp}}} + \frac{\rho'}{\rho_{\text{unp}}^2} e^{-i\phi} \right] \left[\frac{\partial\rho_{\text{unp}}}{\partial\phi} + -i\rho'e^{-i\phi} \right] - \frac{1}{r} \frac{\partial\Phi_{\text{unp}}}{\partial\phi} \end{aligned} \quad (\text{E.31})$$

Now we use equations (2.28) and (D.1) to write is as:

$$RHS = \frac{ip'e^{-i\phi}}{r\rho_{\text{unp}}} \quad (\text{E.32})$$

Equating lhs and rhs, and dividing by $e^{i\phi}$ we get:

$$\boxed{\frac{\partial v'}{\partial t} - iw'\Omega + \frac{u'}{r} \frac{\partial}{\partial r} (r^2\Omega) = \frac{ip'}{r\rho_{\text{unp}}}}. \quad (\text{E.33})$$

E.0.3 Continuity equation

The next equation we use is equation (2.26a):

$$\underbrace{\frac{\partial\rho}{\partial t} + u\frac{\partial\rho}{\partial r} + \frac{v}{r}\frac{\partial\rho}{\partial\phi}}_{\text{LHS}} = \underbrace{-\frac{\rho}{r} \left[\frac{\partial}{\partial r} (ru) + \frac{\partial v}{\partial\phi} \right]}_{\text{RHS}}.$$

$$\begin{aligned} LHS &= \frac{\partial(\rho_{\text{unp}} + \rho'e^{-i\phi})}{\partial t} + \frac{v_{\text{unp}} + v'e^{-i\phi}}{r} \frac{\partial(\rho_{\text{unp}} + \rho'e^{-i\phi})}{\partial\phi} \\ &\quad + (u'e^{-i\phi}) \frac{\partial(\rho_{\text{unp}} + \rho'e^{-i\phi})}{\partial r} \\ &= \frac{\partial\rho_{\text{unp}}}{\partial t} + e^{-i\phi} \frac{\partial\rho'}{\partial t} + \frac{v_{\text{unp}} + v'e^{-i\phi}}{r} \left[\frac{\partial\rho_{\text{unp}}}{\partial\phi} - i\rho'e^{-i\phi} \right] \\ &\quad + (u'e^{-i\phi}) \left[\frac{\partial\rho_{\text{unp}}}{\partial r} + \frac{\partial\rho'}{\partial r} e^{-i\phi} \right] \end{aligned} \quad (\text{E.34})$$

Now we use equations (2.28), (2.27), and (D.1) to write it as:

$$LHS = \frac{\partial \rho'}{\partial t} e^{-i\phi} - i\rho'\Omega e^{-i\phi} + u'e^{-i\phi} \frac{\partial \rho_{\text{unp}}}{\partial r} \quad (\text{E.35})$$

$$\begin{aligned} RHS &= -\frac{\rho_{\text{unp}} + \rho'e^{-i\phi}}{r} \left[\frac{\partial(ru'e^{-i\phi})}{\partial r} + \frac{\partial(v_{\text{unp}} + v'e^{-i\phi})}{\partial \phi} \right] \\ &= -\frac{\rho_{\text{unp}} + \rho'e^{-i\phi}}{r} \left[u'e^{-i\phi} + re^{-i\phi} \frac{\partial u'}{\partial r} + ru' \frac{\partial e^{-i\phi}}{\partial r} + \frac{\partial v_{\text{unp}}}{\partial \phi} - iv'e^{-i\phi} \right] \end{aligned} \quad (\text{E.36})$$

Now we use equations (2.28), (2.27), and (D.1) to write it as:

$$RHS = -\frac{\rho_{\text{unp}}}{r} \left[\frac{\partial(ru')}{\partial r} - iv' \right] e^{-i\phi} \quad (\text{E.37})$$

Equating lhs and rhs and dividing by $e^{i\phi}$:

$$\boxed{\frac{\partial \rho'}{\partial t} - i\rho'\Omega + u' \frac{\partial \rho_{\text{unp}}}{\partial r} = -\frac{\rho_{\text{unp}}}{r} \left[\frac{\partial(ru')}{\partial r} - iv' \right]} \quad (\text{E.38})$$

E.0.4 Pressure equation

The last equation is equation (2.26d):

$$\underbrace{\frac{\partial p}{\partial t} + u \frac{\partial p}{\partial r} + \frac{v}{r} \frac{\partial p}{\partial \phi}}_{\text{LHS}} = \underbrace{-\frac{\gamma p}{r} \left[\frac{\partial ru}{\partial r} + \frac{\partial v}{\partial \phi} \right]}_{\text{RHS}}. \quad (\text{E.39})$$

$$\begin{aligned} LHS &= \frac{\partial(p_{\text{unp}} + p'e^{-i\phi})}{\partial t} + \frac{v_{\text{unp}} + v'e^{-i\phi}}{r} \frac{\partial(p_{\text{unp}} + p'e^{-i\phi})}{\partial \phi} \\ &\quad + (u'e^{-i\phi}) \frac{\partial(p_{\text{unp}} + p'e^{-i\phi})}{\partial r} \\ &= \frac{\partial p_{\text{unp}}}{\partial t} + e^{-i\phi} \frac{\partial p'}{\partial t} + \frac{v_{\text{unp}} + v'e^{-i\phi}}{r} \left[\frac{\partial p_{\text{unp}}}{\partial \phi} - ip'e^{-i\phi} \right] \\ &\quad + (u'e^{-i\phi}) \left[\frac{\partial \rho_{\text{unp}}}{\partial r} + \frac{\partial p'}{\partial r} e^{-i\phi} \right] \end{aligned} \quad (\text{E.40})$$

Now we use equations (2.28), (2.27), and (D.1) to write it as:

$$RHS = \frac{\partial p'}{\partial t} e^{-i\phi} - ip'\Omega e^{-i\phi} + u' e^{-i\phi} \frac{\partial p_{\text{unp}}}{\partial r} \quad (\text{E.41})$$

$$\begin{aligned} LHS &= -\frac{\gamma p_{\text{unp}} + p' e^{-i\phi}}{r} \left[\frac{\partial(ru' e^{-i\phi})}{\partial r} + \frac{\partial(v_{\text{unp}} + v' e^{-i\phi})}{\partial \phi} \right] \\ &= -\frac{\gamma(p_{\text{unp}} + p' e^{-i\phi})}{r} \left[u' e^{-i\phi} + r e^{-i\phi} \frac{\partial u'}{\partial r} + ru' \frac{\partial e^{-i\phi}}{\partial r} \right. \\ &\quad \left. + \frac{\partial v_{\text{unp}}}{\partial \phi} - iv' e^{-i\phi} \right] \end{aligned} \quad (\text{E.42})$$

Now we use equations (2.28), (2.27), and (D.1) to write it as:

$$RHS = -\frac{\gamma p_{\text{unp}}}{r} \left[\frac{\partial(ru')}{\partial r} - iv' \right] e^{-i\phi} \quad (\text{E.43})$$

Equating LHS and RHS, and deviding by $e^{i\phi}$:

$$\boxed{\frac{\partial p'}{\partial t} - ip'\Omega + u' \frac{\partial p_{\text{unp}}}{\partial r} = -\frac{\gamma p_{\text{unp}}}{r} \left[\frac{\partial(ru')}{\partial r} - iv' \right]} \quad (\text{E.44})$$

VERTICAL HYDROSTATIC EQUILIBRIUM

If there is no flow in the z -direction, the sum of all forces acting on a gas particle in that direction is zero. There are two forces acting in the z -direction:

- 1) Due to pressure gradient in the z -direction, a force F_p exists that pushes the gas particle outward: for a particle at $z > 0$, $\vec{F}_p = |F_p|\hat{z}$, for a particle at $z < 0$, $\vec{F}_p = |F_p|(-\hat{z})$

$$F_p = \delta p A$$

- 2) The force of gravity in the z -direction on gas of mass m in a gravitational potential Φ is:

$$\begin{aligned} F_{\text{grav}} &= -m \frac{\partial \Phi}{\partial z} = -\rho \delta z \frac{\partial \Phi}{\partial z} = \rho \delta z \frac{\partial}{\partial z} \left[\frac{M_1 G}{\sqrt{r^2 + z^2}} \right] = \rho \delta z \frac{\partial}{\partial z} \left[\frac{M_1 G}{r \sqrt{1 + (z/r)^2}} \right] \\ &= \text{for } z \ll r \approx \rho \delta z \frac{\partial}{\partial z} \left[\frac{M_1 G}{r} \left(1 - \frac{z^2}{2r^2} \right) \right] = -\rho \delta z \frac{M_1 G z}{r^3} \end{aligned}$$

$$F_p = F_{\text{grav}}$$

$$\delta p A = -\rho \delta z \frac{M_1 G z}{r^3}$$

for $\delta p \approx p$ and $\delta z \approx H = z$

$$p = -\frac{\rho M_1 G H^2}{r^3}$$

From this, we see that pressure is proportional $\rho(H/r)^2$.

Derivation of boundary conditions for the eccentricity equation

The gas equation of state for a locally isothermal disk is:

$$P = \Sigma c_s^2, \quad (\text{G.1})$$

so its the Lagrangian perturbation is:

$$dP = \Sigma dc_s^2 + c_s^2 d(\Sigma). \quad (\text{G.2})$$

We divide it by dt :

$$\frac{dP}{dt} = \Sigma \frac{dc_s^2}{dt} + c_s^2 \frac{d\Sigma}{dt}. \quad (\text{G.3})$$

We use equation (A.9) and the fact that c_s does not explicitly depend on time, to write:

$$\frac{dc_s^2}{dt} = \frac{\partial c_s^2}{\partial t} + u \frac{\partial c_s^2}{\partial r} + \frac{u}{r} \frac{\partial c_s^2}{\partial \phi} = u \frac{\partial c_s^2}{\partial r}. \quad (\text{G.4})$$

We use (equation (2.5)):

$$\frac{d\Sigma}{dt} = -\Sigma \frac{1}{r} \left[\frac{\partial(ru)}{\partial r} + \frac{\partial v}{\partial \phi} \right], \quad (\text{G.5})$$

to write:

$$\frac{dP}{dt} = \Sigma u \frac{\partial c_s^2}{\partial r} - c_s^2 - \Sigma \left[\frac{\partial(ru)}{\partial r} + \frac{\partial v}{\partial \phi} \right]. \quad (\text{G.6})$$

We write equation (G.6) in terms of perturbed velocities:

$$\frac{dP}{dt} = \left[\Sigma u' \frac{\partial(c_s^2)}{\partial r} - c_s^2 \Sigma \frac{1}{r} \left(\frac{\partial(ru')}{\partial r} - iv' \right) \right] e^{-i\phi}, \quad (\text{G.7})$$

and in terms of the eccentricity function:

$$\frac{dP}{dt} = \left[\Sigma i \Omega E r \frac{\partial(c_s^2)}{\partial r} - c_s^2 \Sigma \frac{1}{r} \left(\frac{\partial(ri \Omega E r)}{\partial r} - i \frac{1}{2} \Omega E r \right) \right] e^{-i\phi}. \quad (\text{G.8})$$

We write equation (G.8) as:

$$\frac{dP}{dt} = \left[\Sigma i \Omega E r \frac{\partial(c_s^2)}{\partial r} - c_s^2 \Sigma \frac{1}{r} \left(i E \frac{\partial(r^2 \Omega)}{\partial r} + i r^2 \Omega \frac{\partial E}{\partial r} - i \frac{1}{2} \Omega E r \right) \right] e^{-i\phi}, \quad (\text{G.9})$$

and use (equation (2.61)) to write:

$$\frac{dP}{dt} = \left[\Sigma i \Omega E r \frac{\partial(c_s^2)}{\partial r} - c_s^2 \Sigma \frac{1}{r} \left(i r^2 \Omega \frac{\partial E}{\partial r} \right) \right] e^{-i\phi}. \quad (\text{G.10})$$

If $dP/dt = 0$:

$$E \frac{1}{c_s^4} \frac{\partial(c_s^2)}{\partial r} - \frac{1}{c_s^2} \frac{\partial E}{\partial r} = 0. \quad (\text{G.11})$$

We use:

$$\frac{d}{dr} \frac{E}{c_s^2} = \frac{dE}{dr} \frac{1}{c_s^2} - \frac{d(c_s^2)}{dr} \frac{E}{(c_s^2)^2} \quad (\text{G.12})$$

to write the boundary condition as:

$$\frac{d}{dr} \frac{E}{c_s^2} = 0. \quad (\text{G.13})$$

G.1 An adiabatic disk

The gas equation of state for an adiabatic disk is:

$$P = K \Sigma^\gamma. \quad (\text{G.14})$$

We conduct the same procedure we did for a locally isothermal disk. First we write the Lagrangian differential of pressure:

$$dP = \gamma K \Sigma^{\gamma-1} d\Sigma, \quad (\text{G.15})$$

and divide it by dt :

$$\frac{dP}{dt} = \gamma K \Sigma^{\gamma-1} \frac{d\Sigma}{dt}. \quad (\text{G.16})$$

We again use mass continuity equation (equation (2.5)) to write:

$$\frac{dP}{dt} = \gamma K \Sigma^{\gamma-1} \left[-\Sigma \frac{1}{r} \left(\frac{\partial(ru)}{\partial r} + \frac{\partial v}{\partial \phi} \right) \right]. \quad (\text{G.17})$$

We write the it in terms of velocity perturbations:

$$\frac{dP}{dt} = -\frac{\gamma K \Sigma^\gamma}{r} \left[\frac{\partial(ru')}{\partial r} - iv' \right] e^{-i\phi} \quad (\text{G.18})$$

and eccentricity:

$$\frac{dP}{dt} = -\frac{\gamma K \Sigma^\gamma}{r} \left(\frac{\partial(ri\Omega Er)}{\partial r} - i\frac{1}{2}\Omega Er \right) e^{-i\phi}. \quad (\text{G.19})$$

We can write it in a different way:

$$\frac{dP}{dt} = -\frac{\gamma K \Sigma^\gamma}{r} \left(iE \frac{\partial(r^2\Omega)}{\partial r} + ir^2\Omega \frac{\partial(E)}{\partial r} - i\frac{1}{2}\Omega Er \right) e^{-i\phi}, \quad (\text{G.20})$$

and use $\frac{\partial}{\partial r} (r^2\Omega_{\text{ump},0}) = \frac{1}{2}r\Omega_{\text{ump},0}$ (equation (2.61)) to write:

$$\frac{dP}{dt} = -\frac{\gamma K \Sigma^\gamma}{r} \left(ir^2\Omega \frac{\partial E}{\partial r} \right) e^{-i\phi}. \quad (\text{G.21})$$

Finally, the boundary condition for an adiabatic disk is:

$$\frac{\partial E}{\partial r} = 0. \quad (\text{G.22})$$

Derivation of the eccentricity potential and scaled eccentricity

We compare equations (7.10) and (8.19) to find:

$$P(r) = 3r^{-1} + \frac{\Sigma'}{\Sigma}, \quad (\text{H.1})$$

and:

$$Q(r) = 2\frac{\Sigma'}{\Sigma}r^{-1} + \frac{3q}{2a^6h^2(1+q)^2}r^{-4} - \frac{2\omega}{\Omega_b a^{9/2}h^2}r^{-1/2}. \quad (\text{H.2})$$

We use equation (7.13) to find the scaled eccentricity y as:

$$\begin{aligned} \ln E &= \ln y - \frac{1}{2} \int P(r) dr = \ln y - \frac{1}{2} \int \left[3r^{-1} + \frac{\Sigma'}{\Sigma} \right] dr \\ &= \ln y - \frac{1}{2} [3 \ln r + \ln \Sigma] = \ln \left(yr^{-3/2} \Sigma^{-1/2} \right), \end{aligned} \quad (\text{H.3})$$

or as:

$$E = y(\Sigma r^3)^{-1/2}. \quad (\text{H.4})$$

We use equation (7.14) to write:

$$\begin{aligned} k^2 &= Q(r) - \frac{1}{2}P'(r) - \frac{1}{4}P^2(r) \\ &= 2\frac{\Sigma'}{\Sigma}r^{-1} + \frac{3q}{2a^6h^2(1+q)^2}r^{-4} - \frac{2\omega}{\Omega_b a^{9/2}h^2}r^{-1/2} - \frac{1}{2} \left[-3r^{-2} + \frac{\Sigma''}{\Sigma} - \frac{\Sigma'^2}{\Sigma^2} \right] \\ &\quad - \frac{1}{4} \left[9r^{-2} + \frac{\Sigma'^2}{\Sigma^2} + 6r^{-1} \frac{\Sigma'}{\Sigma} \right] \\ &= \frac{3q}{2a^6h^2(1+q)^2}r^{-4} - \frac{2\omega}{\Omega_b a^{9/2}h^2}r^{-1/2} - \frac{3}{4}r^{-2} - \frac{1}{2} \frac{\Sigma''}{\Sigma} + \frac{1}{4} \frac{\Sigma'^2}{\Sigma} + \frac{1}{2} \frac{\Sigma'}{\Sigma} \end{aligned} \quad (\text{H.5})$$

We verify that using:

$$E = y(\Sigma r^3)^{-1/2}, \quad (\text{H.6})$$

results in a Schrödinger equation. The eccentricity equation is:

$$\begin{aligned}
2\Sigma r^2 \Omega_0 \omega E(r) &= \frac{1}{r} \frac{\partial}{\partial r} \left[\Sigma c_s^2 r^3 \frac{\partial E(r)}{\partial r} \right] + r \frac{d}{dr} (\Sigma c_s^2) E(r) \\
&- \frac{1}{r} \frac{\partial}{\partial r} \left[\Sigma \frac{dc_s^2}{dr} r^3 E(r) \right] + \Sigma \Omega_0^2 E(r) \frac{3q}{2(1+q)^2} a^2.
\end{aligned} \tag{H.7}$$

We calculate different terms of equation (H.7) separately:

$$\begin{aligned}
\text{1st+3rd term of RHS} &= \frac{i}{R} \frac{\partial}{\partial R} \left[\Sigma C_s^2 R^3 \frac{\partial E}{\partial R} - \Sigma \frac{dC_s^2}{dR} R^3 E \right] \\
&= \frac{i}{R} \frac{\partial}{\partial R} \left[\Sigma \frac{h^2 \Omega_b^2 a_b^3 R^3}{R} \frac{\partial}{\partial R} \left(y \Sigma^{-1/2} R^{-3/2} \right) + \Sigma \frac{h^2 \Omega_b^2 a_b^3 R^3}{R^2} y \Sigma^{-1/2} R^{-3/2} \right] \\
&= \frac{i}{R} h^2 \Omega_b^2 a_b^3 \frac{\partial}{\partial R} \left[\Sigma R^2 \frac{\partial}{\partial R} \left(y \Sigma^{-1/2} R^{-3/2} \right) + y \Sigma^{1/2} R^{-1/2} \right] \\
&= i C_s^2 \frac{\partial}{\partial R} \left[\Sigma R^2 \left(y' \Sigma^{-1/2} R^{-3/2} - \frac{1}{2} y \Sigma^{-3/2} \Sigma' R^{-3/2} - \frac{3}{2} y \Sigma^{-1/2} R^{-5/2} \right) + \Sigma^{1/2} R^{-1/2} y \right] \\
&= i C_s^2 \frac{\partial}{\partial R} \left[y' \Sigma^{1/2} R^{1/2} - \frac{1}{2} y \Sigma^{-1/2} \Sigma' R^{1/2} - \frac{3}{2} y \Sigma^{1/2} R^{-1/2} + \Sigma^{1/2} R^{-1/2} y \right] \\
&= i C_s^2 \frac{\partial}{\partial R} \left[y' \Sigma^{1/2} R^{1/2} - \frac{1}{2} y \Sigma^{-1/2} \Sigma' R^{1/2} - \frac{1}{2} y \Sigma^{1/2} R^{-1/2} \right] \\
&= i C_s^2 \left[y'' \Sigma^{1/2} R^{1/2} + \frac{1}{2} y' \Sigma^{-1/2} \Sigma' R^{1/2} + \frac{1}{2} y' \Sigma^{1/2} R^{-1/2} \right. \\
&\quad \left. - \frac{1}{2} y' \Sigma^{-1/2} \Sigma' R^{1/2} + \frac{1}{4} y \Sigma^{-3/2} (\Sigma')^2 R^{1/2} - \frac{1}{2} y \Sigma^{-1/2} \Sigma'' R^{1/2} - \frac{1}{4} y \Sigma^{-1/2} \Sigma' R^{-1/2} \right. \\
&\quad \left. - \frac{1}{2} y' \Sigma^{1/2} R^{-1/2} - \frac{1}{4} y \Sigma^{-1/2} \Sigma' R^{-1/2} + \frac{1}{4} y \Sigma^{1/2} R^{-3/2} \right] \\
&= i C_s^2 \left[y'' \Sigma^{1/2} R^{1/2} + \frac{1}{4} y \Sigma^{-3/2} (\Sigma')^2 R^{1/2} - \frac{1}{2} y \Sigma^{-1/2} \Sigma'' R^{1/2} \right. \\
&\quad \left. - \frac{1}{2} y \Sigma^{-1/2} \Sigma' R^{1/2} + \frac{1}{4} y \Sigma^{1/2} R^{-3/2} \right],
\end{aligned} \tag{H.8}$$

$$\begin{aligned}
\text{2nd RHS term} &= i R \frac{d}{dR} (\Sigma C_s^2) E = i R \frac{d}{dR} \left[\frac{\Sigma h^2 \Omega_b^2 a_b^3}{R} \right] \cdot y \Sigma^{-1/2} R^{-3/2} \\
&= i R^{-1/2} y h^2 \Omega_b^2 a_b^3 \Sigma^{-1/2} \left[\frac{\Sigma'}{R} - \frac{\Sigma}{R} \right] \\
&= i C_s^2 y R^{1/2} \Sigma^{-1/2} \left[\frac{\Sigma'}{R} - \frac{\Sigma}{R^2} \right] \\
&= i C_s^2 \left[y \Sigma' \Sigma^{-1/2} R^{-1/2} - y \Sigma^{1/2} R^{-3/2} \right]
\end{aligned} \tag{H.9}$$

$$\begin{aligned} \text{LHS} &= 2\Sigma R^2 \Omega \frac{\partial E}{\partial t} = 2\Sigma R^2 \Omega i \omega E \\ &= 2\Sigma R^2 \Omega i \omega y \Sigma^{-1/2} R^{-3/2} = 2\Omega i \omega y \Sigma^{1/2} R^{1/2}, \end{aligned} \quad (\text{H.10})$$

$$\text{4th RHS term} = 2\Sigma R^2 \Omega i \Omega f_0 E = 2\Omega^2 i f_0 y \Sigma^{1/2} R^{1/2} \quad (\text{H.11})$$

We sum up all contributions:

$$\begin{aligned} 2\Omega i f_0 y \Sigma^{1/2} R^{1/2} &= i C_s^2 \left[y'' \Sigma^{1/2} R^{1/2} + \frac{1}{4} y \Sigma^{-3/2} (\Sigma')^2 R^{1/2} \right. \\ &\quad - \frac{1}{2} y \Sigma^{-1/2} \Sigma'' R^{1/2} - \frac{1}{2} y \Sigma^{-1/2} \Sigma' R^{-1/2} \\ &\quad \left. + \frac{1}{4} y \Sigma^{1/2} R^{-3/2} + y \Sigma' \Sigma^{-1/2} R^{-1/2} - y \Sigma^{1/2} R^{-3/2} \right] \\ &\quad + 2\Omega^2 i f_0 y \Sigma^{1/2} R^{1/2}, \end{aligned} \quad (\text{H.12})$$

and divide the equation by $C_s^2 \Sigma^{1/2} R^{1/2} i$:

$$y'' + y \frac{2\Omega}{C_s^2} \left[\Omega f_0 + \frac{C_s^2}{2\Omega} \left[\left(\frac{\Sigma'}{2\Sigma} \right)^2 - \frac{1}{2} \frac{\Sigma''}{\Sigma^2} + \frac{1}{2} \frac{\Sigma'}{\Sigma R} + \frac{3}{4R^2} \right] - \omega \right] = 0 \quad (\text{H.13})$$

To rewrite equation (H.13) in a slightly different form, we use:

$$\begin{aligned} \frac{C_s^2}{2\Omega} &= \frac{h^2 \Omega_b^2 a_b^3}{2R \Omega_b \left(\frac{R}{a_b} \right)^{-3/2}} = \frac{h^2 \Omega_b}{2} \frac{a_b^3 a_b^{-3/2} R^2}{R \cdot R^{-3/2} R^2}, \\ &= \frac{h^2 \Omega_b}{2} \frac{a_b^{3/2}}{R^{3/2}} R^2 = \frac{h^2 \Omega_b}{2} \left(\frac{R}{a_b} \right)^{-3/2} R^2, \end{aligned} \quad (\text{H.14})$$

If we define $\omega_{\text{pot}}(r)$ and $k(r)$ as:

$$k^2(\Omega, R) \equiv \frac{2\omega}{C_s^2} [\omega_{\text{pot}}(R) - \omega], \quad (\text{H.15})$$

and:

$$\begin{aligned} \omega_{\text{pot}}(R) &\equiv \Omega f_0 + \frac{h^2 \Omega_b}{2} \left(\frac{R}{a_b} \right)^{-3/2} \left[\frac{R \Sigma'}{2\Sigma} + \left(\frac{R \Sigma'}{2\Sigma} \right)^2 - \frac{R^2 \Sigma''}{2\Sigma} - \frac{3}{4} \right] \\ &= \omega_q \left(\frac{R}{R_{\text{cav}}} \right)^{-7/2} + \frac{\omega_P}{2} \left(\frac{R}{a_b} \right)^{-3/2} \left[\frac{R \Sigma'}{2\Sigma} + \left(\frac{R \Sigma'}{2\Sigma} \right)^2 - \frac{R^2 \Sigma''}{2\Sigma} - \frac{3}{4} \right], \end{aligned} \quad (\text{H.16})$$

the eccentricity equation becomes:

$$\frac{d^2y}{dR^2} + k^2y = 0. \quad (\text{H.17})$$

Scaling the eccentricity equation with a cavity radius

We set $a = 1$ and $\Omega_b = 1$ and use:

$$\Omega_0(r) = \left(\frac{r}{R_{\text{cav}}}\right)^{-3/2} R_{\text{cav}}^{-3/2}, \quad (\text{I.1})$$

and:

$$\frac{d}{dr} = R_{\text{cav}}^{-1} \frac{d}{d\left(\frac{r}{R_{\text{cav}}}\right)}, \quad (\text{I.2})$$

to write the eccentricity equation (equation (9.3)) as:

$$\begin{aligned} 2\Sigma(r)R_{\text{cav}}^{1/2} \left(\frac{r}{R_{\text{cav}}}\right)^{1/2} \frac{\omega}{\omega_Q} E &= \frac{\omega_P}{\omega_Q} \left(\frac{r}{R_{\text{cav}}}\right)^{-1} \frac{d}{d\left(\frac{r}{R_{\text{cav}}}\right)} \left[\Sigma(r)R_{\text{cav}}^{1/2} \frac{dE}{d\left(\frac{r}{R_{\text{cav}}}\right)} \right] \\ &+ \frac{\omega_P}{\omega_Q} \frac{r}{R_{\text{cav}}} \frac{d}{d\left(\frac{r}{R_{\text{cav}}}\right)} \left[\Sigma(r)R_{\text{cav}}^{1/2} \left(\frac{r}{R_{\text{cav}}}\right)^{-1} \right] E \\ &+ \frac{\omega_P}{\omega_Q} \left(\frac{r}{R_{\text{cav}}}\right)^{-1} \frac{d}{d\left(\frac{r}{R_{\text{cav}}}\right)} \left[\Sigma(r)R_{\text{cav}}^{1/2} \left(\frac{r}{R_{\text{cav}}}\right) E \right] \\ &+ \Sigma(r)R_{\text{cav}}^{1/2} \left(\frac{r}{R_{\text{cav}}}\right)^{-3} E. \end{aligned} \quad (\text{I.3})$$

For the density profile (11.1):

$$\begin{aligned} \Sigma(r)R_{\text{cav}}^{1/2} &= \left(r^{-1/2} - Lr^{-1}\right) e^{-(r/R_{\text{cav}})^Z} R_{\text{cav}}^{1/2} \\ &= \left[\left(\frac{r}{R_{\text{cav}}}\right)^{-1/2} - LR_{\text{cav}}^{-1/2} \left(\frac{r}{R_{\text{cav}}}\right)^{-1}\right] e^{-(r/R_{\text{cav}})^Z}, \end{aligned} \quad (\text{I.4})$$

which can only be written in terms of r/R_{cav} if $L = 0$. If $L \neq 0$, the eccentricity solutions depend on the product $LR_{\text{cav}}^{-1/2}$.

Bibliography



- Amaro-Seoane, Pau, Jeff Andrews, Manuel Arca Sedda, *et al.* (Mar. 2022). „Astrophysics with the Laser Interferometer Space Antenna“. In: *arXiv e-prints*, arXiv:2203.06016, arXiv:2203.06016. arXiv: 2203.06016 [gr-qc].
- Amaro-Seoane, Pau, Heather Audley, Stanislav Babak, *et al.* (Feb. 2017). „Laser Interferometer Space Antenna“. In: *arXiv e-prints*, arXiv:1702.00786, arXiv:1702.00786. arXiv: 1702.00786 [astro-ph.IM].
- Arzoumanian, Zaven, Paul T. Baker, Harsha Blumer, *et al.* (Dec. 2020). „The NANOGrav 12.5 yr Data Set: Search for an Isotropic Stochastic Gravitational-wave Background“. In: *ApJL* 905.2, L34, p. L34. arXiv: 2009.04496 [astro-ph.HE].
- Begelman, M. C., R. D. Blandford, and M. J. Rees (Sept. 1980). „Massive black hole binaries in active galactic nuclei“. In: *Nature* 287.5780, pp. 307–309.
- Bellovary, Jillian M., Mordecai-Mark Mac Low, Barry McKernan, and K. E. Saavik Ford (Mar. 2016). „MIGRATION TRAPS IN DISKS AROUND SUPERMASSIVE BLACK HOLES“. In: *The Astrophysical Journal* 819.2, p. L17.
- Bogdanovic, Tamara, M. Coleman Miller, and Laura Blecha (Sept. 2021). „Electromagnetic Counterparts to Massive Black Hole Mergers“. In: *arXiv e-prints*, arXiv:2109.03262, arXiv:2109.03262. arXiv: 2109.03262 [astro-ph.HE].
- Cuadra, J., P. J. Armitage, R. D. Alexander, and M. C. Begelman (Mar. 2009). „Massive black hole binary mergers within subparsec scale gas discs“. In: *MNRAS* 393.4, pp. 1423–1432. arXiv: 0809.0311 [astro-ph].
- D’Orazio, Daniel J. and Paul C. Duffell (June 2021). „Orbital Evolution of Equal-mass Eccentric Binaries due to a Gas Disk: Eccentric Inspirals and Circular Outspirals“. In: *ApJL* 914.1, L21, p. L21. arXiv: 2103.09251 [astro-ph.HE].
- D’Orazio, Daniel J., Zoltán Haiman, Paul Duffell, Andrew MacFadyen, and Brian Farris (July 2016). „A transition in circumbinary accretion discs at a binary mass ratio of 1:25“. In: *MNRAS* 459.3, pp. 2379–2393. arXiv: 1512.05788 [astro-ph.HE].
- D’Orazio, Daniel J., Zoltán Haiman, and Andrew MacFadyen (Dec. 2013). „Accretion into the central cavity of a circumbinary disc“. In: *MNRAS* 436.4, pp. 2997–3020. arXiv: 1210.0536 [astro-ph.GA].

- Duffell, Paul C., Daniel D’Orazio, Andrea Derdzinski, Zoltan Haiman, Andrew MacFadyen, Anna L. Rosen, and Jonathan Zrake (Sept. 2020a). „Circumbinary Disks: Accretion and Torque as a Function of Mass Ratio and Disk Viscosity“. In: *ApJ* 901.1, 25, p. 25. arXiv: 1911.05506 [astro-ph.SR].
- Duffell, Paul C., Daniel D’Orazio, Andrea Derdzinski, Zoltan Haiman, Andrew MacFadyen, Anna L. Rosen, and Jonathan Zrake (Sept. 2020b). „Circumbinary Disks: Accretion and Torque as a Function of Mass Ratio and Disk Viscosity“. In: *ApJ* 901.1, 25, p. 25. arXiv: 1911.05506 [astro-ph.SR].
- Goodchild, Simon and Gordon Ogilvie (May 2006). „The dynamics of eccentric accretion discs in superhump systems“. In: *MNRAS* 368.3, pp. 1123–1131. arXiv: astro-ph/0602492 [astro-ph].
- Klein, Antoine, Enrico Barausse, Alberto Sesana, *et al.* (Jan. 2016). „Science with the space-based interferometer eLISA: Supermassive black hole binaries“. In: *PRD* 93.2, 024003, p. 024003. arXiv: 1511.05581 [gr-qc].
- Lee, Wing-Kit, Adam M. Dempsey, and Yoram Lithwick (Feb. 2019). „Eccentric Modes in Disks with Pressure and Self-gravity“. In: *The Astrophysical Journal* 872.2, p. 184.
- Lommen, Andrea N (June 2012). „Pulsar Timing Arrays: No longer a Blunt Instrument for Gravitational Wave Detection“. In: *Journal of Physics: Conference Series* 363, p. 012029.
- Ma, Zhong-Qi and Bo-Wei Xu (Mar. 2005). „Quantum correction in exact quantization rules“. In: *EPL (Europhysics Letters)* 69.5, pp. 685–691. arXiv: physics/0502109 [physics.comp-ph].
- MacFadyen, Andrew I. and Miloš Milosavljević (Jan. 2008). „An Eccentric Circumbinary Accretion Disk and the Detection of Binary Massive Black Holes“. In: *ApJ* 672.1, pp. 83–93. arXiv: astro-ph/0607467 [astro-ph].
- Muñoz, Diego J. and Yoram Lithwick (Dec. 2020). „Long-lived Eccentric Modes in Circumbinary Disks“. In: *ApJ* 905.2, 106, p. 106. arXiv: 2008.08085 [astro-ph.HE].
- Ogilvie, G. I. (July 2001). „Non-linear fluid dynamics of eccentric discs“. In: *Monthly Notices of the Royal Astronomical Society* 325.1, pp. 231–248.
- Ogilvie, Gordon I. (Aug. 2008). „3D eccentric discs around Be stars“. In: *MNRAS* 388.3, pp. 1372–1380. arXiv: 0805.3128 [astro-ph].
- Perivolaropoulos, L. and F. Skara (Dec. 2022). „Challenges for Λ CDM: An update“. In: *New Astronomy Reviews* 95, 101659, p. 101659. arXiv: 2105.05208 [astro-ph.CO].

- Teyssandier, Jean and Gordon I. Ogilvie (May 2016). „Growth of eccentric modes in disc-planet interactions“. In: *MNRAS* 458.3, pp. 3221–3247. arXiv: 1603.00653 [astro-ph.EP].
- The LIGO Scientific Collaboration, The Virgo Collaboration, The KAGRA Collaboration, *et al.* (2021). *The population of merging compact binaries inferred using gravitational waves through GWTC-3*.
- Tian, Zhi-Jia, Xiao-Wei Liu, Hai-Bo Yuan, *et al.* (May 2018). „Binary Star Fractions from the LAMOST DR4“. In: *Research in Astronomy and Astrophysics* 18.5, 052, p. 052. arXiv: 1802.09690 [astro-ph.SR].
- Tiede, Christopher, Jonathan Zrake, Andrew MacFadyen, and Zoltan Haiman (Sept. 2020). „Gas-driven Inspiral of Binaries in Thin Accretion Disks“. In: *ApJ* 900.1, 43, p. 43. arXiv: 2005.09555 [astro-ph.GA].